

Supporting Information

Highly Tunable Bimane-Based Fluorescent Probes: Design, Synthesis, and Application as Selective Amyloid Binding Dye

Yarra Venkatesh,^a Nicholas P. Marotta,^c Virginia M.-Y. Lee,^c and E. James Petersson^{a,b*}

^aDepartment of Chemistry, University of Pennsylvania, 231 South 34th Street, Philadelphia, Pennsylvania 19104, USA.

^bBiochemistry and Molecular Biophysics Graduate Group, Perelman School of Medicine, University of Pennsylvania, Philadelphia, Pennsylvania 19104, USA.

^cDepartment of Pathology and Laboratory Medicine, Center for Neurodegenerative Disease Research, University of Pennsylvania, 3600 Spruce Street, Philadelphia, Pennsylvania 19104, USA.

*E-mail: ejpetersson@sas.upenn.edu

Table of Contents

General Information	S3
Multi-Gram Scale Synthesis of Bimane Core	S4-S5
Synthesis and Characterization of key precursor 3	S5-6
General Procedure for H-W-E reaction.....	S7
Reaction Optimization for H-W-E reaction.....	S8-S9
Synthesis and Characterization of 5a-5k	S10-S13
Crystal Data and Structure Refinement	S14-S24
General Photophysical Characterization Methods	S25-S26
Photophysical Properties of 3 and 5a-5k in ACN	S27-S28
Solvatochromism of 3 , 5b , 5d , 5j	S29
Fluorescent Quantum Yield Measurements of 5a-5k	S30-S32
Effect of pH on 5h and 5j	S33

Fluorescence Lifetime Measurements of 3 , 5c-5f	S34-S35
Computational Studies	S36-S40
Production of α -Synuclein and 1N4R Tau	S41-S44
Fibril Preparation	S45-S47
Fibril Binding Characterization	S48
Absorbance and Fluorescence Measurements with α S Fibrils	S49-S50
Fluorescent QY and lifetime measurements of 5j and 5k with α S fibrils.....	S51-S52
Excitation and Fluorescence Measurements of 5j , 5k and ThT with Tau Fibrils	S53
Excitation and Fluorescence Measurements of 5j , 5k and ThT with $A\beta_{1-42}$ Fibrils	S54
Experimental Procedure for HEK cell lysate preparation and Selectivity of 5k	S55
Experimental procedure for the fluorescent measurements of 5k with TMAO.....	S56
Patient Tissue Characterization and Amplified Fibril Preparation.....	S57-S60
Fluorescence Measurements with Patient Tissue Lysate Samples	S61
Analysis of Bimane Literature	S62
Photographs of 1 and 5a-5k Solid State Emission	S62
NMR spectra	S63-S73
Optimized Ground and Excited State Geometries	S74-S82
References	S83

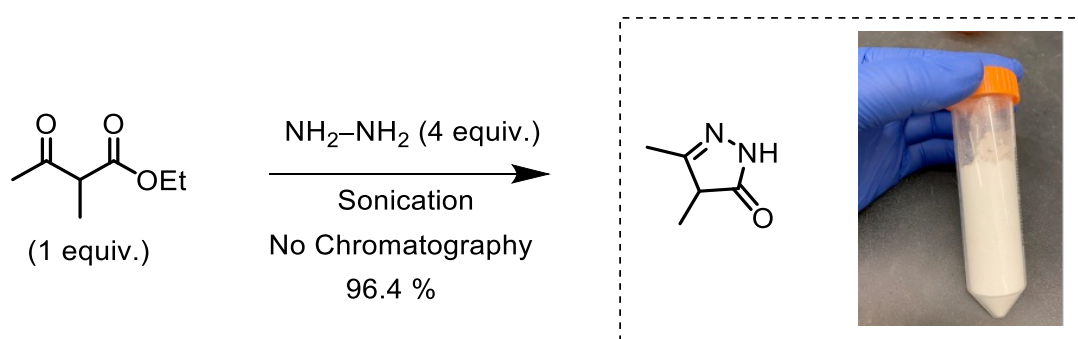
General Information

Materials. Trichloroisocyanuric acid (TCCA), trimethyl phosphite and all other derivatives of aryl aldehydes were purchased from Millipore Sigma (St. Louis, MO, USA). Flash column chromatography was performed using Silicycle silica gel (40-63 μm (230- 400 mesh), 60 \AA irregular pore diameter). Thin-layer chromatography (TLC) was performed on TLC Silica gel 60G F254 plates from Millipore Sigma. Reagents were purchased at the highest commercial quality and used without further purification, unless otherwise stated. The β -amyloid (1-42) peptide, human (Cat. No. RP10017) was purchased from Genscript (Piscataway, NJ).

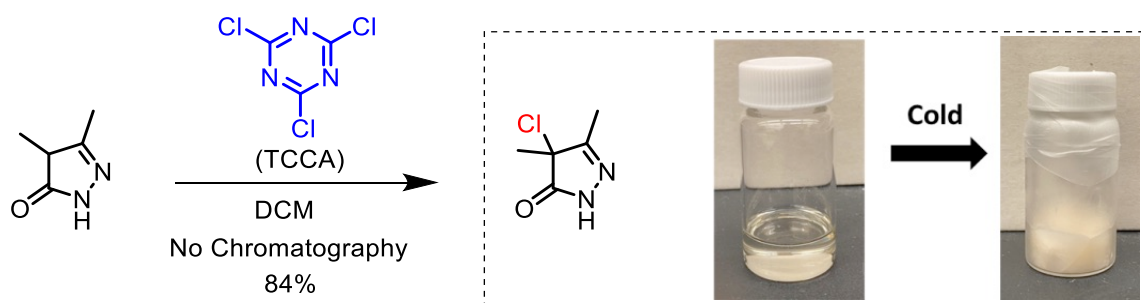
Instruments. Nuclear magnetic resonance (NMR) spectra were obtained on a Bruker UNI-400 MHz or UNI-600 MHz instrument (Billerica, MA, USA) and are calibrated using peaks from residual protic solvent in deuterated solvent. The following abbreviations were used to denote multiplicities: s = singlet, d = doublet, t = triplet, q = quartet, m = multiplet, br = broad). Low-resolution mass spectra (LRMS) were obtained on a Waters Acquity Ultra Performance LC connected to a single quadrupole detector mass spectrometer (Waters Corp.; Milford, MA, USA). High-resolution mass spectra (HRMS) were obtained by Dr. Charles Ross III at the University of Pennsylvania's Mass Spectrometry Center on a High-resolution electrospray ionization mass spectra (ESI-HRMS) using Waters LCT Premier XE liquid chromatograph/mass spectrometer. X-ray diffraction data obtained on a Rigaku XtaLAB Synergy-S diffractometer equipped with an HPC area detector (HyPix-6000HE) and employing confocal multilayer optic-monochromated Mo-K α radiation ($\lambda=0.71073 \text{ \AA}$) or Cu-K α radiation ($\lambda=1.54184 \text{ \AA}$) at a temperature of 100K and solved by Dr. Patrick Carroll at the University of Pennsylvania. Absorbance readings for the DC assay were made on a Tecan M1000 plate reader (Mannedorf, Switzerland). UV-Vis absorption spectra were acquired on a Thermo Scientific Genesys 150 UV-Vis spectrometer (Waltham, MA, USA) using quartz cells with a 1 cm cell path length (Starna Cells, Inc 120ul UV cells). Fluorescence spectra were acquired on a Tecan M1000 plate reader. Quantum yield (QY) measurements were performed using a Jasco FP-8300 Fluorimeter with ILF-835 integrating sphere attachment (Easton, MD, USA). Fluorescence lifetime measurements were made using a Photon Technology International (PTI) QuantaMaster™ 40 fluorescence spectrometer (Birmingham, NJ, USA).

Multi-Gram Scale Synthesis of Bimane Core

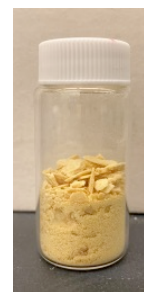
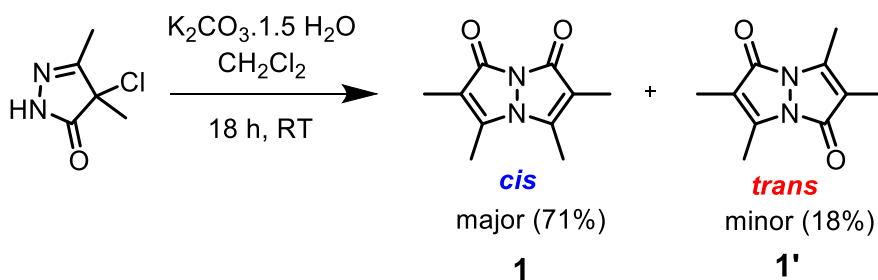
Synthesis of 3,4-dimethyl-2-pyrazolin-5-one. Ethyl 2-methylacetoacetate (30 g, 208.3 mmol, 1 equiv) was condensed with 4 equiv. of hydrazine (26.7 g, 833.2 mmol, 35 wt. % in H₂O) under sonication for 30 min to give a white precipitate. After filtration of the white precipitate and washing several times with ethyl acetate followed by dichloromethane to get rid of the unreacted starting materials, the precipitate was dried overnight to afford 22.485 g of compound 3,4-dimethyl-2-pyrazolin-5-one in 96.4% isolated yield. ¹H NMR and LRMS characterization data matched previous reports.¹



Synthesis of 3,4-dimethyl-4-chloro-2-pyrazolin-5-one. 3,4-dimethyl-2-pyrazolin-5-one (20 g, 178.4 mmol) was dissolved in 200 mL of dichloromethane (DCM). The solution was cooled on an ice bath. Trichloroisocyanuric acid (TCCA, 13.7 g, 59.5 mmol) was slowly added to the reaction mixture over a period of 30 min. After completion of the addition, the reaction mixture was stirred overnight at room temperature and the cyanuric acid byproduct was filtered off. The filtrate was concentrated under reduced pressure at 40 °C to afford 22.05 g of 3,4-dimethyl-4-chloro-2-pyrazolin-5-one in 84 % isolated yield. ¹H NMR and LRMS characterization data matched previous reports.^{1,2}

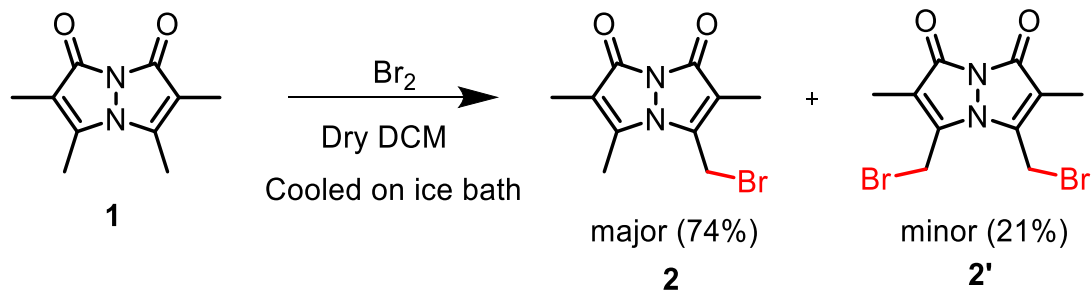


Synthesis of 2,3,5,6-tetramethyl-1H,7H-pyrazolo[1,2-a]pyrazole-1,7-dione (1). 3,4-Dimethyl-4-chloro-2-pyrazolin-5-one (15 g, 102.34 mmol, 1 equiv) was dissolved in 150 mL DCM and cooled on an ice bath. Then add potassium carbonate hydrate ($K_2CO_3 \cdot 1.5 H_2O$) (59.32 g, 429.83 mmol, 4.2 equiv) and stir for 18 hours at room temperature. Then the K_2CO_3 was filtered, and the filtrate concentrated to afford a mixture of *cis* (**1**) and *trans* (**1'**) isomers of bimane. 2,3,5,6-tetramethyl-1*H*,7*H*-pyrazolo[1,2-*a*]pyrazole-1,7-dione, with **1** as the major product. The reaction mixture was purified by column chromatography eluting with 40–70% ethyl acetate in hexane to afford the 71% of compound **1** ($R_f = 0.1$, 70% EtOAc in hexane) and compound **1'** ($R_f = 0.64$, 70% EtOAc in hexane) in 18% yield. 1H NMR and LRMS characterization data matched previous reports.¹

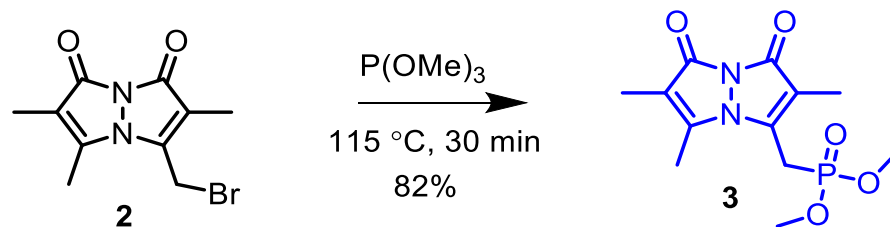


Synthesis and Characterization of 3

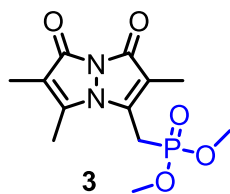
Synthesis of 3-(bromomethyl)-2,5,6-trimethyl-1H,7H-pyrazolo[1,2-a]pyrazole-1,7-dione (2). Compound **1** (3 g, 15.61 mmol) was dissolved in dry 120 mL of DCM. The solution was cooled on an ice bath and a bromine solution (0.8 mL, 15.61 mmol) in 30 mL of DCM solvent was added dropwise over a period of 30 min under cold conditions. Upon completion of the addition, the reaction mixture was stirred for another 30 min under cold conditions. The progress of the reaction was monitored by TLC. Upon completion of the reaction, the resulting mixture was neutralized with cold water and then extracted with DCM. The organic layer was collected and concentrated by rotary evaporation. The crude product was purified by flash column chromatography eluting with 30–60% ethyl acetate in hexane to afford the desired monobrominated product **2** ($R_f = 0.17$, 70% EtOAc in hexane) in 74% yield and we also isolated the dibrominated product **2'** ($R_f = 0.45$, 70% EtOAc in hexane) in 21% yield. 1H and ^{13}C NMR and LRMS characterization data matched previous reports.¹



Synthesis of dimethyl ((2,5,6-trimethyl-1,7-dioxo-1H,7H-pyrazolo[1,2-a]pyrazol-3-yl)methyl)phosphonate (3). A mixture of monobromobimane (**2**, 2.0 g, 7.38 mmol) and trimethyl phosphite (2.85 mL) was heated at 115 °C for 30 min until it became homogeneous and then solidified. After trituration with hexane (50 mL), the mixture was slurried in ethyl acetate and filtered to remove the remaining trimethyl phosphite. Then, the solid product was redissolved in DCM and purified by flash column chromatography using 3% methanol in DCM as an eluent to afford 1.82 g of the phosphonate **3** ($R_f = 0.37$, 3% methanol in DCM) as a light-yellow solid in 82% isolated yield.

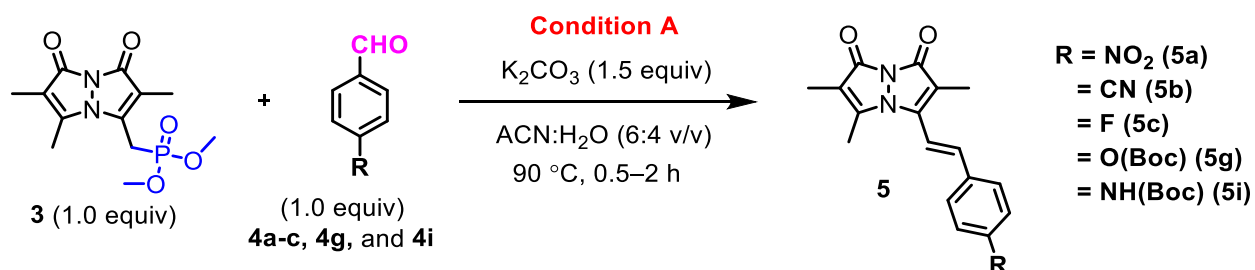


$^1\text{H NMR}$ (400 MHz, CDCl_3) δ 3.78 (d, $J = 11.1$ Hz, 6H), 3.20 (d, $J = 22.0$ Hz, 2H), 2.42 (s, 3H), 1.84 (d, $J = 4.1$ Hz, 3H), 1.80 (s, 3H). $^{13}\text{C NMR}$ (101 MHz, CDCl_3) δ 160.7, 160.2, 146.5, 140.0, 114.7, 113.2, 53.7, 25.2, 23.8, 11.9, 7.0. HRMS (ESI⁺) calcd for $\text{C}_{12}\text{H}_{17}\text{N}_2\text{O}_5\text{P}$ $[\text{M} + \text{H}]^+$, 301.0953; found: 301.0965.

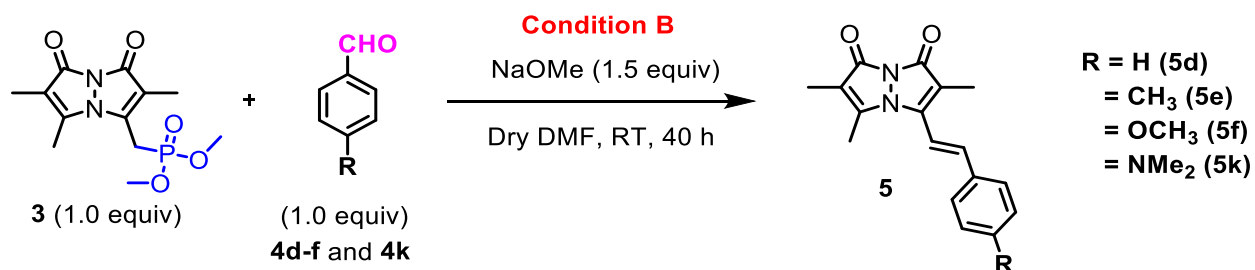


Horner-Wadsworth-Emmons (H-W-E) reactions were performed with one of two general procedures:

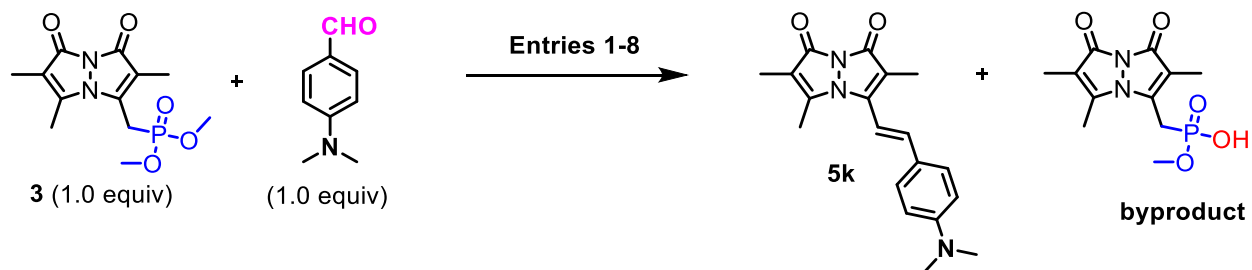
H-W-E General procedure A. To a solution of dimethyl bimanephosphonate **3** (1 mmol) in acetonitrile (ACN)/H₂O (2 mL, 6:4 v/v), add the aryl aldehydes **4a-c**, **4g**, and **4i** (1 mmol) and K₂CO₃ (1.5 mmol) and heat at 90 °C for 30 min-2 h. The reaction progress was checked by TLC, upon completion of the reaction, the solution was cooled to room temperature and the organic layer was extracted with DCM, washed with water (2 x 50 mL), dried using Na₂SO₄, and concentrated under vacuum to yield the crude mixture. Then, the product was purified by recrystallization from MeOH.



H-W-E General procedure B. To a solution of phosphonate **3** (1 mmol) in dry DMF, the aryl aldehydes **4d-f** and **4k** (1 mmol) and NaOMe (1.5 mmol) were added, and the resulting solution was stirred at RT for 40 h under argon atmosphere. The reaction progress was monitored by TLC, and upon completion, the organic layer was extracted with DCM, washed with water (2 x 50 mL), dried using Na₂SO₄, and concentrated under vacuum to yield the crude product. Then, the product was purified by flash column chromatography using 3% methanol in DCM as an eluent.



Scheme S1. Optimization of H-W-E reaction of **3** and 4-(dimethylamino)benzaldehyde^a



Entry	Solvent	Base	Temp	Time (hours)	Yield (%)
1	ACN/H ₂ O	K ₂ CO ₃	RT	40 h	2.3
2	ACN/H ₂ O	K ₂ CO ₃	90 °C	2 h	9
3	DMF	KO ^t Bu	RT	40 h	27
4	DMF	NaOMe	RT	40 h	46
5	DMF	NaOMe	60 °C	40 h	38.4
6	DMSO	KO ^t Bu	RT	40 h	3.5
7	DMSO	NaOMe	RT	40 h	31
8	DMSO	NaOMe	60 °C	40 h	11.5

^aReaction conditions: **3** (1 equiv), aryl aldehyde **4k** (1 equiv), KO^tBu (1.5 equiv) or NaOMe (1.5 equiv), K₂CO₃ (1.5 equiv).

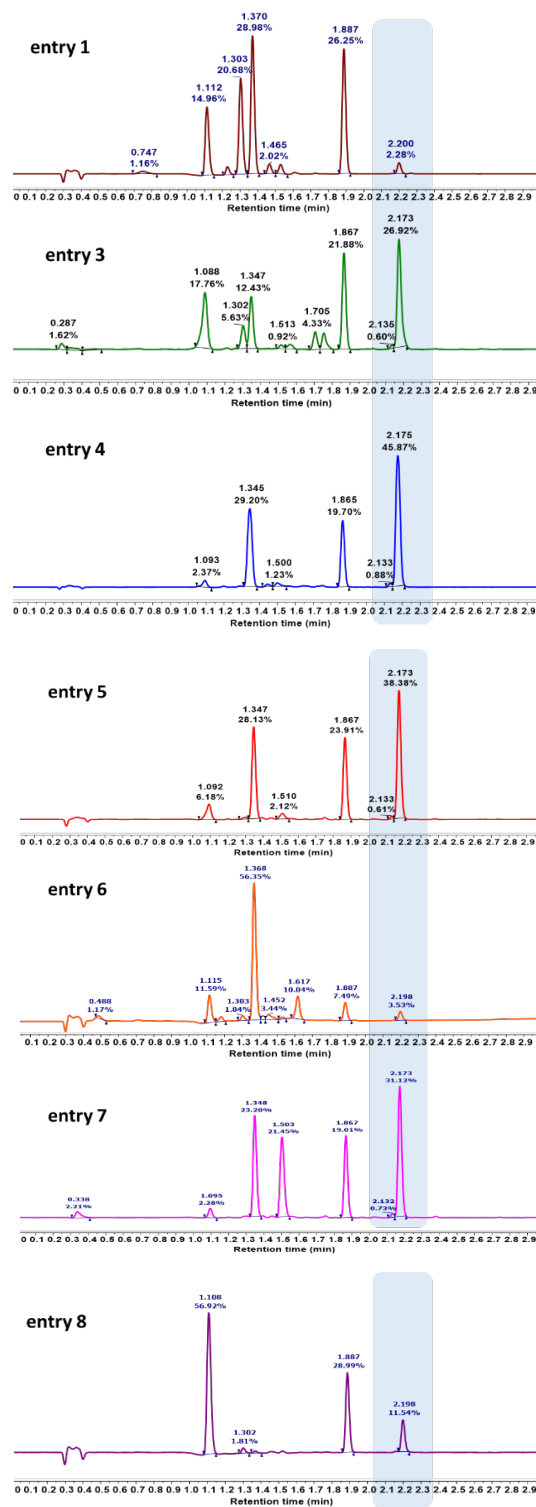
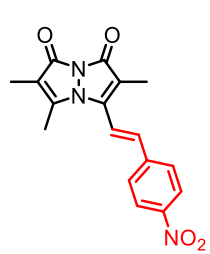


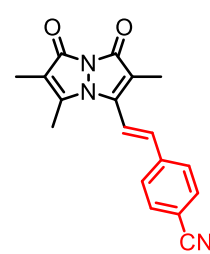
Fig. S1. Liquid Chromatography (LC) chromatogram for the conversion of 5k under different optimized reaction conditions.

Synthesis and Characterization of 5a-5k

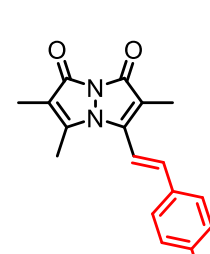
(*E*)-2,3,6-trimethyl-5-(4-nitrostyryl)-1*H*,7*H*-pyrazolo[1,2-*a*]pyrazole-1,7-dione (5a).


Following General Procedure A with 4-nitrobenzaldehyde (**4a**, 50.3 mg, 0.33 mmol, 1 equiv, purchased from Aldrich) at 90 °C for 30 min afforded 106 mg (98 % isolated yield, yellow solid) of **5a**. ¹H NMR (400 MHz, CDCl₃) δ 8.29 (d, *J* = 8.9 Hz, 2H), 7.70 (d, *J* = 8.8 Hz, 2H), 7.17 (d, *J* = 16.5 Hz, 1H), 6.96 (d, *J* = 17.3 Hz, 1H), 2.30 (s, 3H), 2.03 (s, 3H), 1.84 (s, 3H). ¹³C NMR (101 MHz, CDCl₃) δ 161.7, 161.3, 148.5, 146.4, 141.0, 138.5, 128.1, 124.7, 118.3, 115.2, 114.3, 12.7, 8.6, 7.2. HRMS (ESI⁺) calcd for C₁₇H₁₅N₃O₄ [M + H]⁺, 326.1141 ; found: 326.1156.

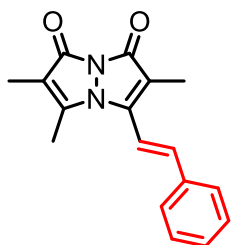
(*E*)-4-(2-(2,5,6-trimethyl-1,7-dioxo-1*H*,7*H*-pyrazolo[1,2-*a*]pyrazol-3-yl)vinyl)benzotrile (5b).


(**5b**). Following General Procedure A with 4-cyanobenzaldehyde (**4b**, 43.6 mg, 0.33 mmol, 1 equiv, purchased from Aldrich) at 90 °C for 1 h afforded 85.3 mg (83.6 % isolated yield, yellow solid) of **5b**. ¹H NMR (400 MHz, CDCl₃) δ 7.73 (d, *J* = 8.4 Hz, 2H), 7.63 (d, *J* = 8.5 Hz, 2H), 7.12 (d, *J* = 16.5 Hz, 1H), 6.91 (d, *J* = 16.5 Hz, 1H), 2.28 (s, 3H), 2.02 (s, 3H), 1.84 (s, 3H). ¹³C NMR (101 MHz, CDCl₃) δ 161.7, 161.3, 148.6, 146.6, 139.1, 139.0, 133.1, 127.9, 118.4, 117.6, 115.0, 114.2, 113.5, 12.7, 8.6, 7.2. HRMS (ESI⁺) calcd for C₁₈H₁₅N₃O₂ [M + H]⁺, 306.1243; found: 306.1235.

(*E*)-3-(4-fluorostyryl)-2,5,6-trimethyl-1*H*,7*H*-pyrazolo[1,2-*a*]pyrazole-1,7-dione (5c).

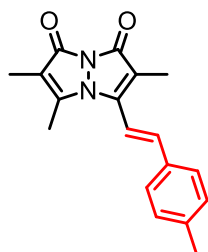

Following General Procedure A with 4-fluorobenzaldehyde (**4c**, 41.3 mg, 0.33 mmol, 1 equiv, purchased from Aldrich) at 90 °C for 2 h afforded 77.2 mg (78 % isolated yield, yellow solid) of **5c**. ¹H NMR (400 MHz, CDCl₃) δ 7.52 (dd, *J* = 8.9, 5.3 Hz, 2H), 7.13 (t, *J* = 8.6 Hz, 2H), 7.07 (d, *J* = 16.4 Hz, 1H), 6.71 (d, *J* = 16.5 Hz, 1H), 2.28 (s, 3H), 2.01 (s, 3H), 1.83 (s, 3H). ¹³C NMR (101 MHz, CDCl₃) δ 164.0 (d, ¹J_{C-F} = 252.7 Hz), 161.8, 161.6, 148.6, 147.5, 140.1, 131.2, 129.4, 129.3, 116.6 (d, ²J_{C-F} = 22.2 Hz), 113.9, 113.7, 12.7, 8.6, 7.2. HRMS (ESI⁺) calcd for C₁₇H₁₅FN₂O₂ [M+H]⁺, 299.1196; found: 299.1193.

(E)-2,3,6-trimethyl-5-styryl-1H,7H-pyrazolo[1,2-a]pyrazole-1,7-dione (5d): Following



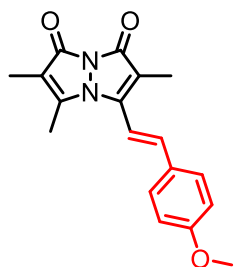
General Procedure B with benzaldehyde (**4d**, 35.3 mg, 0.33 mmol, 1 equiv, purchased from Aldrich) at room temperature for 40 h afforded 67 mg (72.4 % isolated yield, yellow solid) of **5d** after purification by column chromatography (3% methanol in dichloromethane, $R_f = 0.46$). ^1H NMR (400 MHz, CDCl_3) δ 7.53 (dd, $J = 7.9, 1.9$ Hz, 2H), 7.48 – 7.39 (m, 3H), 7.11 (d, $J = 16.5$ Hz, 1H), 6.79 (d, $J = 16.4$ Hz, 1H), 2.29 (s, 3H), 2.02 (s, 3H), 1.84 (s, 3H). ^{13}C NMR (101 MHz, CDCl_3) δ 161.9, 161.7, 148.6, 147.7, 141.4, 135.0, 130.4, 129.4, 127.5, 114.0, 113.9, 113.8, 12.7, 8.6, 7.2. HRMS (ESI⁺) calcd for $\text{C}_{17}\text{H}_{16}\text{N}_2\text{O}_2$ [$\text{M} + \text{H}$]⁺, 281.1290 ; found: 281.1283.

(E)-2,3,6-trimethyl-5-(4-methylstyryl)-1H,7H-pyrazolo[1,2-a]pyrazole-1,7-dione (5e).



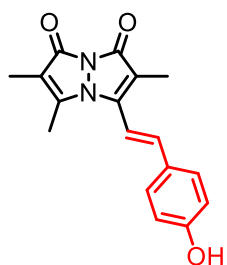
Following General Procedure B with *p*-tolualdehyde (**4e**, 40 mg, 0.33 mmol, 1 equiv, purchased from Aldrich) at room temperature for 40 h afforded 67 mg (68 % isolated yield, yellow solid) of **5e** after purification by column chromatography (3% methanol in dichloromethane, $R_f = 0.47$). ^1H NMR (400 MHz, CDCl_3) δ 7.45 (d, $J = 8.1$ Hz, 2H), 7.28 (d, $J = 2.8$ Hz, 2H), 7.10 (d, $J = 16.5$ Hz, 1H), 6.76 (d, $J = 16.4$ Hz, 1H), 2.43 (s, 3H), 2.31 (s, 3H), 2.04 (s, 3H), 1.86 (s, 3H). ^{13}C NMR (101 MHz, CDCl_3) δ 161.9, 161.7, 148.7, 148.0, 141.4, 140.9, 132.2, 130.1, 127.4, 113.9, 113.4, 112.9, 77.5, 77.2, 76.9, 21.7, 12.7, 8.6, 7.2. HRMS (ESI⁺) calcd for $\text{C}_{18}\text{H}_{18}\text{N}_2\text{O}_2$ [$\text{M} + \text{H}$]⁺, 295.1447; found: 295.1447.

(E)-3-(4-methoxystyryl)-2,5,6-trimethyl-1H,7H-pyrazolo[1,2-a]pyrazole-1,7-dione (5f).



Following General Procedure B with *p*-anisaldehyde (**4f**, 45.3 mg, 0.33 mmol, 1 equiv, purchased from Aldrich) at room temperature for 40 h afforded 61 mg (59 % isolated yield, yellow solid) of **5f** after purification by column chromatography (3% methanol in dichloromethane, $R_f = 0.45$). ^1H NMR (400 MHz, CDCl_3) δ 7.47 (d, $J = 8.8$ Hz, 2H), 7.05 (d, $J = 16.5$ Hz, 1H), 6.95 (d, $J = 8.8$ Hz, 2H), 6.63 (d, $J = 17.1$ Hz, 1H), 3.86 (s, 3H), 2.28 (s, 3H), 2.00 (s, 3H), 1.83 (s, 3H). ^{13}C NMR (101 MHz, CDCl_3) δ 161.7, 161.6, 161.3, 148.5, 148.0, 140.9, 128.9, 127.5, 114.6, 113.6, 112.7, 111.3, 55.5, 12.5, 8.4, 7.0. HRMS (ESI⁺) calcd for $\text{C}_{18}\text{H}_{18}\text{N}_2\text{O}_3$ [$\text{M} + \text{H}$]⁺, 311.1396; found: 311.1408.

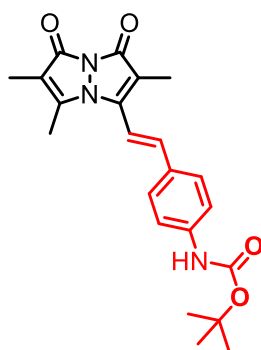
(E)-3-(4-hydroxystyryl)-2,5,6-trimethyl-1H,7H-pyrazolo[1,2-a]pyrazole-1,7-dione (5h).



Following General Procedure A with *tert*-butyl 4-formylphenyl carbonate (**4g**, 74 mg, 0.33 mmol, 1 equiv, purchased from Aldrich) at 90 °C for 2 h afforded 100.3 mg (76 % isolated yield) of *tert*-butyloxycarbonyl (Boc) protected **5g** after purification by column chromatography (3% methanol in dichloromethane, $R_f = 0.41$).

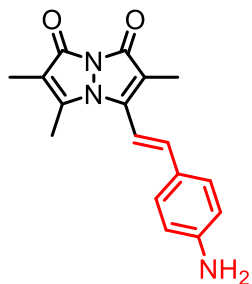
Next, the Boc deprotection of **5g** (100 mg, 0.252 mmol, 1 equiv) was carried out under acidic conditions using trifluoroacetic acid (431.4 mg, 3.78 mmol, 15 equiv) in 2 mL DCM solvent for 6 h. The reaction progress was monitored by the TLC and upon completion, it was dried under vacuum to afford 55.3 mg of the **5h** (74% isolated yield, yellow solid, $R_f = 0.34$ in 3% methanol in dichloromethane). ^1H NMR (600 MHz, DMSO) δ 9.97 (s, 1H), 7.59 (d, $J = 8.7$ Hz, 2H), 7.20 (d, $J = 16.5$ Hz, 1H), 6.97 (d, $J = 16.5$ Hz, 1H), 6.83 (d, $J = 8.7$ Hz, 2H), 2.34 (s, 3H), 1.91 (s, 3H), 1.74 (s, 3H). ^{13}C NMR (151 MHz, DMSO) δ 161.1, 160.9, 159.4, 150.1, 148.8, 141.2, 129.5, 126.3, 115.8, 111.8, 110.6, 110.5, 12.1, 8.0, 6.6. HRMS (ESI⁺) calcd for $\text{C}_{17}\text{H}_{16}\text{N}_2\text{O}_3$ $[\text{M} + \text{H}]^+$, 297.1239; found: 297.1233.

***tert*-butyl (E)-(4-(2-(2,5,6-trimethyl-1,7-dioxo-1H,7H-pyrazolo[1,2-a]pyrazol-3-yl)vinyl)phenyl)carbamate (5i).**



Following General Procedure A with 4-(Boc-amino)benzaldehyde (**4i**, 73.6 mg, 0.33 mmol, 1 equiv) at 90 °C for 2 h afforded 113.5 mg (86 % isolated yield, yellow solid) of **5i** after purification by column chromatography (3% methanol in dichloromethane, $R_f = 0.42$). ^1H NMR (600 MHz, CDCl_3) δ 7.45 (s, 4H), 7.04 (d, $J = 16.4$ Hz, 1H), 6.73 – 6.60 (m, 2H), 2.28 (s, 3H), 2.02 (s, 3H), 1.84 (s, 3H), 1.53 (s, 9H). ^{13}C NMR (151 MHz, CDCl_3) δ 161.9, 161.8, 152.5, 148.7, 148.0, 129.6, 128.4, 118.8, 113.9, 113.2, 112.2, 81.4, 28.5, 12.7, 8.6, 7.2. HRMS (ESI⁺) calcd for $\text{C}_{22}\text{H}_{25}\text{N}_3\text{O}_4$ $[\text{M} + \text{H}]^+$, 396.1923; found: 396.1930.

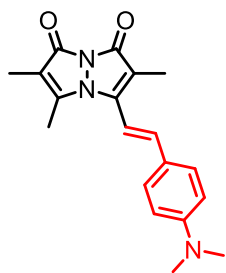
(E)-3-(4-aminostyryl)-2,5,6-trimethyl-1*H*,7*H*-pyrazolo[1,2-*a*]pyrazole-1,7-dione (5j): The deprotection of a Boc-protected **5i** (100 mg, 0.253 mmol, 1 equiv) was carried out under acidic



conditions using trifluoroacetic acid (432.5 mg, 3.79 mmol, 15 equiv) in 2 mL DCM solvent for 6 h. After completion of the reaction, the reaction progress was monitored by the TLC and concentrated the solvent and dried under vacuum to afford 62.8 mg of **5j** (84% isolated yield, red solid, $R_f = 0.39$). ^1H NMR (600 MHz, DMSO) δ 7.43 (d, $J = 8.6$ Hz, 2H), 7.13 (d, $J = 16.3$ Hz, 1H), 6.81 (d, $J = 16.3$ Hz, 1H), 6.60 (d, $J = 8.5$ Hz, 2H), 5.76 (s,

2H), 2.35 (s, 3H), 1.91 (s, 3H), 1.74 (s, 3H). ^{13}C NMR (151 MHz, DMSO) δ 161.6, 161.5, 151.7, 150.5, 149.9, 142.6, 130.0, 122.9, 114.1, 112.2, 109.8, 108.0, 12.6, 8.6, 7.0. HRMS (ESI⁺) calcd for $\text{C}_{17}\text{H}_{17}\text{N}_3\text{O}_2$, $[\text{M} + \text{H}]^+$, 296.1399; found: 296.1405.

(E)-3-(4-(dimethylamino)styryl)-2,5,6-trimethyl-1*H*,7*H*-pyrazolo[1,2-*a*]pyrazole-1,7-dione



(5k). Following General Procedure B with 4-(dimethylamino)benzaldehyde (**4k**, 49.6 mg, 0.33 mmol, 1 equiv, purchased from Aldrich) at room temperature for 40 h afforded 46.3 mg (43 % isolated yield, orange solid) of **5k** after purification by column chromatography (3% methanol in dichloromethane, $R_f = 0.45$). ^1H NMR (600 MHz, CDCl_3) δ 7.40 (d, $J = 8.9$ Hz, 2H), 7.03 (d, $J = 16.3$ Hz, 1H), 6.71 (d, $J = 8.9$ Hz, 2H), 6.53 (d, $J = 16.3$

Hz, 1H), 3.04 (s, 6H), 2.29 (s, 3H), 2.01 (s, 3H), 1.84 (s, 3H). ^{13}C NMR (151 MHz, CDCl_3) δ 162.1, 162.0, 151.9, 149.0, 148.7, 141.8, 129.0, 122.8, 113.6, 112.2, 111.8, 108.4, 40.4, 12.8, 8.7, 7.2. HRMS (ESI⁺) calcd for $\text{C}_{19}\text{H}_{21}\text{N}_3\text{O}_2$, $[\text{M} + \text{H}]^+$, 324.1712; found: 324.1712.

X-ray Structure Determination of Compound 5a

Compound **5a**, C₁₇H₁₅N₃O₄, crystallizes in the monoclinic space group P2₁ (systematic absences 0k0: k=odd) with a=3.85501(8)Å, b=13.3190(3)Å, c=14.7962(3)Å, β=94.880(2)°, V=756.96(3)Å³, Z=2, and d_{calc}=1.427 g/cm³. X-ray intensity data were collected on a Rigaku XtaLAB Synergy-S diffractometer equipped with an HPC area detector (HyPix-6000HE) and employing confocal multilayer optic-monochromated Mo-Kα radiation (λ=0.71073 Å) at a temperature of 100 K. Preliminary indexing was performed from a series of thirty 0.5° rotation frames with exposures of 0.5 sec. A total of 1844 frames (11 runs) were collected employing ω scans with a crystal to detector distance of 34.0 mm, rotation widths of 0.5° and exposures of 5 sec. Rotation frames were integrated using CrysAlisPro, producing a listing of unaveraged F² and σ(F²) values. A total of 19219 reflections were measured over the ranges 4.122 ≤ 2θ ≤ 50.682°, -4 ≤ h ≤ 4, -16 ≤ k ≤ 16, -17 ≤ l ≤ 17 yielding 2782 unique reflections (R_{int} = 0.0272). The intensity data were corrected for Lorentz and polarization effects and for absorption using SCALE3 ABSPACK (minimum and maximum transmission 0.8029, 1.0000). The structure was solved by direct methods - ShelXT. Refinement was by full-matrix least squares based on F² using SHELXL-2018. All reflections were used during refinement. The weighting scheme used was w=1/[σ²(F_o²) + (0.0390P)² + 0.1383P] where P = (F_o² + 2F_c²)/3. Non-hydrogen atoms were refined anisotropically and hydrogen atoms were refined using a riding model. Refinement converged to R1=0.0237 and wR2=0.0626 for 2734 observed reflections for which F > 4σ(F) and R1=0.0241 and wR2=0.0629 and GOF =1.029 for all 2782 unique, non-zero reflections and 220 variables. The maximum Δ/σ in the final cycle of least squares was 0.000 and the two most prominent peaks in the final difference Fourier were +0.12 and -0.15 e/Å³.

Table S1. lists cell information, data collection parameters, and refinement data. **Tables S2.** and **S3.** list bond distances and bond angles. **Fig. S2.** is an ORTEP representation of the molecule with 50% probability thermal ellipsoids displayed.

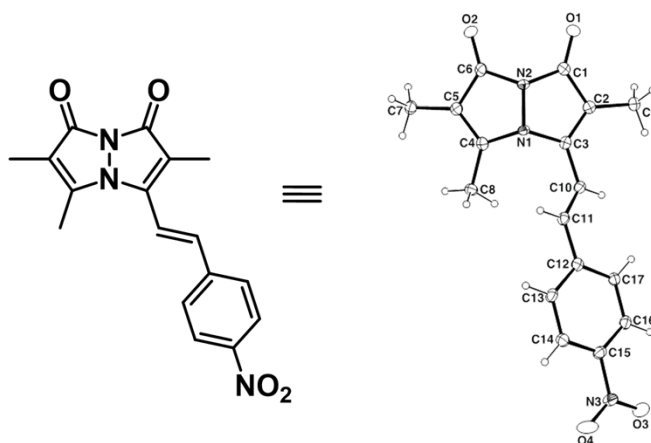


Fig. S2. X-ray diffraction data and ORTEP drawing of **5a** with 50% thermal ellipsoids.

Table S1. Summary of Structure Determination of **5a**

Empirical formula	C ₁₇ H ₁₅ N ₃ O ₄
Formula weight	325.32
Diffractometer	Rigaku XtaLAB Synergy-S
Temperature/K	100
Crystal system	monoclinic
Space group	P2 ₁
a	3.85501(8)Å
b	13.3190(3)Å
c	14.7962(3)Å
β	94.880(2)°
Volume	756.96(3)Å ³
Z	2
d _{calc}	1.427 g/cm ³
μ	0.104 mm ⁻¹
F(000)	340.0
Crystal size, mm	0.2 × 0.07 × 0.07
2θ range for data collection	4.122 - 50.682°
Index ranges	-4 ≤ h ≤ 4, -16 ≤ k ≤ 16, -17 ≤ l ≤ 17
Reflections collected	19219

Independent reflections	2782[R(int) = 0.0272]
Data/restraints/parameters	2782/1/220
Goodness-of-fit on F ²	1.029
Final R indexes [I ≥ 2σ (I)]	R ₁ = 0.0237, wR ₂ = 0.0626
Final R indexes [all data]	R ₁ = 0.0241, wR ₂ = 0.0629
Largest diff. peak/hole	0.12/-0.15 eÅ ⁻³
Flack parameter	-0.3(3)

Table S2. Bond Distances in Compound **5a**, Å

C1-C2	1.456(3)	C1-N2	1.419(2)	C1-O1	1.216(2)
C2-C3	1.361(3)	C2-C9	1.491(3)	C3-C10	1.453(2)
C3-N1	1.416(2)	C4-C5	1.354(3)	C4-C8	1.484(2)
C4-N1	1.418(2)	C5-C6	1.450(3)	C5-C7	1.493(3)
C6-N2	1.435(2)	C6-O2	1.213(2)	C10-C11	1.345(3)
C11-C12	1.463(2)	C12-C13	1.405(3)	C12-C17	1.404(3)
C13-C14	1.384(3)	C14-C15	1.388(3)	C15-C16	1.388(3)
C15-N3	1.469(2)	C16-C17	1.381(3)	N1-N2	1.400(2)
N3-O3	1.230(2)	N3-O4	1.227(2)		

Table S3. Bond Angles in Compound **5a**, °

N2-C1-C2	105.09(15)	O1-C1-C2	130.24(18)	O1-C1-N2	124.61(17)
C1-C2-C9	121.50(16)	C3-C2-C1	108.59(17)	C3-C2-C9	129.84(18)
C2-C3-C10	127.42(17)	C2-C3-N1	109.79(16)	N1-C3-C10	122.17(16)
C5-C4-C8	127.80(17)	C5-C4-N1	109.57(16)	N1-C4-C8	122.51(16)
C4-C5-C6	109.23(16)	C4-C5-C7	128.84(17)	C6-C5-C7	121.91(16)
N2-C6-C5	104.84(15)	O2-C6-C5	131.29(17)	O2-C6-N2	123.87(17)
C11-C10-C3	123.89(16)	C10-C11-C12	126.40(17)	C13-C12-C11	117.83(16)
C17-C12-C11	123.28(17)	C17-C12-C13	118.89(17)	C14-C13-C12	121.02(17)
C13-C14-C15	118.21(17)	C14-C15-C16	122.51(17)	C14-C15-N3	118.40(17)
C16-C15-N3	119.07(16)	C17-C16-C15	118.66(17)	C16-C17-C12	120.70(17)
C3-N1-C4	130.54(15)	N2-N1-C3	106.78(14)	N2-N1-C4	107.10(14)
C1-N2-C6	128.21(15)	N1-N2-C1	109.73(13)	N1-N2-C6	109.04(14)
O3-N3-C15	118.26(17)	O4-N3-C15	118.47(16)	O4-N3-O3	123.26(17)

X-ray Structure Determination of Compound 5c

Compound **5c**, $C_{17}H_{15.25}FN_2O_{2.125}$, crystallizes in the orthorhombic space group $Fdd2$ (systematic absences hkl : $h+k=\text{odd}$ and $k+l=\text{odd}$, $h0l$: $h+1\neq 4n$, and $0kl$: $k+1\neq 4n$) with $a=29.9395(3)\text{\AA}$, $b=27.5788(3)\text{\AA}$, $c=7.07968(9)\text{\AA}$, $V=5845.66(12)\text{\AA}^3$, $Z=16$, and $d_{\text{calc}}=1.366\text{ g/cm}^3$. X-ray intensity data were collected on a Rigaku XtaLAB Synergy-S diffractometer equipped with an HPC area detector (HyPix-6000HE) and employing confocal multilayer optic-monochromated $\text{Cu}=\text{K}\alpha$ radiation ($\lambda=1.54184\text{ \AA}$) at a temperature of 100K. Preliminary indexing was performed from a series of sixty 0.5° rotation frames with exposures of 15 sec. for $\theta = \pm 47.04^\circ$ and 60 sec. for $\theta = 107.75^\circ$. A total of 7042 frames (47 runs) were collected employing ω scans with a crystal to detector distance of 34.0 mm, rotation widths of 0.5° and exposures of 2 sec. for $\theta = \pm 47.04^\circ$ and 8 sec. for $\theta = -86.25$ and 107.75° . Rotation frames were integrated using CrysAlisPro, producing a listing of unaveraged F^2 and $\sigma(F^2)$ values. A total of 35147 reflections were measured over the ranges $8.718 \leq 2\theta \leq 149.006^\circ$, $-37 \leq h \leq 35$, $-33 \leq k \leq 34$, $-8 \leq l \leq 8$ yielding 2976 unique reflections ($R_{\text{int}} = 0.0563$). The intensity data were corrected for Lorentz and polarization effects and for absorption using SCALE3 ABSPACK (minimum and maximum transmission 0.58523, 1.00000). The structure was solved by dual space methods - SHELXT. Refinement was by full-matrix least squares based on F^2 using SHELXL. All reflections were used during refinement. The weighting scheme used was $w=1/[\sigma^2(F_o^2) + (0.0568P)^2 + 4.6832P]$ where $P = (F_o^2 + 2F_c^2)/3$. Non-hydrogen atoms were refined anisotropically and hydrogen atoms were refined using a riding model. Refinement converged to $R1=0.0365$ and $wR2=0.0978$ for 2938 observed reflections for which $F > 4\sigma(F)$ and $R1=0.0369$ and $wR2=0.0982$ and $\text{GOF} = 1.087$ for all 2976 unique, non-zero reflections and 207 variables. The maximum Δ/σ in the final cycle of least squares was 0.001 and the two most prominent peaks in the final difference Fourier were $+0.15$ and -0.21 e/\AA^3 .

Table S4. lists cell information, data collection parameters, and refinement data. **Tables S5 and S6.** list bond distances and bond angles. **Figure S3.** is an ORTEP representation of the molecule with 50% probability thermal ellipsoids displayed.

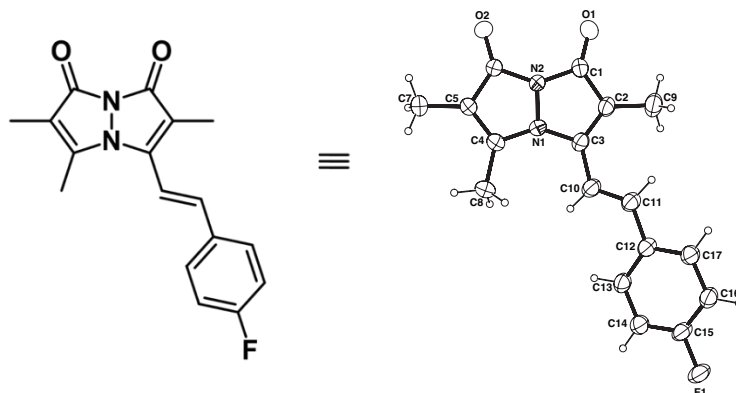


Fig. S3. X-ray diffraction data and ORTEP drawing of **5c** with 50% thermal ellipsoids.

Table S4. Summary of Structure Determination of **5c**

Empirical formula	C ₁₇ H _{15.25} FN ₂ O _{2.125}
Formula weight	300.56
Diffractometer	Rigaku XtaLAB Synergy-S (HyPix-6000HE)
Temperature/K	100
Crystal system	orthorhombic
Space group	Fdd2
a	29.9395(3)Å
b	27.5788(3)Å
c	7.07968(9)Å
α	90°
β	90°
γ	90°
Volume	5845.66(12)Å ³
Z	16
d _{calc}	1.366 g/cm ³
μ	0.829 mm ⁻¹
F(000)	2516.0
Crystal size, mm	0.25 × 0.12 × 0.08
2θ range for data collection	8.718 - 149.006°
Index ranges	-37 ≤ h ≤ 35, -33 ≤ k ≤ 34, -8 ≤ l ≤ 8
Reflections collected	35147

Independent reflections	2976[R(int) = 0.0563]
Data/restraints/parameters	2976/1/207
Goodness-of-fit on F ²	1.087
Final R indexes [$I \geq 2\sigma(I)$]	R ₁ = 0.0365, wR ₂ = 0.0978
Final R indexes [all data]	R ₁ = 0.0369, wR ₂ = 0.0982
Largest diff. peak/hole	0.15/-0.21 eÅ ⁻³
Flack parameter	0.10(6)

Table S5. Bond Distances in Compound **5c**, Å

C1-C2	1.452(3)	C1-N2	1.417(3)	C1-O1	1.221(3)
C2-C3	1.374(3)	C2-C9	1.490(3)	C3-C10	1.450(3)
C3-N1	1.387(3)	C4-C5	1.368(3)	C4-C8	1.483(3)
C4-N1	1.374(3)	C5-C6	1.448(3)	C5-C7	1.487(3)
C6-N2	1.398(3)	C6-O2	1.219(3)	C10-C11	1.346(3)
C11-C12	1.464(3)	C12-C13	1.403(3)	C12-C17	1.392(3)
C13-C14	1.388(3)	C14-C15	1.380(3)	C15-C16	1.371(3)
C15-F1	1.357(3)	C16-C17	1.392(3)	N1-N2	1.375(3)

Table S6. Bond Angles in Compound **5c**, °

N2-C1-C2	104.22(18)	O1-C1-C2	131.6(2)	O1-C1-N2	124.2(2)
C1-C2-C9	121.2(2)	C3-C2-C1	109.11(19)	C3-C2-C9	129.5(2)
C2-C3-C10	130.4(2)	C2-C3-N1	108.07(19)	N1-C3-C10	121.5(2)
C5-C4-C8	130.0(2)	C5-C4-N1	108.1(2)	N1-C4-C8	122.0(2)
C4-C5-C6	109.28(19)	C4-C5-C7	127.9(2)	C6-C5-C7	122.8(2)
N2-C6-C5	103.76(18)	O2-C6-C5	131.4(2)	O2-C6-N2	124.86(19)
C11-C10-C3	121.2(2)	C10-C11-C12	127.4(2)	C13-C12-C11	123.9(2)
C17-C12-C11	117.1(2)	C17-C12-C13	118.9(2)	C14-C13-C12	120.3(2)
C15-C14-C13	118.5(2)	C16-C15-C14	123.2(2)	F1-C15-C14	118.2(2)
F1-C15-C16	118.6(2)	C15-C16-C17	117.7(2)	C12-C17-C16	121.4(2)
C4-N1-C3	142.1(2)	C4-N1-N2	108.70(18)	N2-N1-C3	109.15(18)
C6-N2-C1	140.38(18)	N1-N2-C1	109.45(18)	N1-N2-C6	110.16(17)

This report has been created with Olex2 [6], compiled on 2021.10.07 svn.r9718050b for OlexSys.

X-ray Structure Determination of Compound 5k

Compound **5k**, $C_{20}H_{25}N_3O_3$, crystallizes in the monoclinic space group $P2_1/c$ (systematic absences $0k0$: $k=\text{odd}$ and $h0l$: $l=\text{odd}$) with $a=7.0514(6)\text{\AA}$, $b=17.1123(10)\text{\AA}$, $c=30.720(2)\text{\AA}$, $\beta=91.352(8)^\circ$, $V=3705.8(5)\text{\AA}^3$, $Z=8$, and $d_{\text{calc}}=1.274\text{ g/cm}^3$. X-ray intensity data were collected on a Rigaku XtaLAB Synergy-S diffractometer equipped with an HPC area detector (Dectris Pilatus3 R 200K) and employing confocal multilayer optic-monochromated Mo-K α radiation ($\lambda=0.71073\text{ \AA}$) at a temperature of 100 K. Preliminary indexing was performed from a series of thirty 0.5° rotation frames with exposures of 10 seconds. A total of 1272 frames (13 runs) were collected employing ω scans with a crystal to detector distance of 50.0 mm, rotation widths of 0.5° and exposures of 60 seconds.

The crystal grew as a non-merohedral twin. The Ewald Explorer extension in CrysAlisPro was used to index the diffraction images and to determine the twinning mechanism. The crystal was twinned by a rotation of 180° about the 001 real direction. Rotation frames were integrated using CrysAlisPro, producing a listing of unaveraged F^2 and $\sigma(F^2)$ values. A total of 49137 reflections were measured over the ranges $4.636 \leq 2\theta \leq 52.95^\circ$, $-8 \leq h \leq 8$, $-21 \leq k \leq 21$, $-37 \leq l \leq 38$ yielding 13556 unique reflections ($R_{\text{int}} = 0.081$). The intensity data were corrected for Lorentz and polarization effects and for absorption using SCALE3 ABSPACK (minimum and maximum transmission 0.85,80 1.0000). The structure was solved by dual space methods - SHELXT. Refinement was by full-matrix least squares based on F^2 using SHELXL. All reflections were used during refinement. The weighting scheme used was $w=1/[\sigma^2(F_o^2) + (0.1260P)^2 + 0.9687P]$ where $P = (F_o^2 + 2F_c^2)/3$. Non-hydrogen atoms were refined anisotropically and hydrogen atoms were refined using a riding model. Refinement converged to $R1=0.0719$ and $wR2=0.1949$ for 9577 observed reflections for which $F > 4\sigma(F)$ and $R1=0.1047$ and $wR2=0.2144$ and $GOF = 1.047$ for

all 13556 unique, non-zero reflections and 484 variables. The maximum Δ/σ in the final cycle of least squares was 0.000 and the two most prominent peaks in the final difference Fourier were +0.40 and -0.33 e/Å³. The twinning parameter refined to a value of 0.5079(16).

Table S7. lists cell information, data collection parameters, and refinement data. **Tables S8.** and **S9.** list bond distances and bond angles. **Fig. S4.** is an ORTEP representation of the molecule with 50% probability thermal ellipsoids displayed.

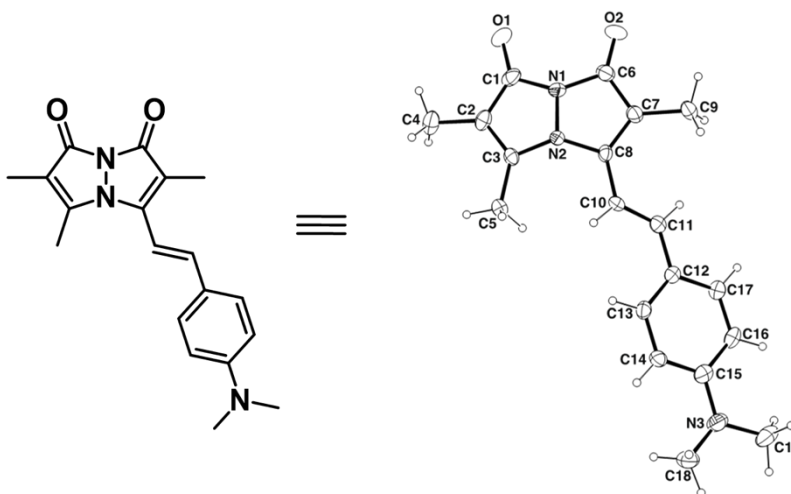


Fig. S4. X-ray diffraction data and ORTEP drawing of **5k** with 50% thermal ellipsoids.

Table S7. Summary of Structure Determination of Compound **5c**

Empirical formula	C ₂₀ H ₂₅ N ₃ O ₃
Formula weight	355.43
Diffractometer	Rigaku XtaLAB Synergy-S (Dectris Pilatus3 R 200K)
Temperature/K	100
Crystal system	monoclinic
Space group	P2 ₁ /c
a	7.0514(6)Å
b	17.1123(10)Å
c	30.720(2)Å
β	91.352(8)°
Volume	3705.8(5)Å ³
Z	8
d _{calc}	1.274 g/cm ³
μ	0.087 mm ⁻¹

F(000)	1520.0
Crystal size, mm	0.26 × 0.19 × 0.04
2θ range for data collection	4.636 - 52.95°
Index ranges	-8 ≤ h ≤ 8, -21 ≤ k ≤ 21, -37 ≤ l ≤ 38
Reflections collected	49137
Independent reflections	13556[R(int) = 0.081]
Data/restraints/parameters	13556/0/484
Goodness-of-fit on F ²	1.047
Final R indexes [$I \geq 2\sigma(I)$]	R ₁ = 0.0719, wR ₂ = 0.1949
Final R indexes [all data]	R ₁ = 0.1047, wR ₂ = 0.2144
Largest diff. peak/hole	0.40/-0.33 eÅ ⁻³

Table S8. Bond Distances in Compound **5k**, Å

O1-C1	1.235(4)	O2-C6	1.219(4)	N1-N2	1.369(4)
N1-C1	1.409(4)	N1-C6	1.421(4)	N2-C3	1.392(4)
N2-C8	1.394(4)	N3-C15	1.373(4)	N3-C18	1.438(5)
N3-C19	1.455(5)	C1-C2	1.430(5)	C2-C3	1.357(4)
C2-C4	1.510(5)	C3-C5	1.477(5)	C6-C7	1.437(5)
C7-C8	1.364(5)	C7-C9	1.508(4)	C8-C10	1.445(4)
C10-C11	1.339(4)	C11-C12	1.453(4)	C12-C13	1.391(5)
C12-C17	1.401(4)	C13-C14	1.378(5)	C14-C15	1.398(5)
C15-C16	1.414(5)	C16-C17	1.380(5)	O1'-C1'	1.215(4)
O2'-C6'	1.225(4)	N1'-N2'	1.370(4)	N1'-C1'	1.404(4)
N1'-C6'	1.401(4)	N2'-C3'	1.385(4)	N2'-C8'	1.378(4)
N3'-C15'	1.362(5)	N3'-C18'	1.445(5)	N3'-C19'	1.459(4)
C1'-C2'	1.459(5)	C2'-C3'	1.348(4)	C2'-C4'	1.490(5)
C3'-C5'	1.482(4)	C6'-C7'	1.445(5)	C7'-C8'	1.373(5)
C7'-C9'	1.490(5)	C8'-C10'	1.444(5)	C10'-C11'	1.347(4)
C11'-C12'	1.452(5)	C12'-C13'	1.398(5)	C12'-C17'	1.403(4)
C13'-C14'	1.367(5)	C14'-C15'	1.422(4)	C15'-C16'	1.409(5)
C16'-C17'	1.369(5)	O3-C20	1.404(5)	O3'-C20'	1.372(5)

Table S9. Bond Angles in Compound **5k**, °

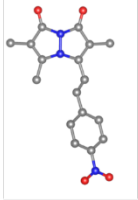
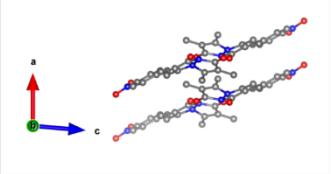
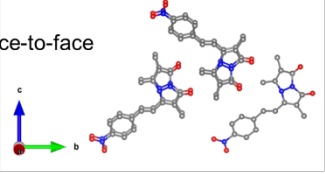
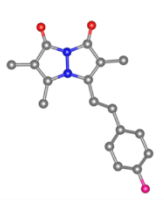
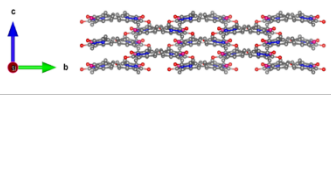
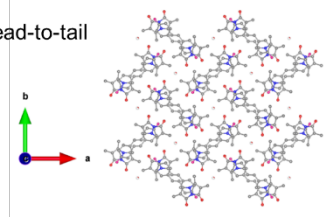
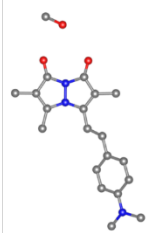
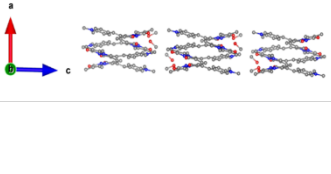
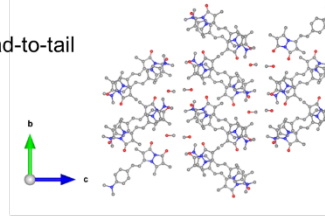
N2-N1-C1	109.1(3)	N2-N1-C6	109.6(2)	C1-N1-C6	139.1(3)
N1-N2-C3	108.6(2)	N1-N2-C8	108.4(3)	C3-N2-C8	140.0(3)
C15-N3-C18	120.4(3)	C15-N3-C19	120.1(3)	C18-N3-C19	117.6(3)
O1-C1-N1	122.9(3)	O1-C1-C2	132.3(3)	N1-C1-C2	104.8(3)
C1-C2-C4	123.6(3)	C3-C2-C1	109.4(3)	C3-C2-C4	127.0(3)
N2-C3-C5	121.6(3)	C2-C3-N2	108.0(3)	C2-C3-C5	130.4(3)
O2-C6-N1	123.6(3)	O2-C6-C7	132.1(3)	N1-C6-C7	104.3(3)
C6-C7-C9	122.0(3)	C8-C7-C6	109.3(3)	C8-C7-C9	128.5(3)
N2-C8-C10	120.6(3)	C7-C8-N2	108.3(3)	C7-C8-C10	131.0(3)
C11-C10-C8	122.6(3)	C10-C11-C12	126.5(3)	C13-C12-C11	123.7(3)
C13-C12-C17	116.6(3)	C17-C12-C11	119.7(3)	C14-C13-C12	122.5(3)
C13-C14-C15	121.0(3)	N3-C15-C14	121.0(3)	N3-C15-C16	121.9(3)
C14-C15-C16	117.1(3)	C17-C16-C15	121.0(3)	C16-C17-C12	121.9(3)
N2'-N1'-C1'	109.9(3)	N2'-N1'-C6'	109.7(2)	C6'-N1'-C1'	139.8(3)
N1'-N2'-C3'	108.5(2)	N1'-N2'-C8'	109.1(3)	C8'-N2'-C3'	141.9(3)
C15'-N3'-C18'	120.9(3)	C15'-N3'-C19'	121.4(3)	C18'-N3'-C19'	117.6(3)
O1'-C1'-N1'	124.5(3)	O1'-C1'-C2'	131.7(3)	N1'-C1'-C2'	103.7(3)
C1'-C2'-C4'	122.7(3)	C3'-C2'-C1'	109.1(3)	C3'-C2'-C4'	128.1(3)
N2'-C3'-C5'	122.2(3)	C2'-C3'-N2'	108.7(3)	C2'-C3'-C5'	129.1(3)
O2'-C6'-N1'	124.2(3)	O2'-C6'-C7'	131.5(3)	N1'-C6'-C7'	104.2(3)
C6'-C7'-C9'	121.2(3)	C8'-C7'-C6'	109.1(3)	C8'-C7'-C9'	129.1(3)
N2'-C8'-C10'	120.6(3)	C7'-C8'-N2'	107.8(3)	C7'-C8'-C10'	131.6(3)
C11'-C10'-C8'	124.1(3)	C10'-C11'-C12'	126.1(3)	C13'-C12'-C11'	123.4(3)
C13'-C12'-C17'	116.7(3)	C17'-C12'-C11'	119.9(3)	C14'-C13'-C12'	122.0(3)
C13'-C14'-C15'	121.3(3)	N3'-C15'-C14'	120.7(3)	N3'-C15'-C16'	122.7(3)
C16'-C15'-C14'	116.5(3)	C17'-C16'-C15'	121.1(3)	C16'-C17'-C12'	122.3(3)

This report has been created with Olex2 [6], compiled on 2021.08.20 svn.r13c46975 for OlexSys.

Table S10. Comparison of selected bond lengths and bond angles of **5a**, **5c**, and **5k**.

probe	bond length (Å)		bond angles °	packing
	C1-O1	N2-N1	φ (C1-N2-C6)	
5a	1.216(2)	1.400(2)	128.21(15)	face-to-face
5c	1.221(3)	1.375(3)	140.38(18)	head-to-tail
5k	1.235(4)	1.369(4)	139.1(3)	head-to-tail

Table S11. Crystal structures of probes **5a**, **5c**, and **5k** showing their asymmetric units and representative sections of their crystal lattices (ORTEP-style with 50% thermal ellipsoids).

Probe	Asymmetric unit ^a	Side view	Top view
5a			
5c			
5k ^b			

^aProbes **5a**, **5c**, and **5k** exhibit several molecules per asymmetric unit, only one of which shown here. ^bProbe **5k** includes interstitial methanol molecules. Atoms are colored as follows: C, gray; N, blue; O, red; F, pink. Hydrogen atoms have been omitted for clarity.

General Photophysical Characterization Methods

Absorbance measurements. Key precursor **3** and bimeane derivatives **5a-5k** were dissolved in DMSO to make 10 mM starting stock solutions. Samples were individually diluted to the final concentration of 25 μM (500 μL) using 50:50 acetonitrile in phosphate buffered saline (ACN/PBS). The absorbance spectrum of each derivative (150 μL) was measured on a Thermo Scientific Genesys 150 UV-Vis spectrometer, using 50:50 ACN/PBS as a blank.

Fluorescence measurements. 10 mM stock solutions of **3** and **5a-5k** in DMSO were individually diluted to the final concentration of 25 μM (500 μL) using 50:50 ACN/PBS. The fluorescence spectrum of each derivative (150 μL) was measured on a Photon Technology International (PTI) QuantaMaster™ 40 fluorescence spectrometer by excitation at the maximum absorption wavelength for each compound.

Molar absorptivity determination. 10 mM stock solutions of **3** and **5a-5k** in DMSO were individually diluted to the final concentration of 25 μM (500 μL) using 50:50 ACN/PBS. The absorbance spectrum of each derivative (150 μL) was measured on a Thermo Scientific Genesys 150 UV-Vis spectrometer, using 50:50 ACN/PBS as a blank. Then, the molar absorptivity of each derivative was calculated by using the Beer–Lambert law for solutions, $A = \epsilon lc$, where A = absorbance at maximum wavelength, l = optical path length in cm, c = concentration of the solution (25 μM), ϵ = molar absorptivity.

Solvatochromic measurements. 10 mM stock solution of **3**, **5b**, **5d**, **5j**, and **5k** in DMSO were individually diluted into six different organic solvents (toluene, dichloromethane, ACN, dimethyl formamide, dimethyl sulfoxide, and ethanol) to the final concentration of 25 μM (1000 μL). The fluorescence spectrum of each derivative (150 μL) was measured on a PTI QuantaMaster™ 40 fluorescence spectrometer by excitation at the maximum absorption wavelength for each compound. The remaining 850 μL solution was used to obtain fluorescence images under a handheld 365 nm UV lamp.

pH measurements. 10 mM stock solutions of **5h** and **5j** in DMSO were individually diluted into ACN/PBS buffer (50:50 v/v) having different pH ranging from pH 2 – 11 with 25 μ M (500 μ L) of final concentration. For pH screening of **5h** and **5j**, PBS buffer solutions were prepared, then adjusted the pH 2, 4, and 7 by adding 6 M hydrochloric acid, pH 9 and 11 by adding 5 M sodium hydroxide. Then, we have recorded the absorption and fluorescence spectra by using Thermo Scientific Genesys 150 UV-Vis spectrometer, followed by PTI QuantaMaster™ 40 fluorescence spectrometer by excitation with maximum absorption wavelength.

Viscosity measurements. As a representative example, we have measured the viscosity of **5k** (25 μ M, 10 mM stock in DMSO) in glycerol/ethylene glycol (G/EG) mixtures, varying the glycerol percentage 0-90%. Then, the emission spectra were recorded using a PTI QuantaMaster™ 40 fluorescence spectrometer by excitation with 385 nm wavelength.

Photophysical Properties of **3** and **5a-5k** in ACN

Table S12. Photophysical properties of the bimane derivatives **3** and **5a-5k** in ACN.

Entry	Substituent (Ph-R)	Absorbance $\lambda_{\text{max}}(\text{nm})^{\text{a}}$	Emission $\lambda_{\text{max}}(\text{nm})^{\text{b}}$	Molar Absorptivity $(\epsilon)(\text{M}^{-1}\text{cm}^{-1})^{\text{c}}$	Stokes shift $(\text{nm})^{\text{d}}$	Fluorescence quantum yield $(\%)^{\text{e}}$
3	–	375	432	6121	57	77.7
5a	NO ₂	332	432	37871	100	0.2
5b	CN	316	522	43238	206	1.4
5c	F	315	492, 520	28940	177	2.8
5d	H	316	492, 522	32724	176	3.1
5e	CH ₃	325	490, 520	24426	165	3.4
5f	OCH ₃	342	488, 518	34554	146	3.5
5h	OH	342	486, 518	29910	144	3.1
5i	NH(Boc)	348	490, 520	37555	142	3.4
5j	NH ₂	378	540	32091	162	1.5
5k	NMe ₂	402	568	24742	166	7.5

^aMaximum absorption wavelength, ^bMaximum emission wavelength, ^cMolar absorption coefficients at maximum absorption wavelength, ^dDifference between maximum absorption wavelength and maximum emission wavelength, ^eFluorescence quantum yield (error limit within ± 5). Final probe concentration is 25 μM in ACN.

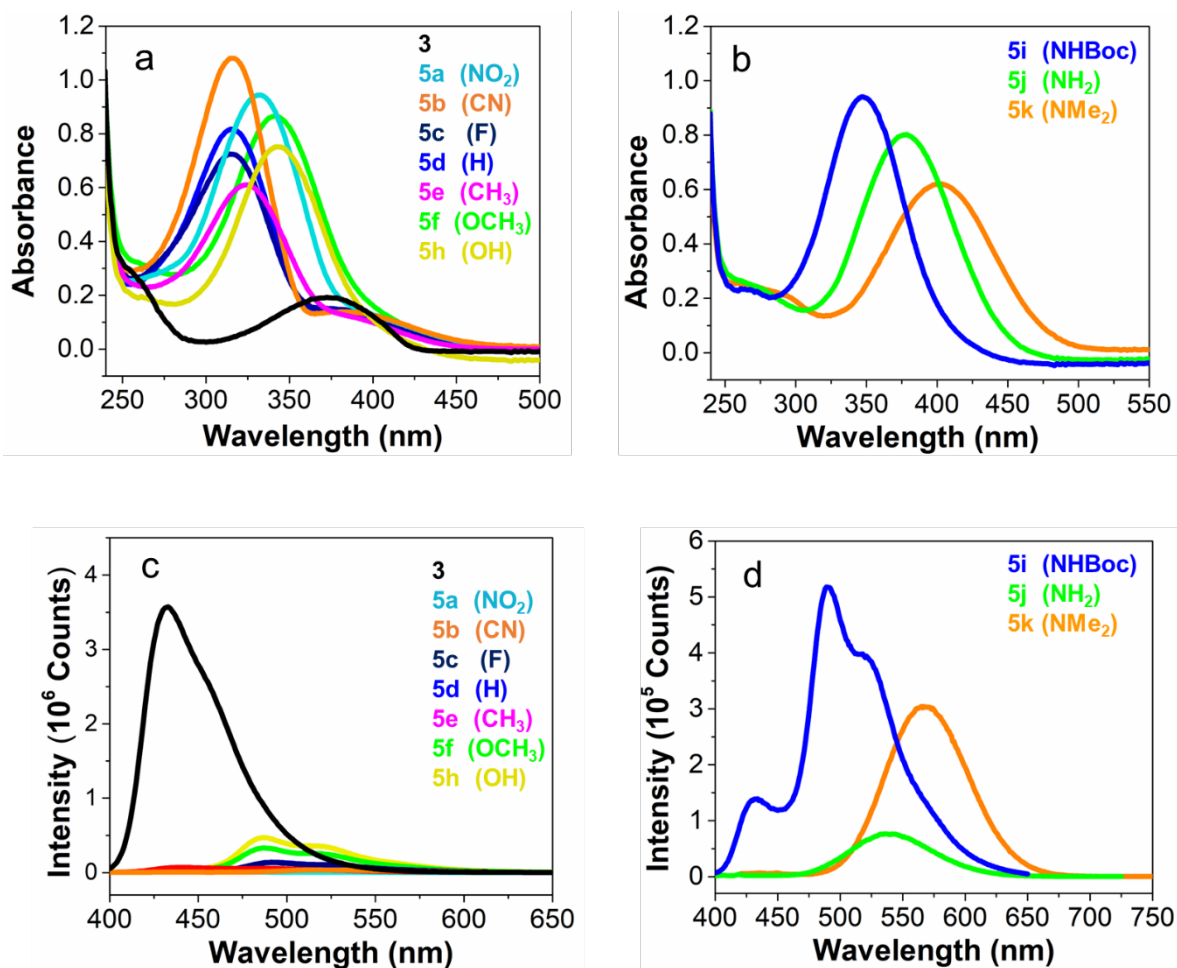


Fig. S5. Photophysical properties of **3** and **5a-5k** in ACN solvent. (a) Absorption spectra of **3** and **5a-5f** and **5h** (b) Absorption spectra of **5i-5k**, (c) Fluorescence spectra of **3** and **5a-5f** and **5h**, and (d) Fluorescence spectra of **5i-5k**. Final probe concentration is 25 μ M. Fluorescence spectra were measured at their maximum absorption wavelength.

Solvatochromism of **3**, **5b**, **5d** and **5j**

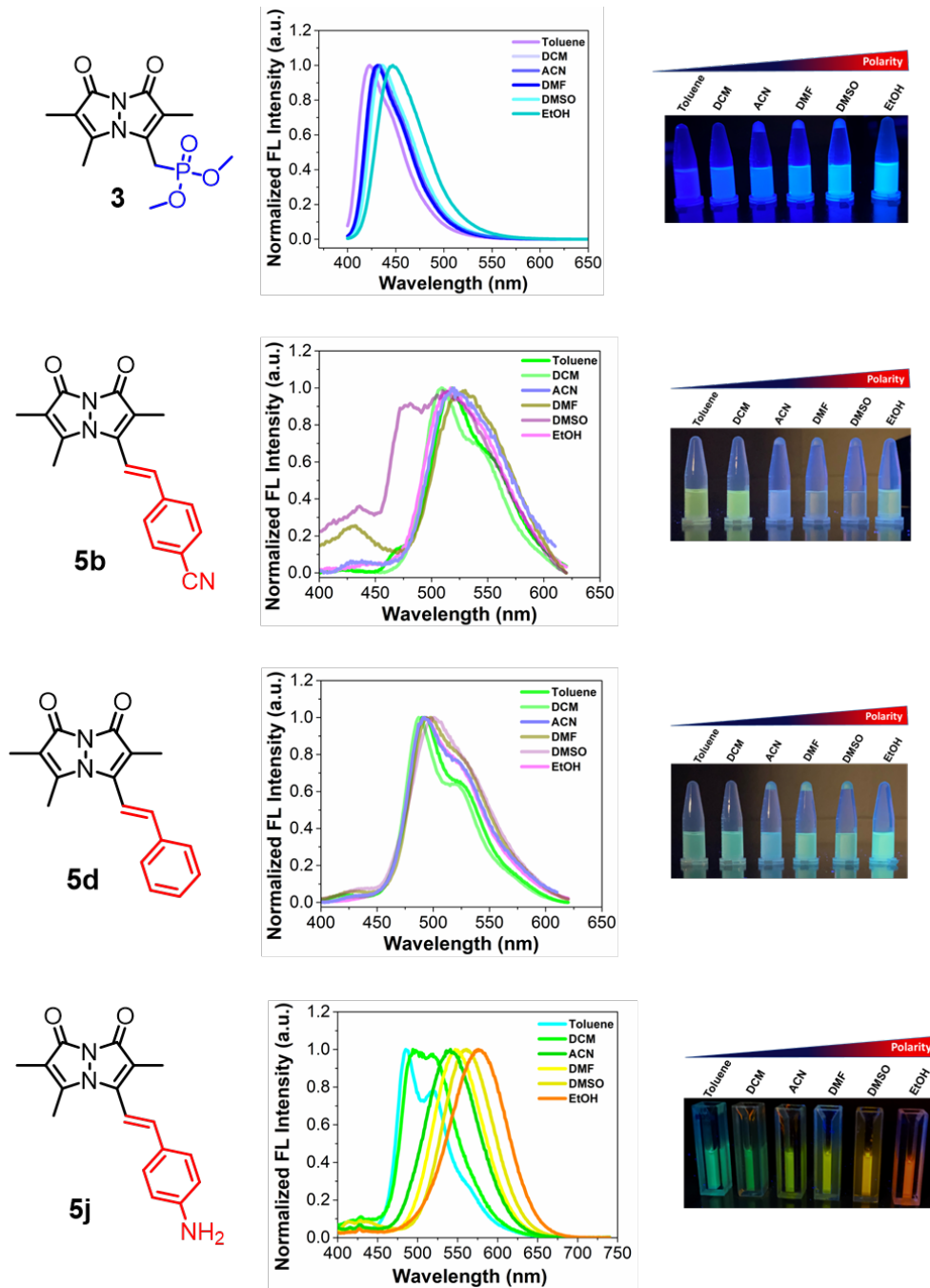


Fig. S6. Solvatochromism of **3**, **5b**, **5d** and **5j**. Left: Normalized fluorescence spectra in different solvents. Right: Fluorescence image taken under handheld UV lamp at 365 nm. Probe concentration 25 μM and excitation wavelength is 384 nm for **3**, 320 nm for **5b** and **5d**, and 418 nm for **5j**.

Fluorescent Quantum Yield Measurements of **3** and **5a-5k**

Fluorescent quantum yield (QY) measurements. For each QY measurement, the incident excitation light spectrum was collected with 1 mL of solvent. After measuring the incident light intensity, dye (**3** and **5a-5k**) was added to the solvent from a concentrated stock solution to a final concentration of 500 μM and the new spectrum (fluorescence intensity and new incident light intensity) was collected. Using the JASCO Quantum Yield Software, the dye QY was calculated by dividing the dye fluorescence intensity by the difference in incident light intensity in the presence and absence of dye. The minimum excitation wavelength for a full excitation incident spectrum using this setup is 360 nm. QY values are reported in Table S1 and in main text Table 2.

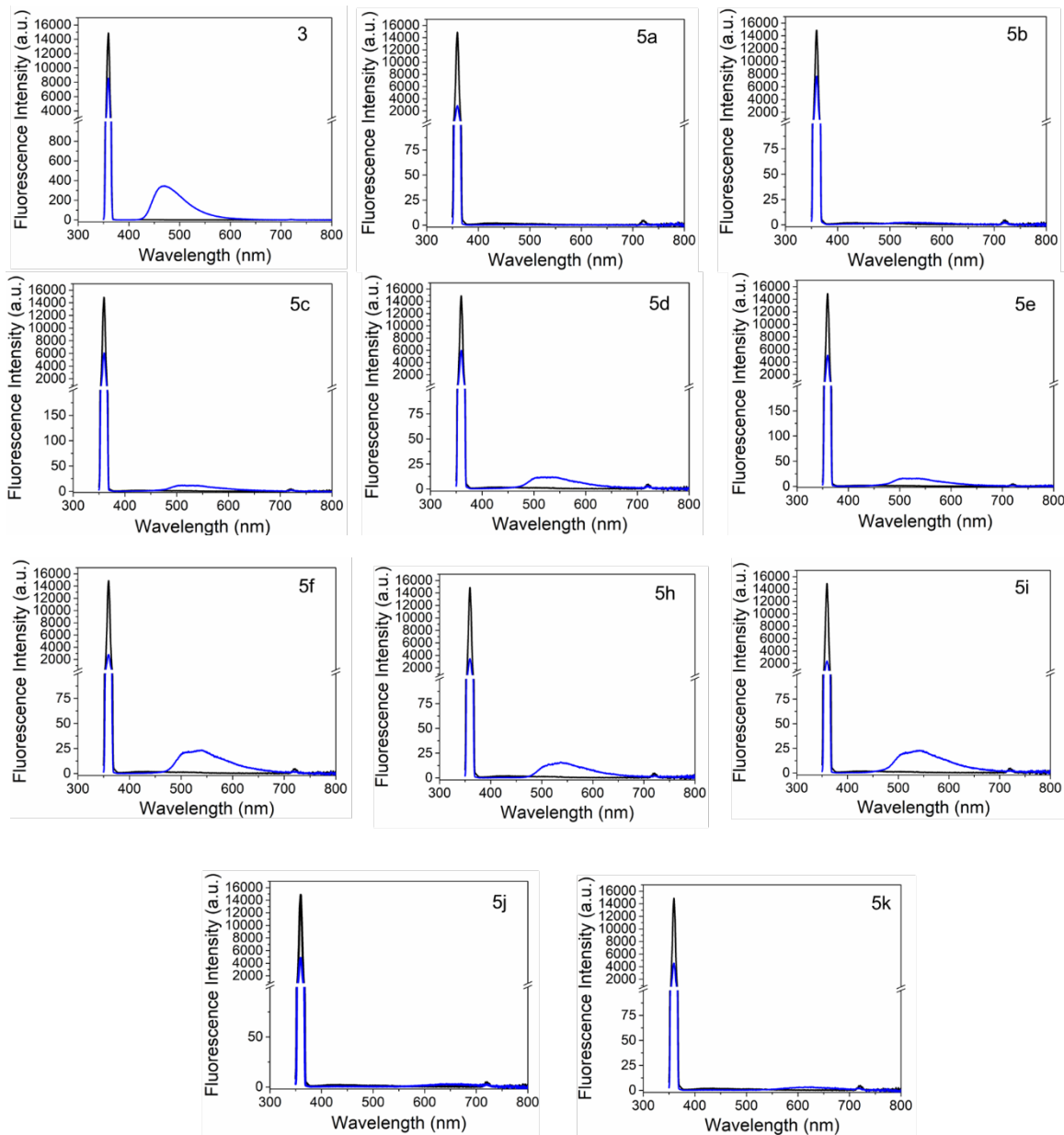


Fig. S7. Representative QY acquisitions of **3** and **5a-f**, **5h-k** in ACN/PBS buffer (50:50). All had consistent excitation (360 nm) and spectral collection (350–800 nm) parameters. Final concentration of the probe is 500 μ M. Black line indicates incident light and blue line indicates sample spectrum.

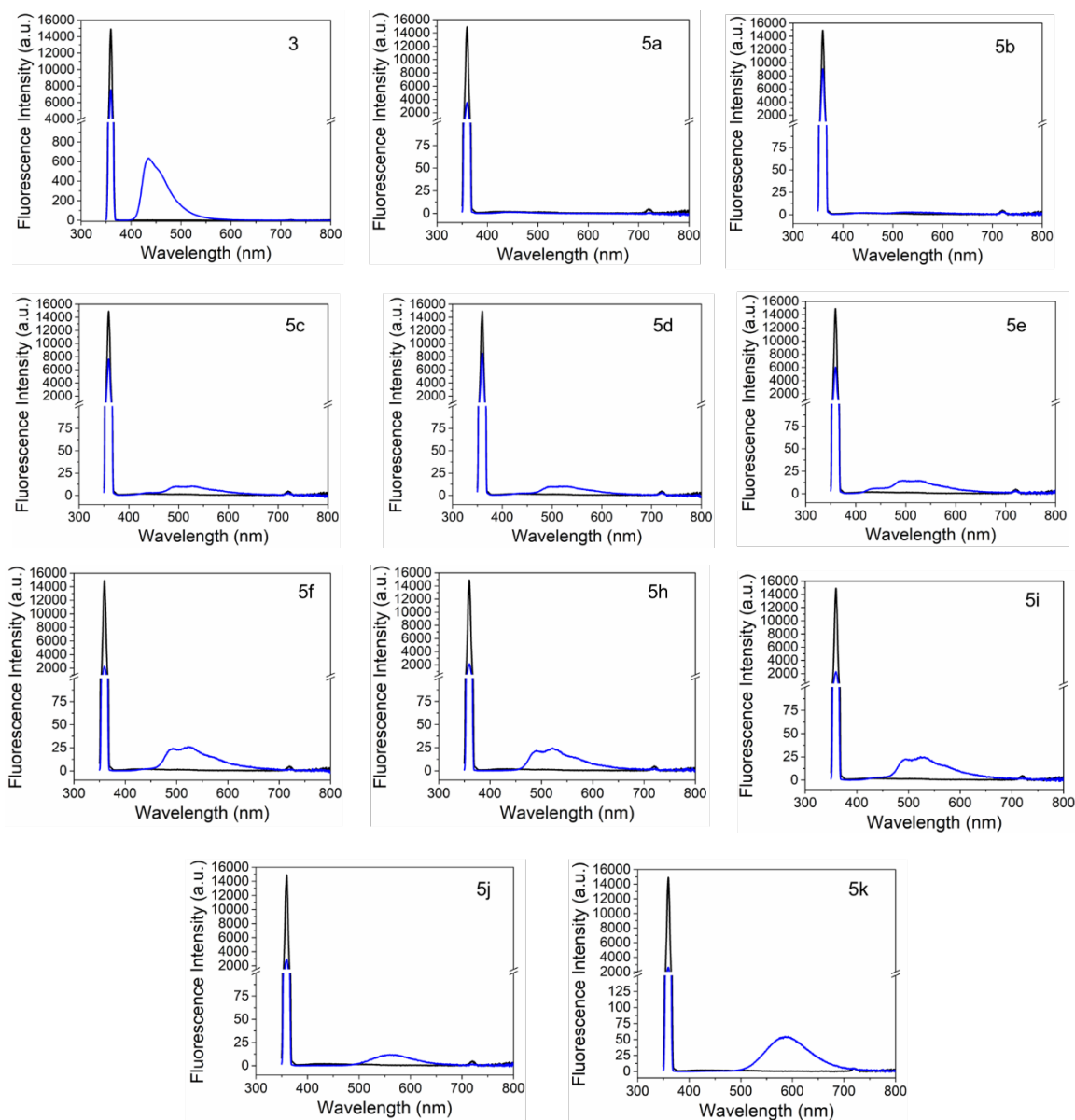


Fig. S8. Representative QY acquisitions of **3** and **5a-f**, **5h-k** in ACN solvent. All had consistent excitation (360 nm, slit width 10 nm) and spectral collection (350-800 nm) parameters. Final concentration of the probe is 500 μ M. Black line indicates incident light and blue line indicates sample spectrum.

Effect of pH on 5h and 5j

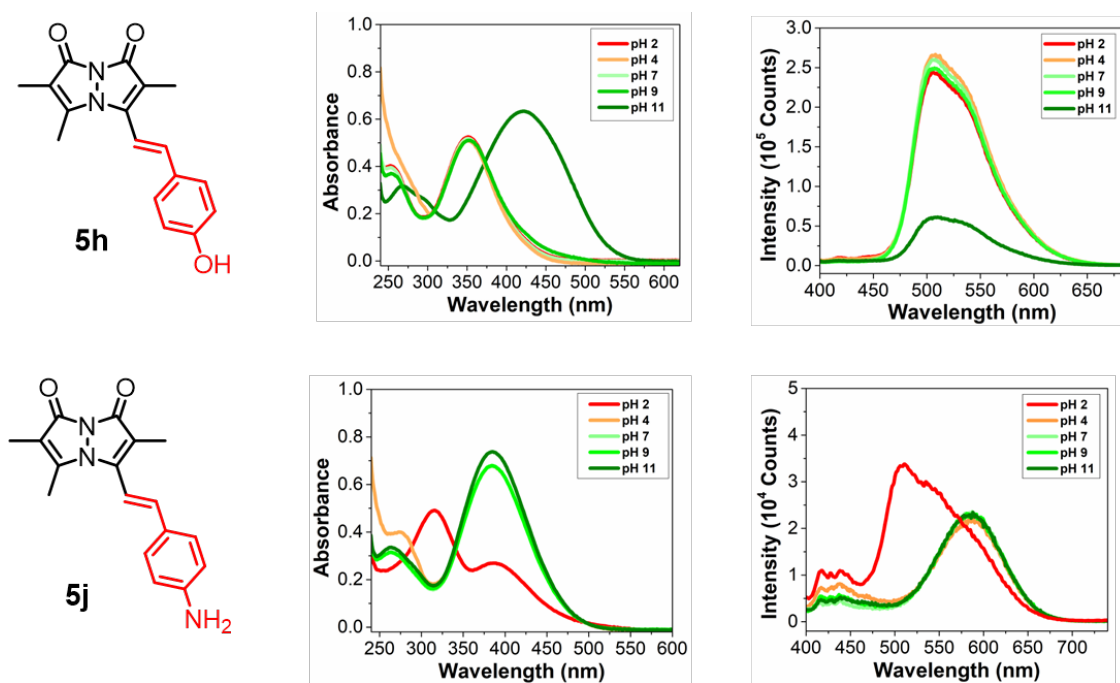


Fig. S9. Effect of pH on absorption and emission of **5h** and **5j**. Final concentration of the probe is 25 μ M. For pH screening of **5h** and **5j**, PBS buffer solutions were prepared, then adjusted the pH 2, 4, and 7 by adding 6 M hydrochloric acid, pH 9 and 11 by adding 5 M sodium hydroxide. Emission spectra were measured by the excitation wavelength 354 nm for **5h** and 385 nm for **5j**.

Fluorescence Lifetime Measurements of **3** and **5c-5f**

Fluorescence lifetime measurements. Time correlated single photon counting (TCSPC) measurements of fluorescence lifetime decays for 100 μM solutions of dyes (**3** and **5c-f**) in ACN/PBS buffer (50:50 v/v) were collected with the PTI Quantamaster TM 40 using a pulsed LED with a maximum emission at 340 nm. Fluorescence emission was collected at the indicated wavelength for each dye with 20 nm slit widths. The instrument response function (IRF) was collected under identical conditions. Data analysis was performed with FluoFit software (PicoQuant GmbH; Berlin, Germany) using an exponential decay model. Lifetime values are reported in Table S13 and in main text Table 2.

Table S13. Fluorescence lifetime measurements of **3** and selected probes **5c-f** in ACN/PBS buffer (50:50 v/v) and fit χ^2 values.^a

Probe	Ar-R	Lifetime (ns)	χ^2
3	-	2.32 ± 0.01	1.099
5c	F	1.07 ± 0.003	1.017
5d	H	1.02 ± 0.004	0.942
5e	CH ₃	1.28 ± 0.004	1.089
5f	OCH ₃	1.31 ± 0.004	0.932

^aTCSPC data were collected at 540 nm emission for **5c-f** and 464 nm emission for **3**. Excitation wavelength 340 nm.

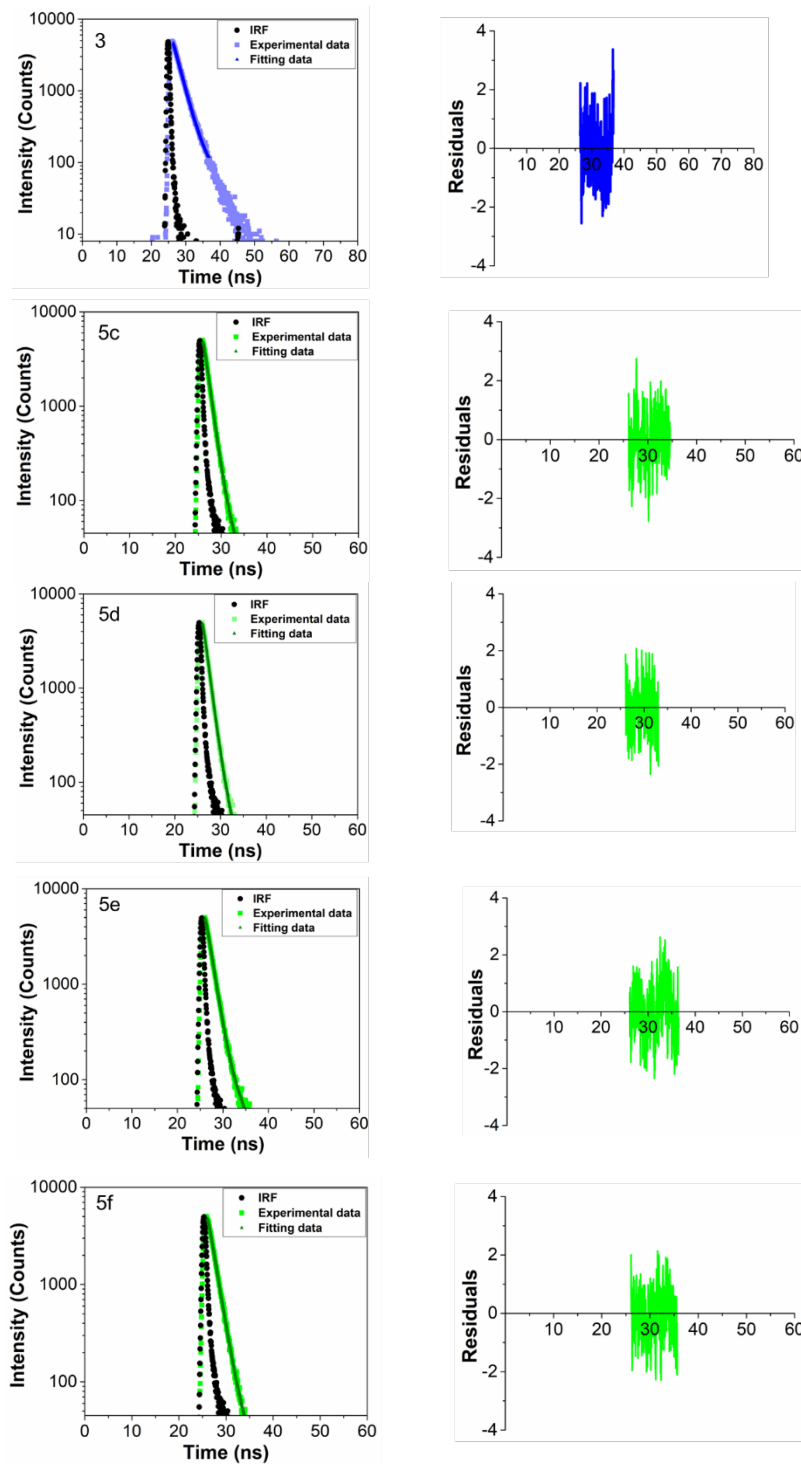


Fig. S10. Fluorescence lifetime measurements in ACN/PBS buffer (50:50 v/v). Lifetime measurements with exponential fits shown at left and residuals after fitting shown at right. TCSPC data were collected at 540 nm emission for **5c-5f** and 464 nm emission for **3**. Excitation wavelength 340 nm.

Computational Studies

Methods. All calculations were performed employing the APF-D density functional as implemented in the Gaussian16TM suite of programs with the 6-311+G (2d,p) basis set.³ Geometry optimizations and energies were calculated for selected bimane derivatives **5a-f**, **5h**, **5j**, and **5k** compounds. The HOMO-LUMO energy gaps between the ground state (S_0) and the first excited state (S_1) of the bimane derivatives were calculated and are shown below. All structures are ground-state minima according to the analysis of their vibrational frequencies, which showed no negative value.

Table S14. Calculation of the Energy Gaps of Bimane Derivatives in Water (H_2O).

Compound	Hammett Constant (σ_p)	Absorbance Wavelength (nm) ^a	HOMO (eV)	LUMO (eV)	#LUMO-#HOMO Transition	LUMO-HOMO Δ (eV)
5a (NO_2)	0.778	335	-6.547	-3.232	86-85	3.315
5b (CN)	0.66	320	-6.523	-2.827	81-80	3.696
5c (F)	0.062	321	-6.419	-2.506	79-78	3.912
5d (H)	0	321	-6.430	-2.514	75-74	3.915
5e (CH_3)	-0.17	332	-6.351	-2.470	79-78	3.881
5f (OCH_3)	-0.268	348	-6.146	-2.420	83-82	3.726
5h (OH)	-0.37	354	-6.192	-2.420	79-78	3.772
5j (NH_2)	-0.66	385	-5.812	-2.383	79-78	3.429
5k (NMe_2)	-0.83	418	-5.528	-2.356	87-86	3.172

^aAbsorbance spectra recorded in ACN:PBS buffer (50:50 v/v).

HOMO-LUMO gap calculations. We have analyzed the correlation between the photophysical properties of bimane derivatives and the electronic properties of the substituents to understand the mechanism of fluorescence tuning of the bimane scaffold. It is generally accepted that the absorption wavelength (λ_{abs}) and emission wavelength (λ_{em}) correlate well with the energy gap between HOMO and LUMO as determined by simple electronic structure calculations. Relative energy levels of HOMO and LUMO were calculated using APF-D/6-311+G (2d,p) density functional theory (DFT) calculations. Representative compounds **5e** (CH_3), **5f** (OCH_3), **5h** (OH), **5j** (NH_2), and **5k** (NMe_2), with electron donating groups at the *para*-position, showed a decrease

in HOMO-LUMO gap with more electron donating substituents that matched well with red-shifts of the UV-Vis absorbance (Table S3 and Fig. S10). Interestingly, compounds with electron withdrawing substituents, **5a** (NO₂), **5b** (CN), and **5c** (F) showed a shallower correlation of UV-Vis absorbance with HOMO-LUMO gap, indicative of a change in excitation mechanism (Fig. S10). The change in mechanism can be explained by examination of the HOMO and LUMO of these compounds (Fig. S11). For compounds with electron-withdrawing substituents such as **5a**, the electrons move from a HOMO centered on the bimane group to a LUMO centered on the styryl group. In contrast, for compounds with electron-donating substituents such as **5k**, the electrons move from a HOMO centered on the styryl group to a LUMO centered on the bimane group. This is similar to our observations of the changes in λ_{abs} with the Hammett constant in **Fig. 1** in the main text.

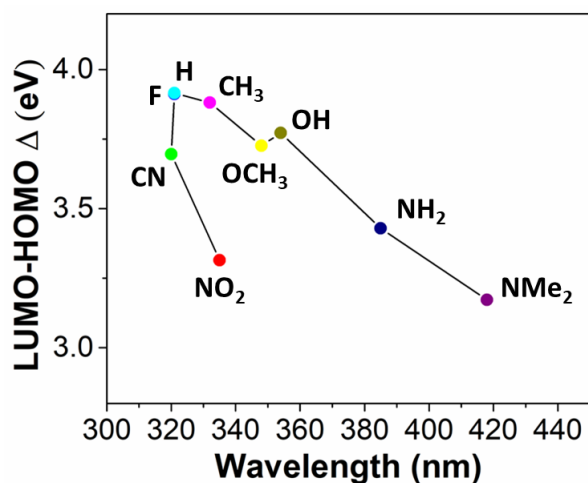


Fig. S11. Correlation between HOMO-LUMO energy gap (eV) compared to experimentally measured UV-Vis absorption maximum (nm) of **5a-5f**, **5h**, **5j**, and **5k**. Maximum UV-Vis absorption wavelengths were obtained in ACN/PBS buffer (50:50 v/v).

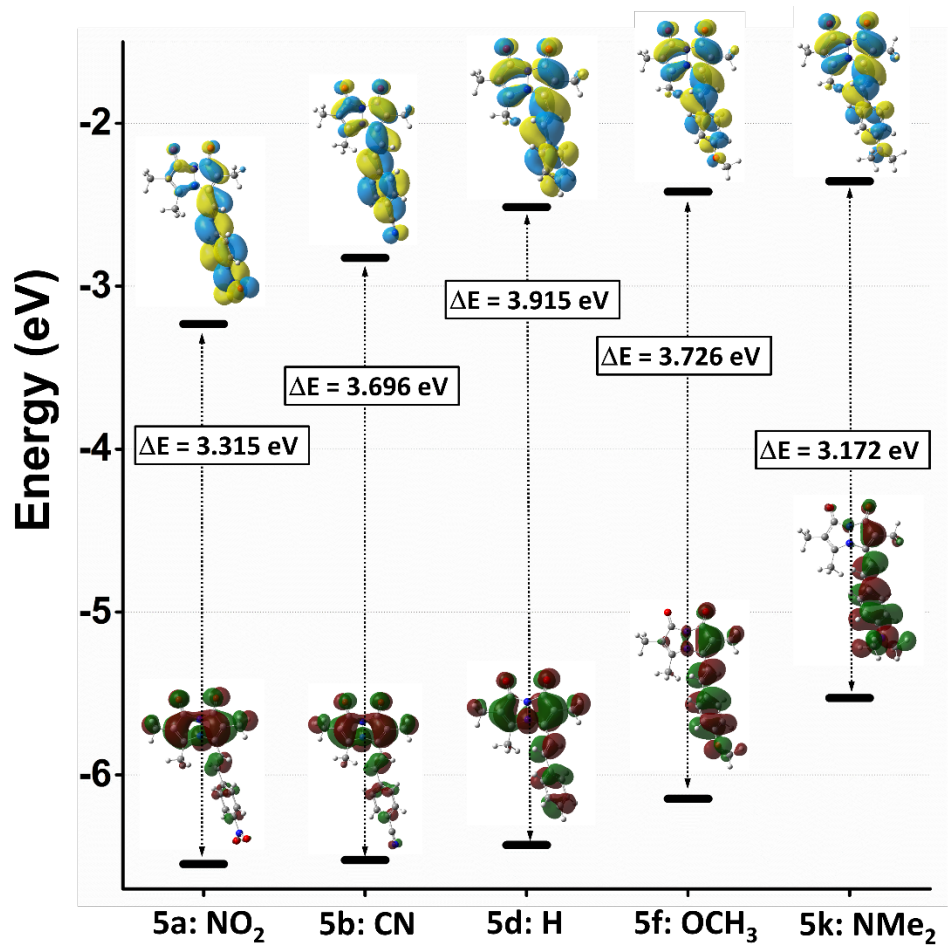


Fig. S12. Relative HOMO-LUMO energy gap (eV) of selected bimane derivatives.

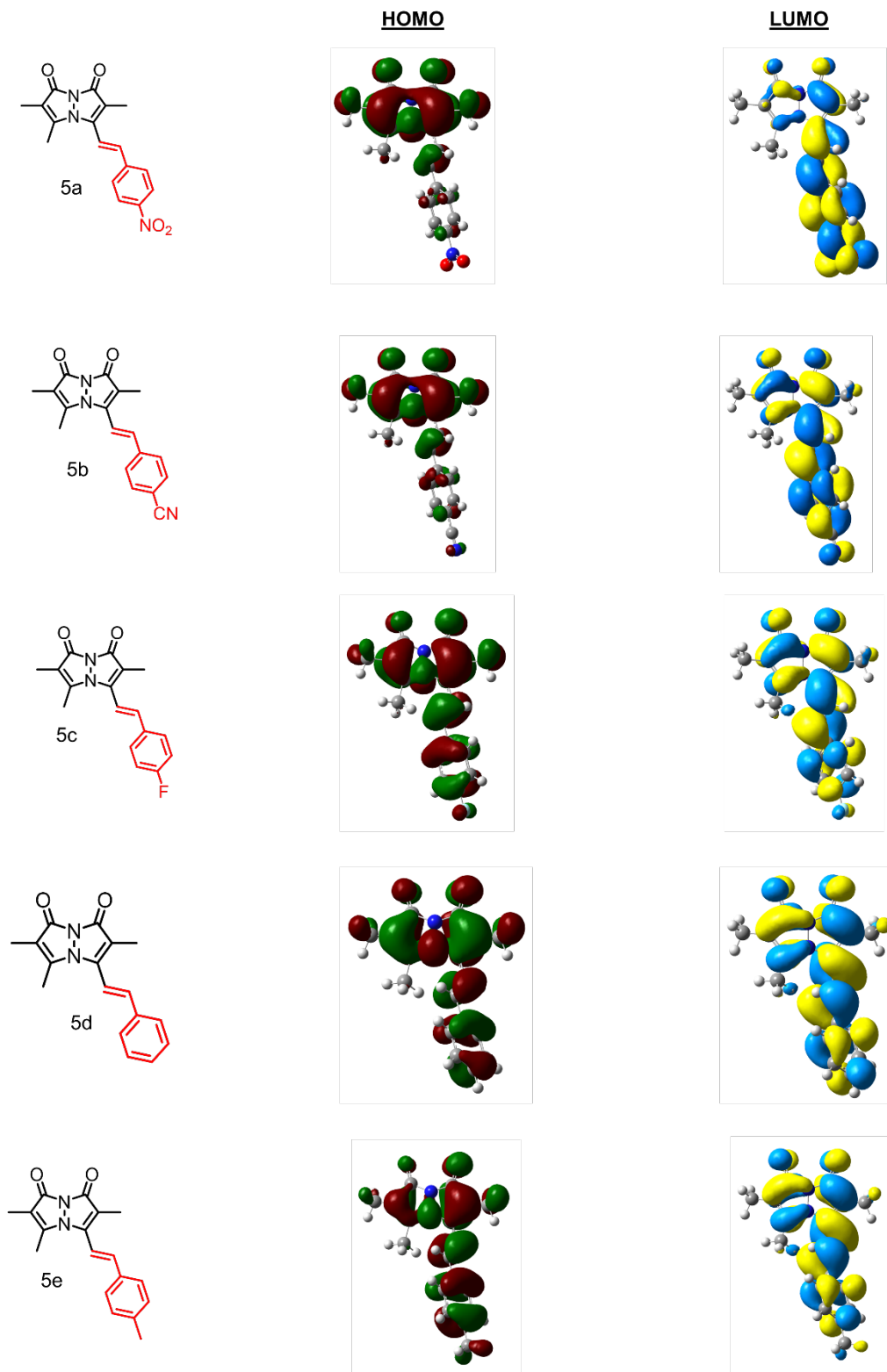


Fig. S13. HOMO and LUMO MOs of **5a-5e**.

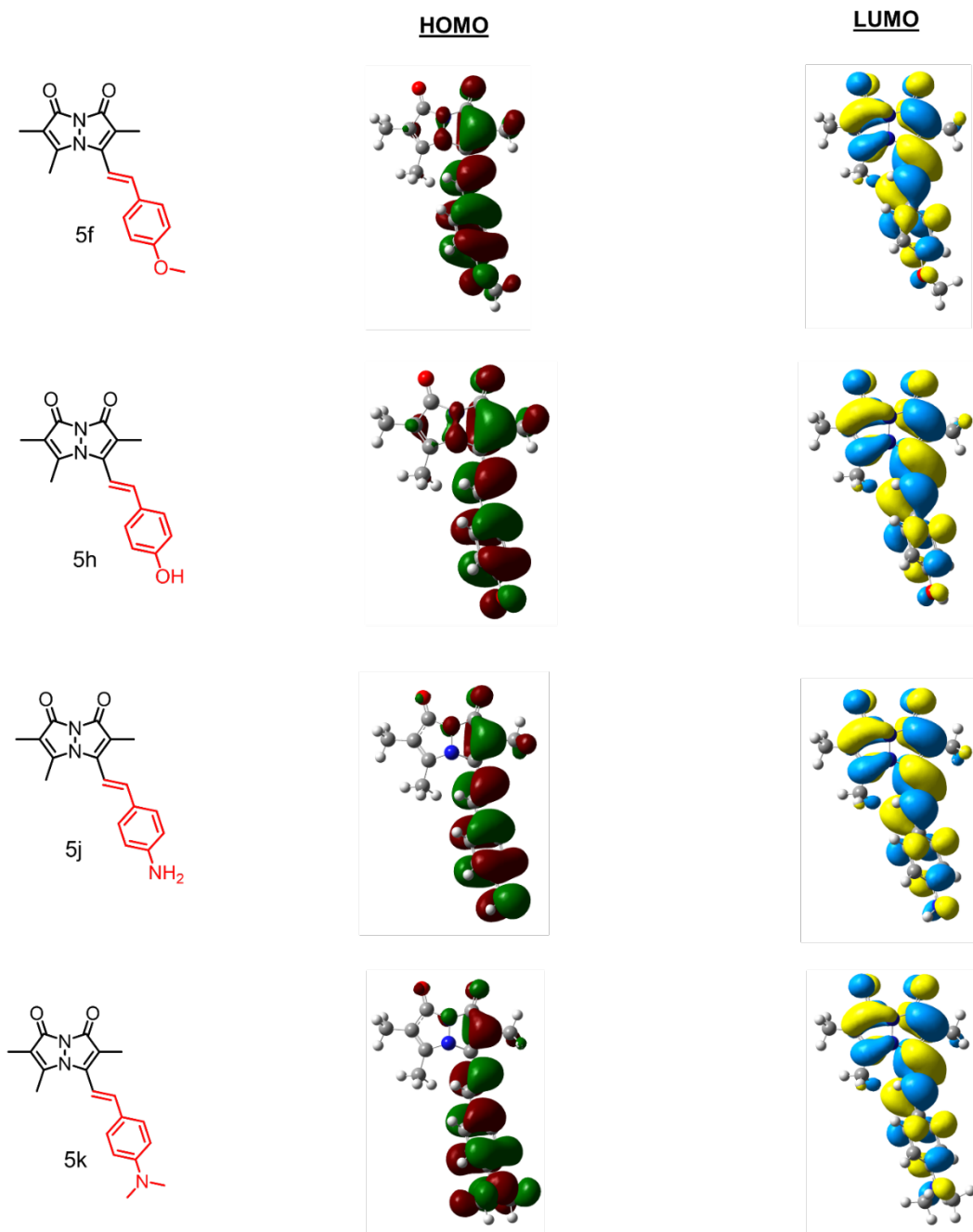


Fig. S14. HOMO and LUMO MOs of **5f**, **5h**, **5j**, and **5k**.

Production of α -Synuclein and 1N4R Tau

α -Synuclein production. α -Synuclein (α S) was expressed and purified as previously described with slight modifications.⁴ Human α S with a C-terminal intein-His₆ fusion was transformed into *Escherichia coli* (*E. coli*) BL21 cells and plated on ampicillin plates (100 μ g/mL). A single colony was then inoculated into a 5 ml primary culture containing ampicillin (100 μ g/mL) in Luria-Bertain (LB) media and grown for 5-6 h with shaking (250 rpm) at 37 °C. The primary culture was then transferred to 1 L LB containing ampicillin (100 μ g/mL) and grown as previously described until reaching an optical density (OD₆₀₀) of 0.8-1.0. At this stage, protein production was induced by the addition of isopropyl β -D-1-thiogalactopyranoside (IPTG) to 1 mM final concentration, and the culture was grown with shaking (250 rpm) overnight at 18 °C. The following day, cells were harvested by centrifugation at 4 °C for 20 min at 4000 rpm (Sorvall GS3 rotor). Pellets were then re-suspended in 20 mL/L culture of 40 mM Tris, pH 8.3 supplemented with EDTA-free protease inhibitor tablets (Pierce Biotechnology; Waltham, MA, USA) and transferred to a metal cup for sonication. Cells were lysed by sonication on ice with a Q700 probe sonicator (QSonica LLC; Newtown, CT, USA) with the following settings: Amplitude 50, Process Time 2-3 min, Pulse-ON Time 1 s, Pulse-OFF Time 1 s. Crude lysate was then transferred to 50 mL centrifugation tubes and clarified via centrifugation at 14,000 rpm for 45 min (Sorvall SS34 rotor). Following centrifugation, supernatant was removed and transferred to a 50 mL Falcon tube. Then, 5 ml of nickel agarose resin (GoldBio; St. Louis, MO, USA) was added, and the lysate-nickel mixture was incubated with nutation at 4 °C for 1 h. The lysate-nickel mixture was then poured into a 20 mL fritted column, and the flowthrough was saved. The remaining resin was then washed with ~20 mL Wash Buffer 1 (50 mM HEPES buffer, pH 7.5), ~20 mL Wash Buffer 2 (50 mM HEPES, 5 mM imidazole, pH 7.5), and eluted with 12 mL Elution Buffer (50 mM HEPES, 300mM imidazole, pH 7.5). Then 2-mercaptoethanol (Bio-Rad Laboratories; Hercules, CA, USA) was added to crude lysate (200 mM final concentration), and the mixture was allowed to incubate with nutation at room temperature overnight. The resulting cleaved protein was dialyzed against 20 mM Tris pH 8.0 for 8-10 h. The resulting dialysate was then treated with 5 mL nickel agarose resin and incubated with nutation at 4 °C for 1-2 h. The mixture was then applied to a 20 mL fritted column and flowthrough containing α S was collected in a 15 mL Falcon tube. The resulting enriched protein mixture was then dialyzed against 20 mM Tris, pH 8.0 overnight and purified via

FPLC using a 5 mL HiTrap Q-HP column (Cytiva; Marlborough, MA, USA) using the following method: Buffer A: 20 mM Tris, pH 8.0; Buffer B: 20 mM Tris, 1 M NaCl, pH 8.0; Gradient: 0% Buffer B – 5 column volumes, 0 – 10% Buffer B – 5 column volumes, 20-30% Buffer B – 20 column volumes, 30-100% Buffer B – 10 column volumes; flow rate 3 mL/min. The resulting fractions were then assessed for purity via MALDI MS, and pure fractions were combined. Protein was then concentrated, and buffer exchanged into PBS (NaCl 137 mM, KCl 2.7 mM, Na₂HPO₄ 10 mM, KH₂PO₄ 1.8 mM) to a final concentration of 100-200 μM via Amicon 3 kDa MWCO filters (Millipore Sigma; St. Louis, MO, USA). Purified protein was aliquoted into 1.5 mL tubes and stored at -80 °C until further use. MALDI MS [M+H]⁺ calcd: 14460, found: 14457.

Tau 1N4R protein production: Tau (1N4R) (Tau) was expressed and purified as previously described, with slight modifications.⁵ Using a fresh transformation of Tau 1N4R plasmid transformed into *E. coli* BL21 cells and plated on ampicillin plates (100 μg/mL), single colony was inoculated into a 5 mL primary culture containing ampicillin (100 μg/ml) in LB media and grown for 5-6 h with shaking (250 rpm) at 37 °C. The primary culture was then transferred to 1 L LB containing ampicillin (100 μg/ml) and grown until reaching an OD₆₀₀ of 0.4-0.6. At this stage, protein production was induced by the addition of IPTG to 1 mM final concentration, and the culture was grown with shaking (250 rpm) overnight at 16 °C. The following day, cells were harvested by centrifugation at 4 °C for 20 min at 4000 rpm (Sorvall GS3 rotor). Pellets were then re-suspended in 15 mL Ni-NTA Buffer A (50 mM Tris pH 8, 500 mM NaCl, and 10 mM Imidazole) with 1mg/mL (chicken egg white) lysozyme, 1 tablet of EDTA-free protease inhibitor and 1 mM PMSF. The suspension was sonicated on ice for 1 minute 40 seconds, 1 second on/2 seconds off, power set to 50 W. Cellular debris was then transferred to 50 mL centrifugation tubes and clarified via centrifugation at 20,000 x g for 30 min (Sorvall SS34 rotor). Following centrifugation, supernatant was removed and filtered with a 0.22 μm syringe filter into a 50 mL Falcon tube. Then, 5 – 7 mL of nickel agarose resin was prepared and equilibrated with ~30 mL of Ni Buffer A. Then supernatant-nickel mixture was incubated with nutation at 4 °C for 1 h. Supernatant-nickel mixture was then poured into a 20 mL fritted column, and the flowthrough was saved. The remaining resin was then washed with ~30 mL Ni-NTA Buffer A and eluted with ~15 mL Ni-NTA Buffer B (50 mM Tris pH 8, 500 mM NaCl, and 400 mM imidazole). The nickel

column was cleaned by running more Ni-NTA Buffer B through the column and then re-equilibrated with Ni-NTA Buffer A. The elution was then concentrated to ~1 mL in an Amicon concentrator (10 kDa MWCO) and the following were added 25 μ M TEV, and 1 mM DTT from fresh 1 M DTT stock. The mixture was allowed to incubate with nutation at 4 °C overnight and then the buffer was exchanged back to Ni-NTA Buffer A (2 cycles of 15 mL) using an Amicon concentrator. The resulting dialysate was then treated with 5 – 7 mL nickel agarose resin and incubated with nutation at 4 °C for 1 h. The mixture was then applied to a 20 mL fritted column and flowthrough containing 1N4R tau was collected in a 15 mL Falcon tube. The resulting enriched protein mixture was then concentrated, and buffer exchanged two times into Ni-NTA Buffer C (25 mM Tris pH 8, 100 mM NaCl, 1 mM EDTA, and 1 mM TCEP) using an Amicon concentrator and concentrated down to 1 mL before filtering the solution using a 0.22 μ m filter. Then, the protein was purified via FPLC using a size exclusion column (S200, HiLoadc16/60cSuperdex 200 pg) using the following method: isocratic elution: 100 % Ni-NTA Buffer C, – 1.2 column volumes with flowrate 0.5 mL/min. The purity of the fractions was checked by SDS-PAGE gel and the clean fractions were combined, concentrated, and the buffer exchanged into PBS to a final concentration of 100-200 μ M via Amicon 10 kDa MWCO filters and stored at -80 °C until further use. MALDI MS $[M+H]^+$ calcd: 43111, found: 43109.

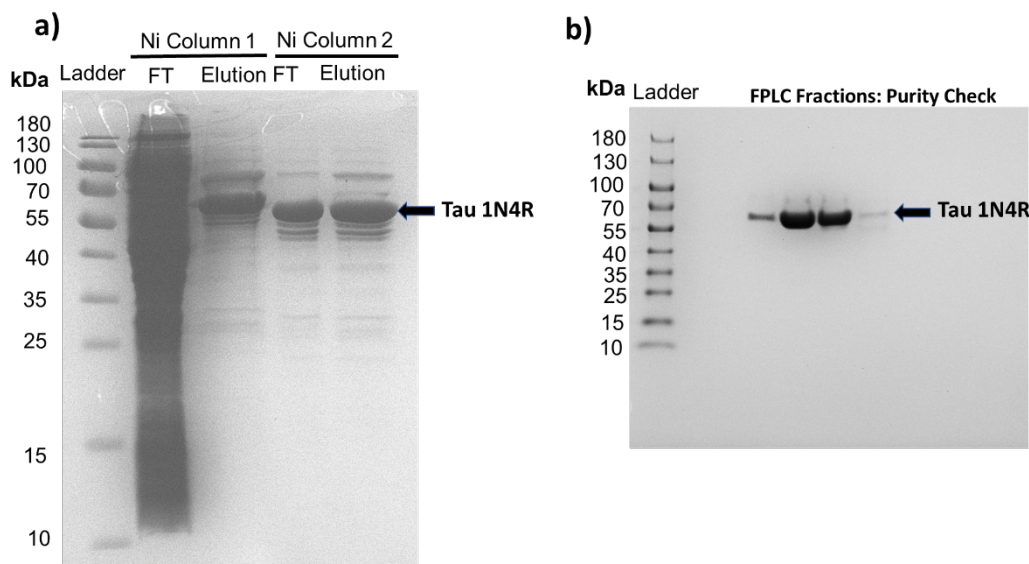


Fig. S15. Protein purification and cleavage of 1N4R tau. (a) nickel purification visualized by a Coomassie stained 10% SDS-Page gel and (b) FPLC purification fractions by SDS-PAGE gel.

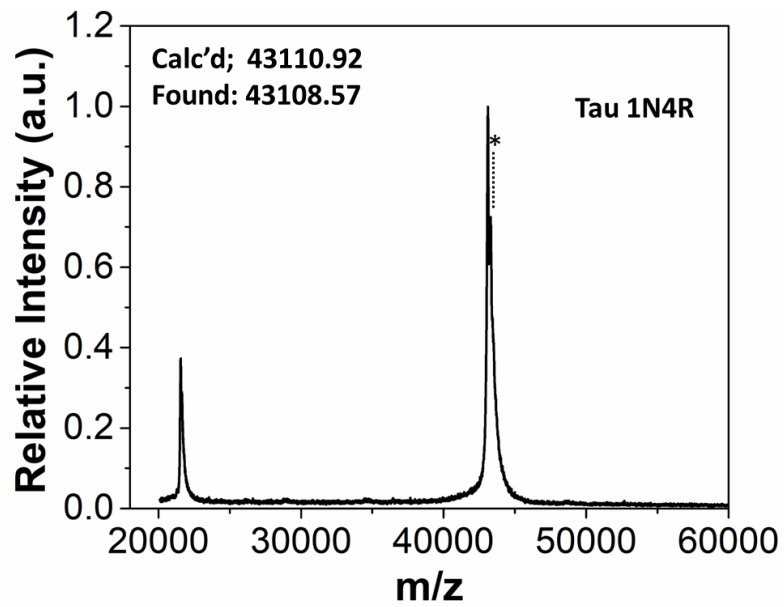
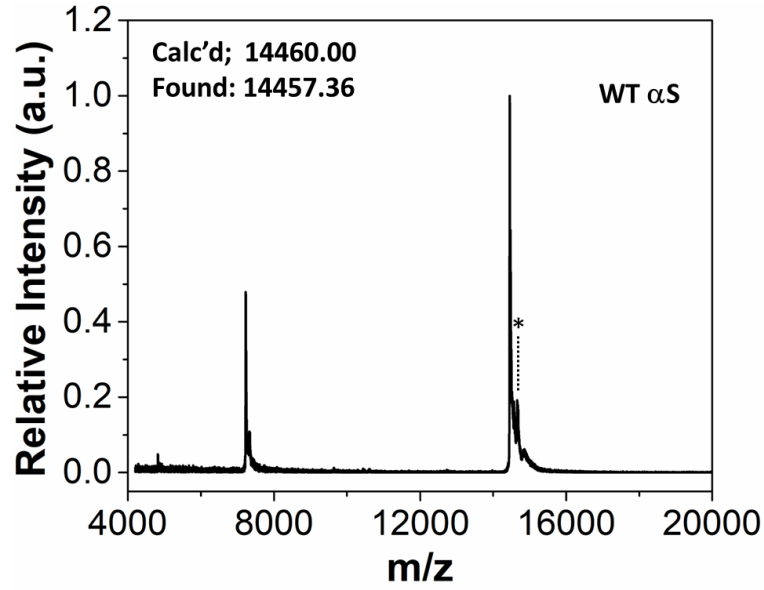


Fig. S16. MALDI MS characterization of WT α S (Top) and tau 1N4R (Bottom). On each plot matrix adduct peaks are marked with *.

Fibril Preparation

α S fibril preparation. 100 μ M final concentration of α S monomer in PBS buffer (500 μ L, 1.5 mL tube) at pH 7 was sealed with Teflon tape followed by parafilm and then incubated at 37 °C with shaking at 1300 rpm for 7 days in an IKA MS3 control orbital shaker (Wilmington, NC, USA) to get α S fibrils.⁴

1N4R Tau fibril preparation. 50 μ M final concentration of 1N4R tau monomer in PBS buffer (200 μ L) at pH 7.4 along with 100 μ M of DTT and 12.5 μ M of heparin was sealed with Teflon tape followed by parafilm incubated at 37 °C with shaking at 1300 rpm for 72 h in an IKA MS3 control orbital shaker (Wilmington, NC, USA) to get tau fibrils.⁵

A β ₁₋₄₂ fibril preparation. Using 1 mg of the commercially available A β ₁₋₄₂ (β -Amyloid (1-42), human, Genscript Cat. No. RP10017) 1 mg, a 1 mM stock solution was made by adding 222 μ L hexafluoroisopropanol (HFIP) directly to the vial containing lyophilized powder through the rubber septum. After the peptide completely dissolved, the septum was pierced with a syringe needle to release the vacuum. The A β ₁₋₄₂-HFIP solution was incubated for 30 min at room temperature. Using a positive displacement pipette, 100 μ L aliquots of the solution (0.45 mg) were transferred into Eppendorf tubes and the HFIP was allowed to evaporate in the open tubes in a fume hood. The tubes were then dried on a vacuum centrifuge for 1 h without heating to remove any remaining trace amount of HFIP. To make a 1 mM stock solution of A β ₁₋₄₂ fibrils in 10 mM Phosphate buffer at pH 7.4, 0.45 mg of A β ₁₋₄₂ was dissolved in 10 μ L DMSO with addition of 10 μ L of 10 mM of NaOH and sealed in an Eppendorf tube with Teflon tape followed by parafilm, then incubated at 37 °C with shaking at 500 rpm for 5 days in an IKA MS3 control orbital shaker (Wilmington, NC, USA).^{6,7}

Gel-based quantification of protein in fibrils. Following completion of aggregation, fibrils were pelleted by centrifugation in a bench top centrifuge at 13,200 rpm for 90 min at 4 °C. The supernatant was then carefully removed, and the fibril pellet resuspended in aggregation buffer with vortexing. Then 10 μ L from each sample was transferred into an individual 0.6 mL Eppendorf tube and 2 μ L 150 mM SDS in water was added (final concentration: 25 mM SDS). The tubes were then capped and heated to \sim 100 °C for 15-20 min. Then the tubes were placed on ice to cool for 5-10 min, and 3 μ L 4X gel loading was added and the supernatant and pellet were run on an SDS-PAGE along with a monomer standard at a known concentration. After running the gel, the bands were quantified by ImageJ software to estimate the percentage in fibrils (pellet). This was used with the initial monomer concentration in the aggregation reactions to determine the concentration of fibrils for dye binding experiments.

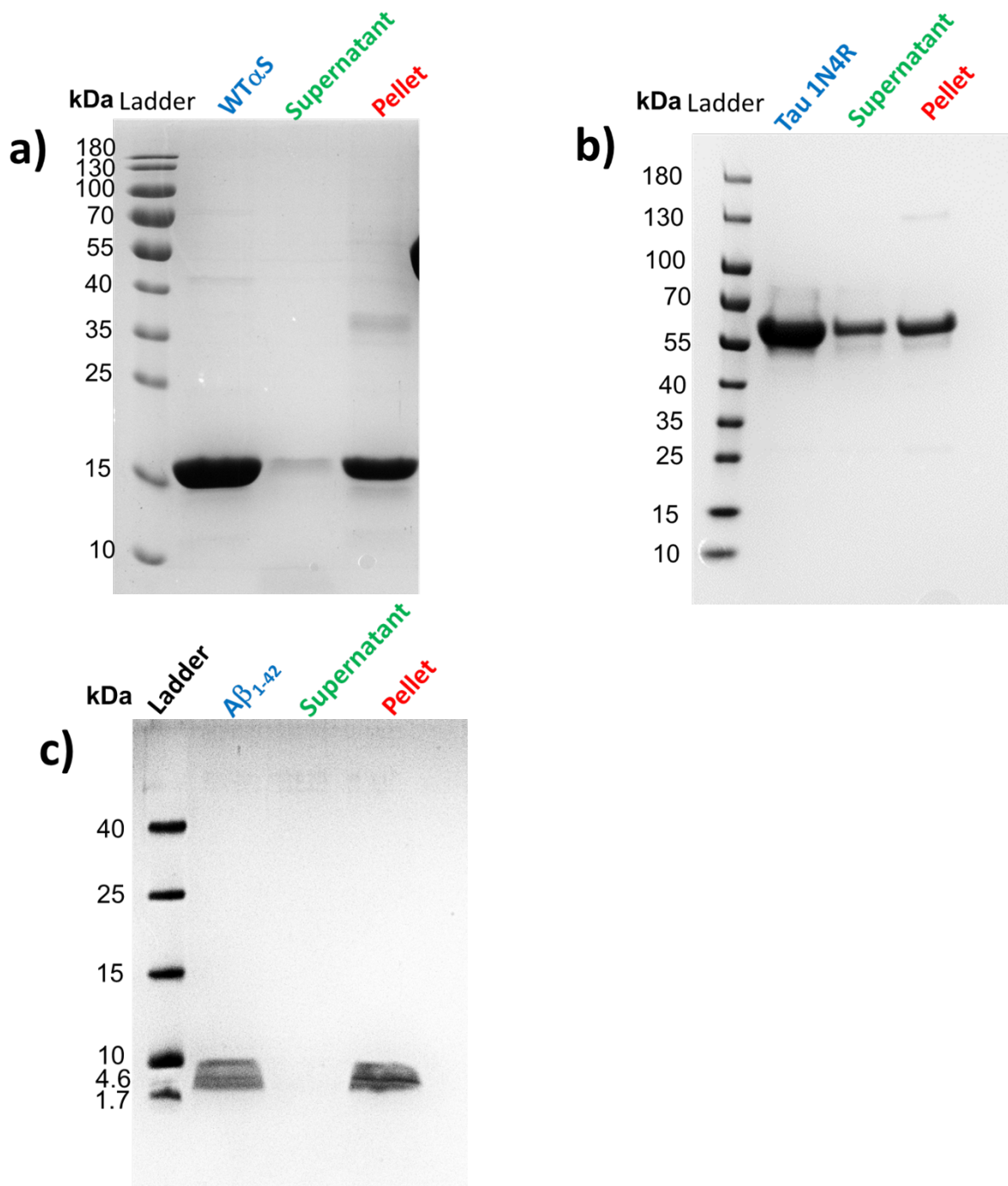


Fig. S17. Gel-based quantification of protein in α S (a), 1N4R tau (b), and A β ₁₋₄₂ (c) fibrils.

Fibril Binding Characterization

Probe binding (K_d) measurements with α S fibrils. α S fibrils (100 μ M) in PBS buffer were incubated with varying **5k** concentrations (0, 0.01, 0.1, 0.5, 1, 3, 5, 7, and 10 μ M) from concentrated 10 mM DMSO stock solutions in Greiner 96 well flat black $\frac{1}{2}$ area plates at 37 °C with shaking at 500 rpm for 15 min in an IKA MS3 control orbital shaker (Wilmington, NC, USA). After 15 min incubation, fluorescence intensity measurements were obtained with a Tecan Spark plate reader (Männedorf, Switzerland) by excitation with $\lambda_{ex}/\lambda_{em} = 463/580$ nm for **5k**, using the following parameters: excitation and emission bandwidth 5 nm, delay time 0 μ s, integration time 40 μ s. Averages and standard deviations were calculated from at least 3 independent measurements at each probe concentration. The resulting binding curve was fit to the following equation (modified from the One site -- Total, accounting for ligand depletion model) in Graphpad Prism 9 (San Diego, CA, USA), from which the K_d was determined.

$$Y = \frac{a}{2} \left(b - (b^2 - 4c)^{\frac{1}{2}} \right)$$

$$b = R_t + X + K_d \quad \text{and} \quad c = R_t X$$

X = total probe added in μ M, Y: measured fluorescence emission, K_d : Dissociation constant in μ M, a: fluorescence counts/ μ M probe bound, and R_t = maximum probe occupancy (set to 3.3 μ M based on B_{max} observed in prior radioligand binding studies).⁷ We note that variation of R_t from 1 to 10 does not significantly change the fitted K_d value (less than 2-fold change).

Absorbance and Fluorescence Measurements with α S Fibrils

Fluorescence spectra with α S fibrils. Fluorescence measurements were performed using a PTI QuantaMaster™ 40 fluorescence spectrometer. Fluorescence spectra of 10 μ M probes (concentrated stock solution prepared as 10 mM in DMSO) (**5b-5f** and **5h**) in PBS buffer were measured by excitation at their absorbance maximum wavelength in the absence and presence of 50 μ M α S fibrils (stock solution 100 μ M α S fibrils in PBS buffer).

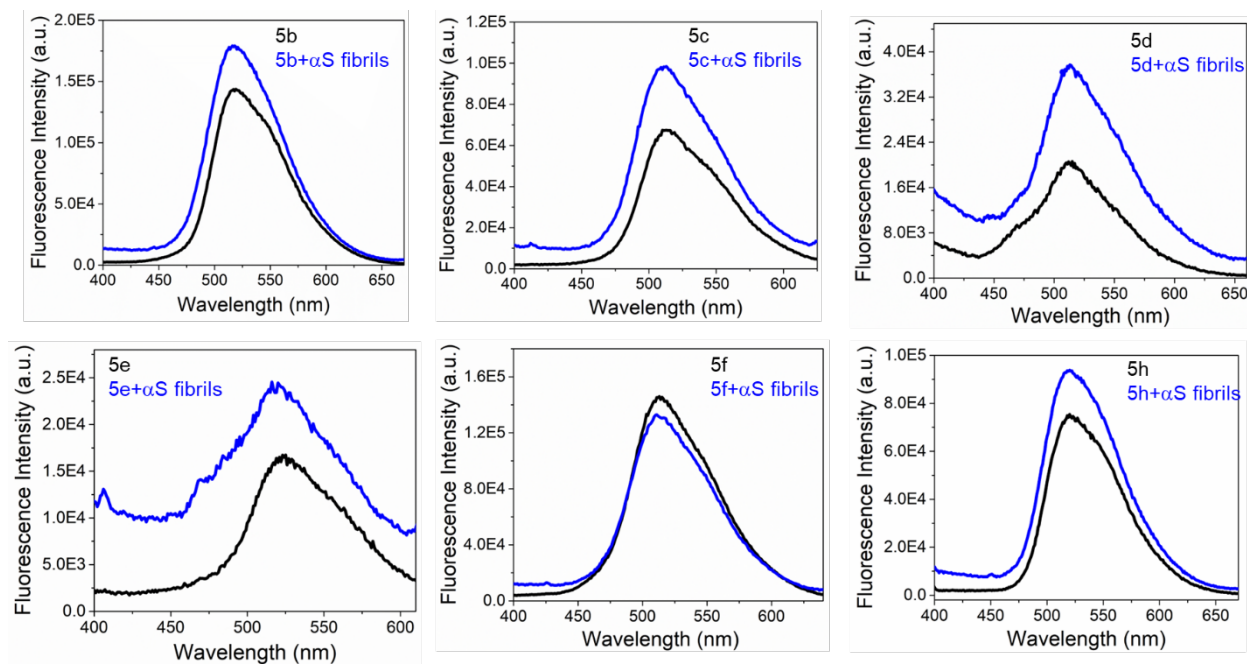


Fig. S18. Fluorescence spectra of probes (**5b-5f** and **5h**) with and without α S fibrils. Final concentrations of probes and α S fibrils were 10 μ M and 50 μ M, respectively. Emission spectra collected at each dye's maximum absorption wavelength. Ex/Em slit widths: 3 nm/3 nm.

Absorbance spectra with α S fibrils. Absorption measurements were performed using Thermo Scientific Genesys 150 UV Vis spectrometer. Absorption spectra of 10 μ M probes (concentrated stock solution prepared as 10 mM in DMSO) (**5j** and **5k**) in PBS buffer were measured in the absence and presence of 50 μ M α S fibrils (stock solution 100 μ M α S fibrils in PBS buffer).

Excitation spectra with α S fibrils. Excitation spectral measurements were performed using a PTI QuantaMaster™ 40 fluorescence spectrometer. Excitation spectra of 10 μ M probes (concentrated stock solution prepared as 10 mM in DMSO) (**5j** and **5k**) in PBS buffer were measured in the absence and presence of 50 μ M α S fibrils (stock solution 100 μ M α S fibrils in PBS buffer).

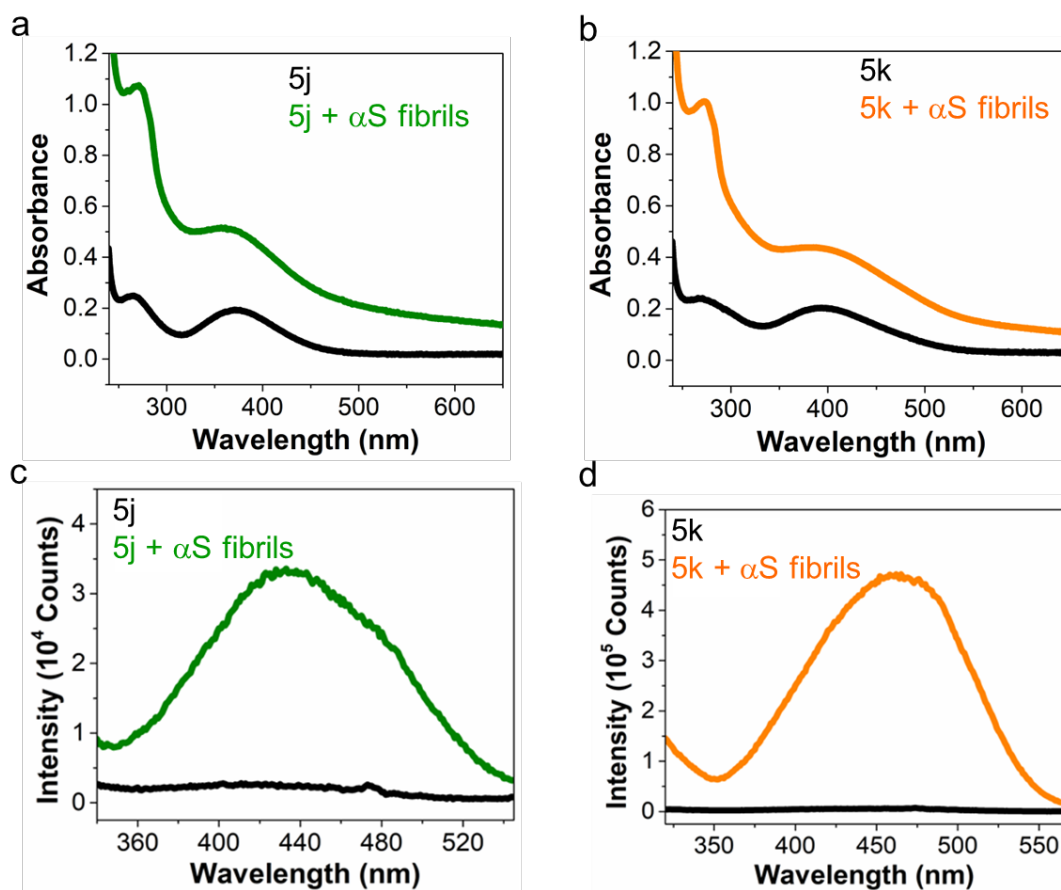


Fig. S19. Absorbance (a, b) and excitation spectra (c, d) of probes **5j** and **5k** with and without α S fibrils. Final probe and fibrils concentrations were 10 μ M and 50 μ M, respectively. Final probe and fibril concentrations were 10 μ M and 50 μ M, respectively. Emission wavelengths were 575 nm for **5j**, 580 nm for **5k**. Ex/Em slit widths: 3 nm/3 nm.

Fluorescent QY measurements of 5j and 5k with α S fibrils. For each QY measurement, the incident excitation light spectrum was collected with 100 μ L of probes (100 μ M) in PBS buffer. After measuring the incident light intensity, probes (**5j** and **5k**) were added to the α S fibrils (100 μ M) from a concentrated stock solution (10 mM in DMSO) to a final concentration of 100 μ M and the new spectrum (fluorescence intensity and new incident light intensity) was collected. Using the JASCO Quantum Yield Software, the dye QY was calculated by dividing the dye fluorescence intensity by the difference in incident light intensity in the presence and absence of fibrils.

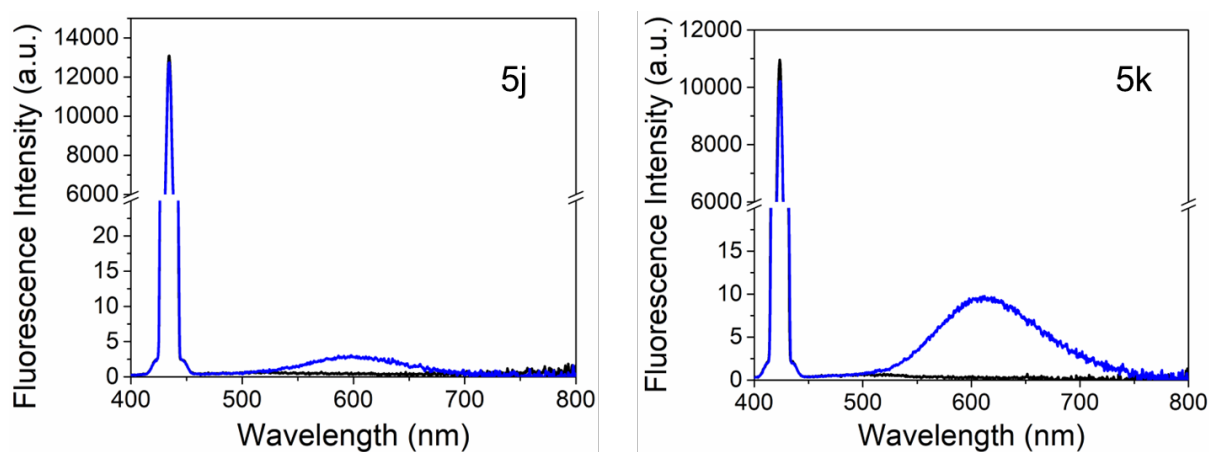


Fig. S20. Representative QY acquisitions of **5j** and **5k** with α S fibrils. Black line indicates incident light (α S fibrils without probe) and blue line indicates sample (α S fibrils with probe). Excitation at $\lambda_{\text{exc}} = 435$ nm for **5j** and $\lambda_{\text{exc}} = 463$ nm for **5k** and spectral collection (400-800 nm). Final concentrations of the probe and α S fibrils are the 100 μ M. Ex/Em slit widths: 5 nm/5 nm.

Fluorescence lifetime measurements of probes with α S fibrils. TCSPC measurements of fluorescence lifetime decays for 100 μ M dyes in the presence of 100 μ M α S fibrils were collected with the PTI Quantamaster TM 40 using a pulsed LED with a maximum emission at 486 nm. Fluorescence emission was collected at the indicated wavelength for each dye with 20 nm slit widths. The IRF was collected under identical conditions. Data analysis was performed with FluoFit software using an exponential decay model.

Table S15. Fluorescence lifetime measurements of α S fibrils with probes **5j** and **5k** in PBS buffer and fit χ^2 values.^a

Probe	Lifetime (ns)	χ^2
5j	1.90 \pm 0.01	1.221
5k	2.27 \pm 0.01	1.079

^aEmission wavelength collected at 575 nm for **5j** and 580 nm for **5k**. Final concentrations of the probe and α S fibrils were 100 μ M.

Fluorescence Measurements with Tau Fibrils

Fluorescence spectra with tau fibrils. Fluorescence measurements were performed using a PTI QuantaMaster™ 40 fluorescence spectrometer. Fluorescence spectra of 5 μM probes (concentrated stock solution prepared as 10 mM in DMSO) (**5j**, **5k**, and **ThT**) in PBS buffer were measured in the absence and presence of 25 μM tau fibrils (stock solution 32 μM tau fibrils in PBS buffer).

Excitation spectra with tau fibrils. Excitation spectral measurements were performed using a PTI QuantaMaster™ 40 fluorescence spectrometer. Excitation spectra of 5 μM probes (concentrated stock solution prepared as 10 mM in DMSO) (**5j**, **5k**, and **ThT**) in PBS buffer were measured in the absence and presence of 25 μM tau fibrils (stock solution 32 μM tau fibrils in PBS buffer).

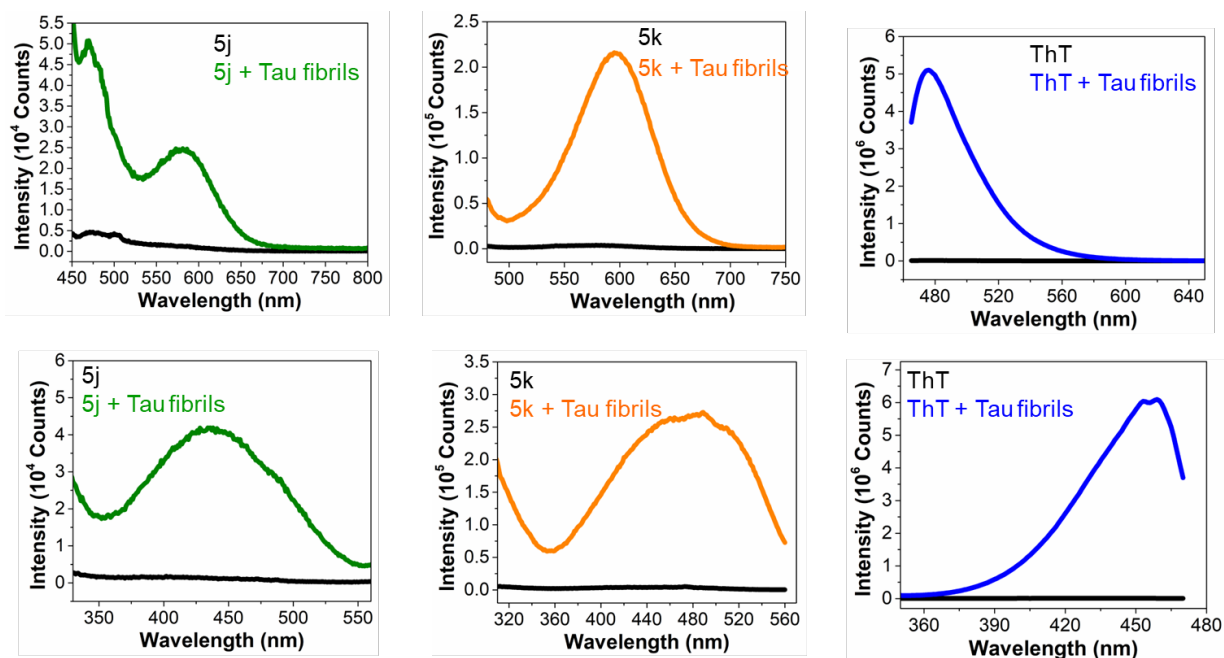


Fig. S21. Fluorescence spectra (a-c) and excitation spectra (d-f) of **5j**, **5k** and **ThT** with and without tau fibrils. Final probe and tau fibril concentrations were 5 μM and 25 μM , respectively. Excitation at $\lambda_{\text{exc}} = 435$ nm for **5j**, $\lambda_{\text{exc}} = 463$ nm for **5k**, $\lambda_{\text{exc}} = 450$ nm for **ThT**. Emission wavelengths were 575 nm for **5j**, 580 nm for **5k**, and 482 nm for **ThT**. Ex/Em slit widths: 3 nm/3 nm.

Fluorescence Measurements with A β ₁₋₄₂ Fibrils

Fluorescence spectra with A β ₁₋₄₂ fibrils. Fluorescence measurements were performed using a PTI QuantaMaster™ 40 fluorescence spectrometer. Fluorescence spectra of 10 μ M probes (concentrated stock solution prepared as 10 mM in DMSO) (5j, 5k and ThT) in PBS buffer were measured in the absence and presence of 50 μ M A β ₁₋₄₂ fibrils (stock solution 1 mM A β ₁₋₄₂ in 10 mM phosphate buffer, pH 7.4).

Excitation spectra with A β ₁₋₄₂ fibrils. Excitation spectral measurements were performed using a PTI QuantaMaster™ 40 fluorescence spectrometer. Excitation spectra of 10 μ M probes (concentrated stock solution prepared as 10 mM in DMSO) (5j, 5k and ThT) in PBS buffer were measured in the absence and presence of 50 μ M A β ₁₋₄₂ fibrils (stock solution 1 mM A β ₁₋₄₂ in phosphate buffer).

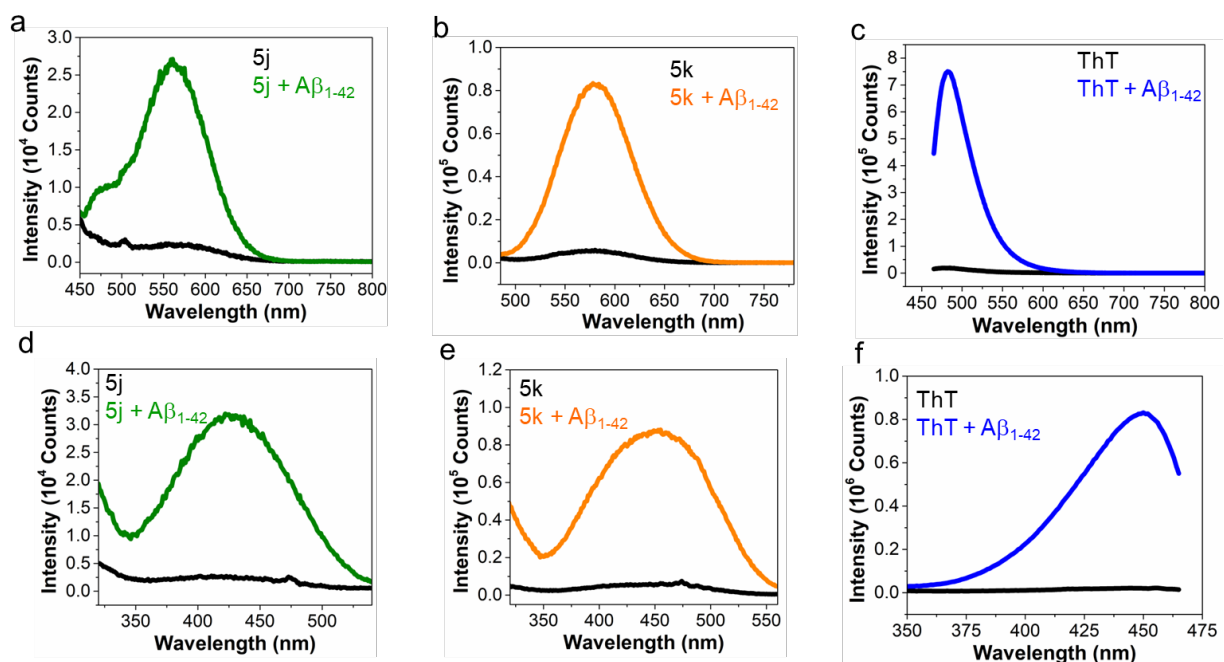


Fig. S22. Fluorescence spectra (a-c) and excitation spectra (d-f) of **5j**, **5k** and **ThT** with and without A β ₁₋₄₂ fibrils. Final probe and fibrils concentrations were 10 μ M and 50 μ M. Excitation at $\lambda_{\text{exc}} = 435$ nm for **5j**, $\lambda_{\text{exc}} = 463$ nm for **5k**, and $\lambda_{\text{exc}} = 450$ nm for **ThT**. Emission wavelengths were 575 nm for **5j**, 580 nm for **5k**, and 482 nm for **ThT**. Ex/Em slit widths: 3 nm/3 nm.

HEK cell lysate preparation. HEK 293T cells were grown on 150 mm dishes in sterile-filtered Dulbecco's modified Eagle's medium (Gibco, Thermo Fisher) supplemented with 10% fetal bovine serum (FBS), 1% penicillin/streptomycin (Mediatech, 10 mg/ml each). Cells were then washed with PBS and harvested in 5 mL PBS by scraping. Cells were pelleted by centrifugation at 1000 rpm for 5 min, and the supernatant was removed. The resulting cell pellet was re-suspended in 300-500 μ L PBS buffer with 0.1% Triton X-100 (Bio-Rad) and 1x HALT protease inhibitor cocktail without EDTA (Thermo Fisher), then lysed by sonication for two 30 s cycles (cycle 1: 2s on 2s off, amp 50; cycle 2: 2s on 2s off, amp 55) using a QSonica Q700 sonicator fitted with a microtip. Following sonication, lysate was centrifuged at 13,200 rpm for 60 min to separate membrane and cytosolic protein fractions. The resulting lysate cytosolic or membrane fraction was then used immediately after concentration determination by DC protein assay (Bio-Rad).

Selectivity of probe 5k binding with α S fibrils in HEK cell lysate. Probe 5k in PBS buffer (1 μ M, the stock solution prepared as 10 mM in DMSO) were incubated with different α S fibril concentrations (0, 5, 10, 25 and 50 μ M) in the presence of 10 mg/mL HEK cell lysate in Greiner 96 well flat black $\frac{1}{2}$ area plates at 37 $^{\circ}$ C with shaking at 500 rpm for 15 min in an IKA MS3 control orbital shaker. After 15 min incubation, fluorescence intensity measurements were obtained with a Tecan Spark plate reader (Männedorf, Switzerland) by excitation with $\lambda_{ex}/\lambda_{em} = 463/580$ nm for 5k, using the following parameters: excitation and emission bandwidth 5 nm, delay time 0 μ s, integration time 40 μ s.

Experimental procedure for the fluorescent measurements of 5k with TMAO: A 1 mM stock solution of 5k in DMSO and a 6.5 M stock solution of trimethylamine *N*-oxide (TMAO) in Tris buffer at pH 7.4 were prepared. From these stocks, the fluorescence measurements of probe 5k (10 μ M) were carried out with and without α S monomer (50 μ M) at different concentrations of TMAO (2 M, 4 M and 6 M) diluted with the Tris buffer. The solutions were mixed and then the spectra were measured using a Photon Technology International (PTI) QuantaMaster™ 40 fluorescence spectrometer with excitation at 418 nm.

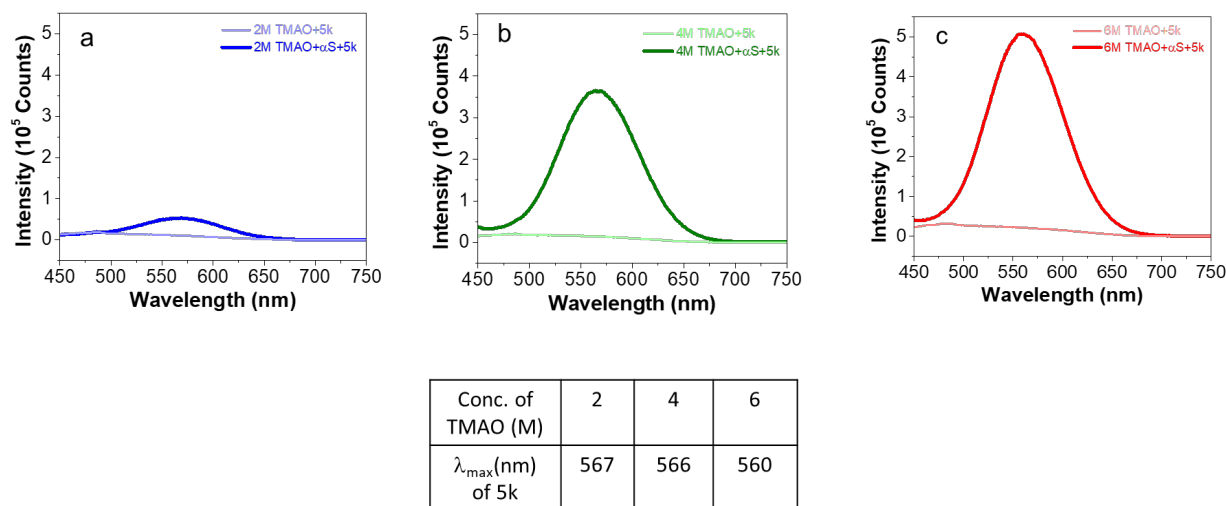


Fig. S23. Fluorescence spectra of probe 5k (10 μ M) with and without α S monomer (50 μ M) in different TMAO concentrations. (a) 2 M TMAO, (b) 4 M TMAO, (c) 6 M TMAO, and tabulated λ_{\max} (λ_{em}) of 5k with increasing TMAO concentrations. Excitation wavelength for 5k is 418 nm. Ex/Em slit widths: 3 nm/3 nm.

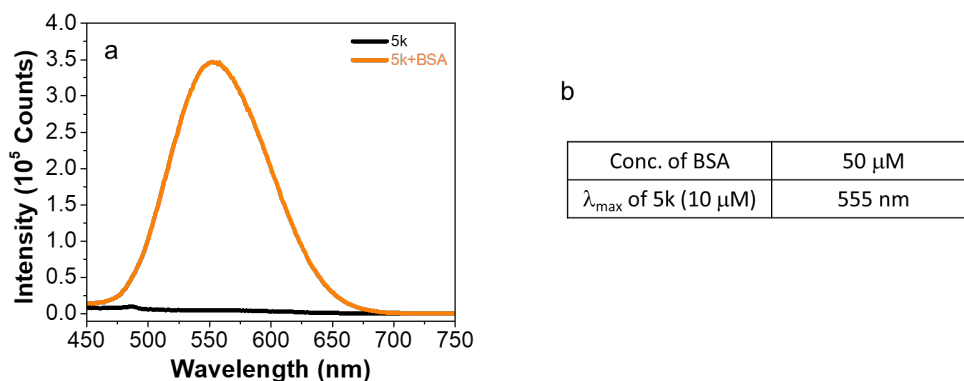


Fig. S24. (a) Fluorescence spectra of probe 5k (10 μ M) with BSA (50 μ M) and (b) Tabulated λ_{\max} (λ_{em}) of 5k. Excitation wavelength for 5k is 418 nm. Ex/Em slit widths: 3 nm/3 nm.

Patient Tissue Characterization and Amplified Fibril Preparation

Preparation of sarkosyl-insoluble α S from disease and control brains. All procedures were performed in accordance with local institutional review board guidelines. Written informed consent for autopsy and analysis of tissue sample data was obtained either from patients themselves or their next of kin. Frozen postmortem human frontal cortex brain tissues from three patients diagnosed with Alzheimer's disease (AD) and three patients diagnosed with Parkinson's disease with dementia (PDD) were selected for sequential extraction of α S aggregates based on a high burden of α S pathology determined by immunohistochemical staining using previously established methods.⁹ In brief, 5–10 g of frontal cortical gray matter were homogenized in five volumes (W/V) of high-salt (HS) buffer (50 mM Tris–HCl pH 7.4, 750 mM NaCl, 10 mM NaF, 5 mM EDTA) with protease and protein phosphatase inhibitors, incubated on ice for 20 min and centrifuged at 100,000 \times g for 30 min. The pellets were then re-extracted with HS buffer, followed by sequential extractions with five volumes of 1% Triton X-100-containing HS buffer and 1% Triton X-100-containing HS buffer with 30% sucrose. The pellets were then re-suspended and homogenized in 1% sarkosyl-containing HS buffer, rotated at room temperature for 2 h or at 4 °C overnight and centrifuged at 100,000 \times g for 30 min. The resulting sarkosyl-insoluble pellets were washed once with Dulbecco's PBS (DPBS) and re-suspended in DPBS by sonication (QSonica Microson XL-2000; 50 pulses; setting 2; 0.5 s per pulse). These final sarkosyl-insoluble fractions are referred to as "brain extracts.": The amount of α S in the brain extracts was determined by sandwich ELISA using Syn9027, a mono-clonal antibody (Mab) to α S, and the protein concentrations were examined by bicinchoninic acid (BCA) assay as previously described.⁹ Total protein in AD cases ranged from 5 to 13 mg/mL and total protein in PDD cases ranged from 9 to 12 mg/mL. α S concentration in AD cases ranged from 36 to 43 μ g/mL and total protein in PDD cases ranged from 24 to 33 μ g/mL.

***In vitro* amplification of α S fibrils from brain extracts.** Brain-derived α S aggregates in extract samples from three AD and three PDD cases (Fig. S23a) were used as seeds for templated aggregation of recombinant α S monomer. Brain lysates were sonicated on high for 20 cycles of 30 s on, followed by 30 s off (Diagenode Biorupter UCD-300 bath sonicator) and diluted to 350 nM (based on sandwich ELISA) in DPBS (pH 7.4, without Mg^{2+} and Ca^{2+}) containing sufficient monomer for a final α S concentration of 35 μ M (1% patient-derived seed, 99% monomer) and

incubated at 37° C with constant shaking at 1000 rpm for 7 days. The resulting aggregates were termed amplified fibrils (AFs). After seven days of incubation, amplification progress was determined by removing an aliquot and diluting tenfold in DPBS to a final α S concentration of 3.5 μ M. Samples were centrifuged at 45k rpm for 30 min at 10°C in a TLA-55 rotor (Beckman Coulter). The supernatants were removed, and the pellets were resuspended in DPBS. Equal volumes of supernatant and pellet fractions were analyzed on SDS-PAGE gels and Western blot, with amplified aggregates migrating to the pellet fraction (Fig. S23b). Primary mouse hippocampal neurons were then treated with the AFs to confirm they retained the characteristic pathological phenotype of the original brain lysate and were distinct from recombinant PFFs. Primary mouse neurons were prepared from the hippocampus of embryonic day E16–E18 CD1 mouse embryos as previously described 10. All procedures were performed according to the National Institutes of Health Guide for the Care and Use of Experimental Animals and were approved by the University of Pennsylvania Institutional Animal Care and Use Committee. Primary mouse hippocampal neurons were plated at 17.5k cells per well in 96-well plates and were treated with 50 ng per well of brain-derived, AFs, or recombinant PFFs at seven days in vitro and maintained for two weeks post-treatment. Cells were grown in Neurobasal medium supplemented with B27, 2 mM GlutaMax, and 100 U/ml penicillin/ streptomycin (ThermoFisher). Following fixation with 4% paraformaldehyde, 4% sucrose, and 1% Triton-X100, cultures were probed with antibodies for MAP2 (17028) and pSer-129 α S (81A) Patient-derived fibrils and AFs induce discrete, dense inclusions in cell bodies with little neuritic pathology while PFF induce predominantly small neuritic puncta and threads (Fig. S24).

Control sample preparation. Control samples for comparison to AFs in fluorescence binding experiments below were prepared as follows. “Lysate” controls used a portion of the same brain extracts from AD cases 1-3 and PDD cases 1-3, but were not subjected to amplification. These should contain the same concentration of patient-derived α S and other insoluble proteins as the AF samples, but no seeded fibrils. Pre-formed fibril (PFF) controls took these lysates and added α S fibrils, generated as described above for binding studies of the pure fibrils, to match the α S monomer concentration used in generating AFs (35 μ M). Thus, they would have the same fibril content as an amplification reaction which went to completion, but with a fibril morphology that is not templated by the patient-derived α S aggregates.

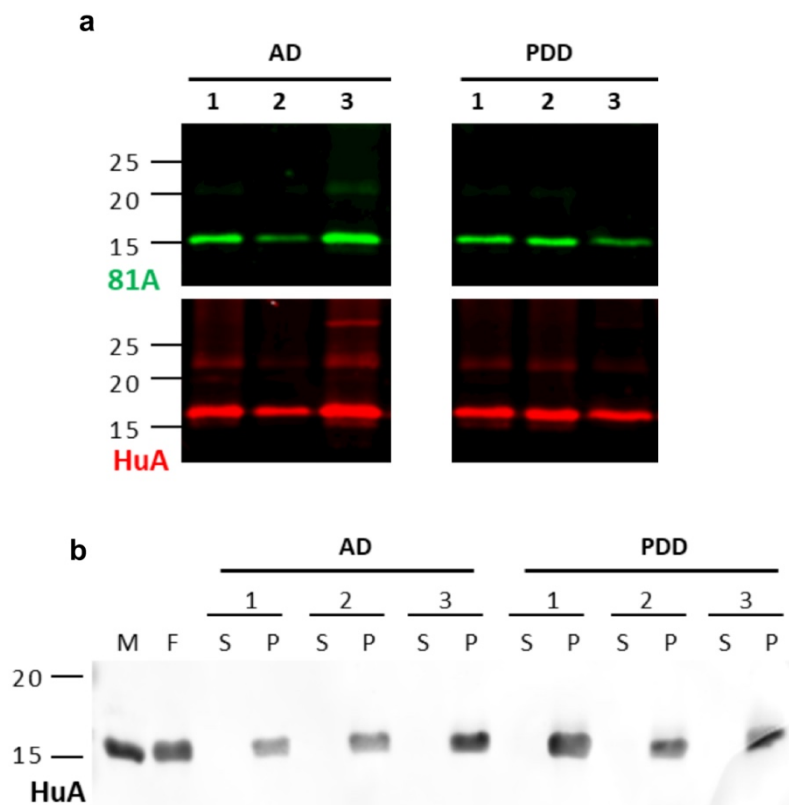


Fig. S25. Preparation of fibrils amplified from patient-derived α -synuclein aggregates. (a) Western blots of the final brain lysate samples extracted from AD and PDD patient brains. Membranes were probed with anti-pSer-129 α S (81A) or total α S (HuA). (b) Western blot of sedimentation results for amplified fibrils (AFs) after seven days of incubation. Supernatant (S) and pellet (P) fractions were run for each reaction with monomer (M) and PFF (F) as loading controls. The membrane was probed with HuA.

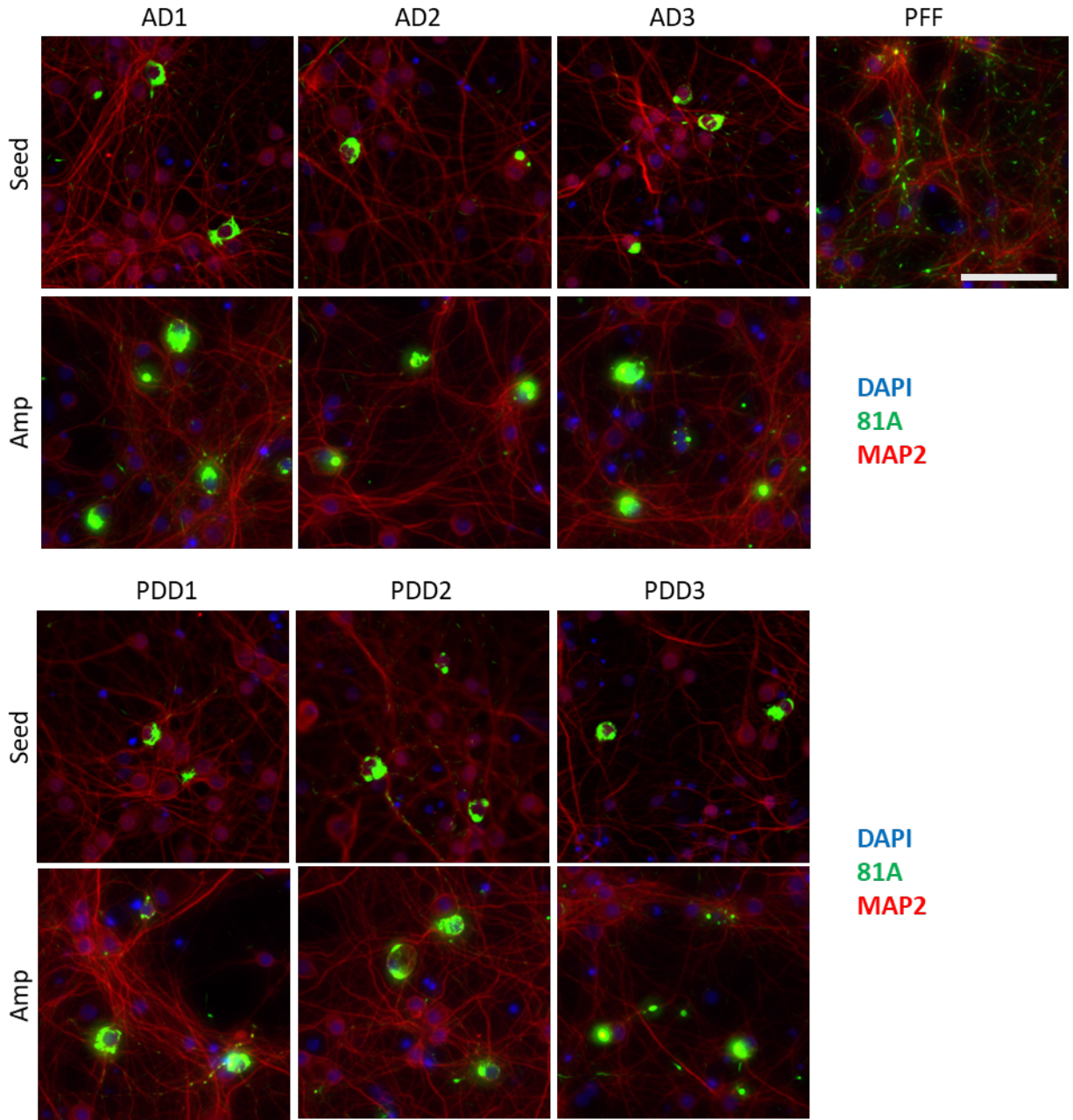


Fig. S26. Representative images of pathology induced in primary mouse hippocampal neurons for seeds and AFs (Amp) for each case, or PFFs. Probed with 81A (green), anti-MAP2 (red) and DAPI (blue). Scale bar 50 μ m.

Fluorescence Measurements with Patient Tissue Lysate Samples

Fluorescence measurements of 5k and ThT with AD and PDD patient cases. Probe binding was tested with 7 μM stock concentrations of patient tissue samples from 3 different AD patient cases (AD1, AD2, and AD3) with 3 different conditions: lysate only, amplified αS fibrils (AFs), preformed αS fibrils (PFFs), all prepared as described above. Final samples were prepared in a Greiner 384-well small volume microplate by diluting to 1 μM final concentration with PBS buffer from each condition's stock in a 5 μL final volume. To this was added bimane probes **5k** and **ThT** at 1 μM probe concentration (10 mM stock of **5k** and **ThT** in DMSO and 5 mM stock of ThT in PBS buffer), then incubated at 37 °C with shaking at 500 rpm for 15 min in an IKA MS3 control orbital shaker. After 15 min of incubation, fluorescence intensity measurements were obtained with a Tecan Spark plate reader by excitation $\lambda_{\text{ex}}/\lambda_{\text{em}} = 463/580$ nm for **5k** and $\lambda_{\text{ex}}/\lambda_{\text{em}} = 450/482$ nm for **ThT**, using the following parameters: excitation and emission bandwidth 5 nm, delay time 0 μs , integration time 40 μs . Identical experiments were performed for 7 μM stock concentrations of patient tissue samples from 3 different PDD patient cases (PDD1, PDD2, and PDD3) with 3 different conditions: lysate only, amplified αS fibrils (AFs), preformed αS fibrils (PFFs).

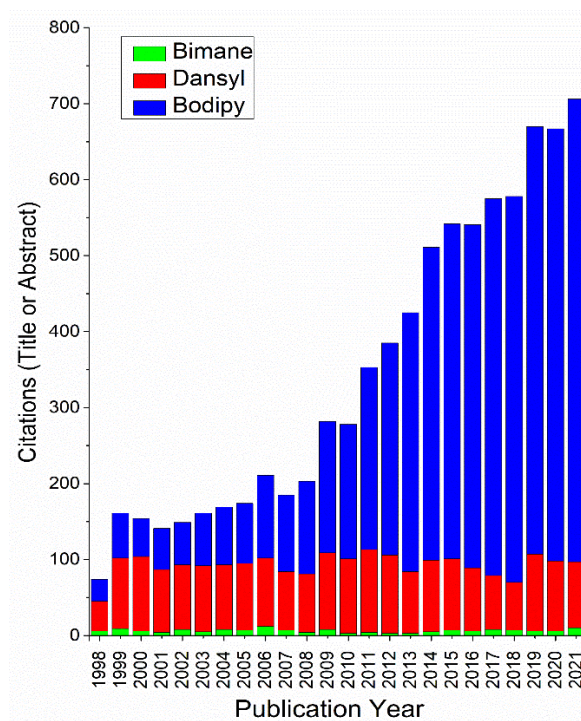


Fig. S27. Analysis of bimane literature relative to similar fluorophores such as BODIPY and Dansyl fluorophores (<https://www.webofscience.com/wos/woscc/basic-search>).

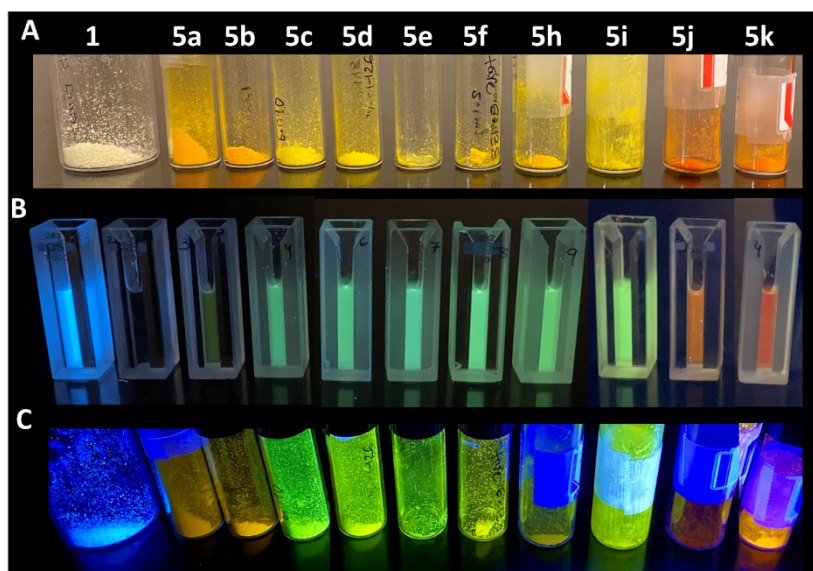


Fig. S28. Photophysical properties of **1** and **5a-f, 5h-k**. (A) Photograph under ambient light, (B) Solution state fluorescence of 25 μM probe in ACN/PBS buffer (50:50 v/v) under handheld UV lamp (365 nm), and (C) Amorphous solid-state fluorescence under handheld UV lamp (365 nm).

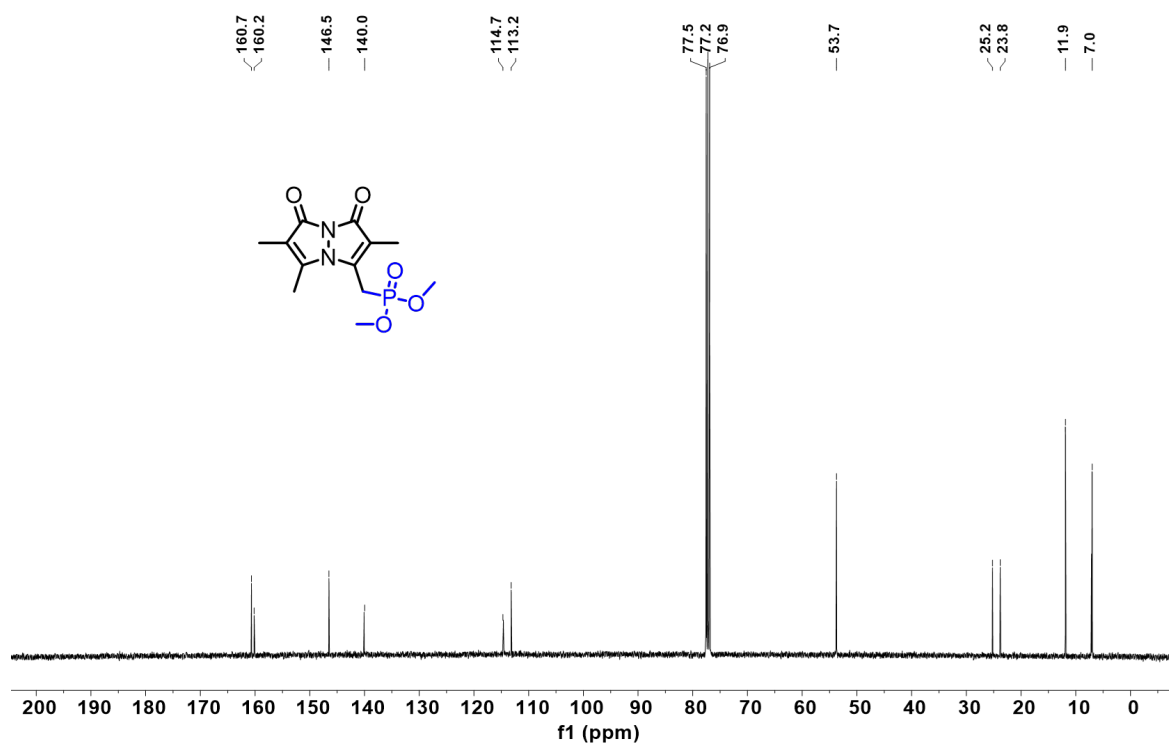
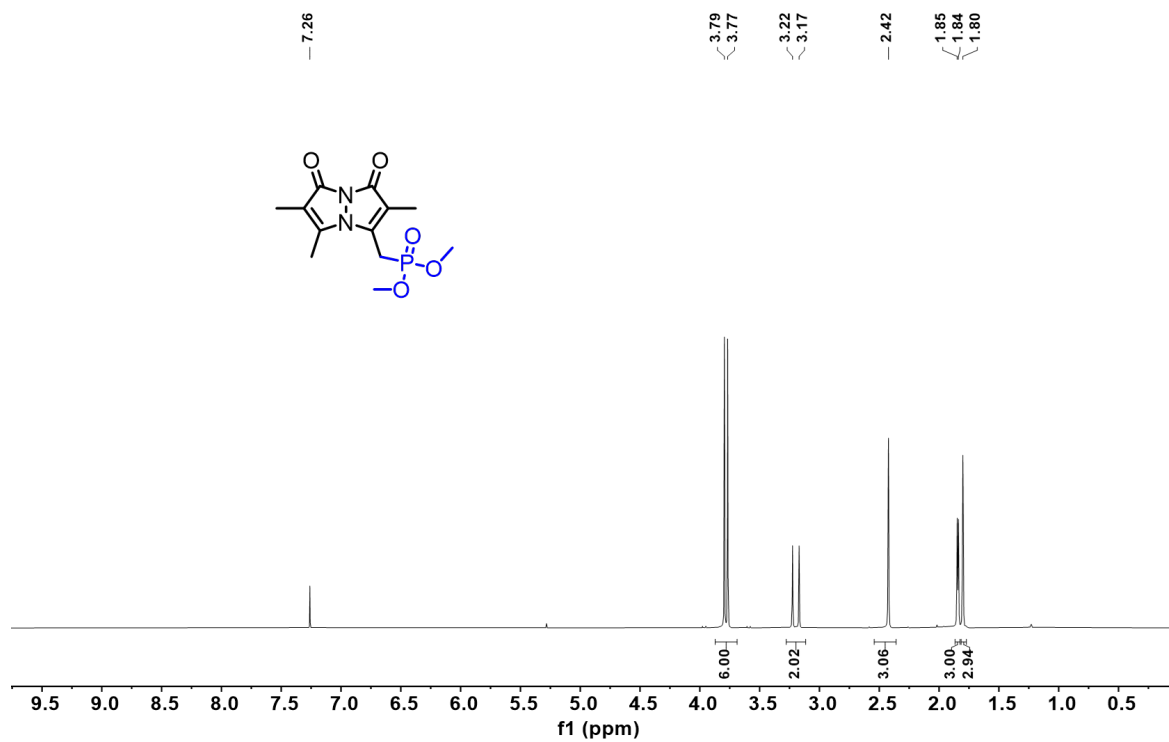


Fig. S29. ¹H NMR and ¹³C NMR spectrum of **3** in CDCl₃.

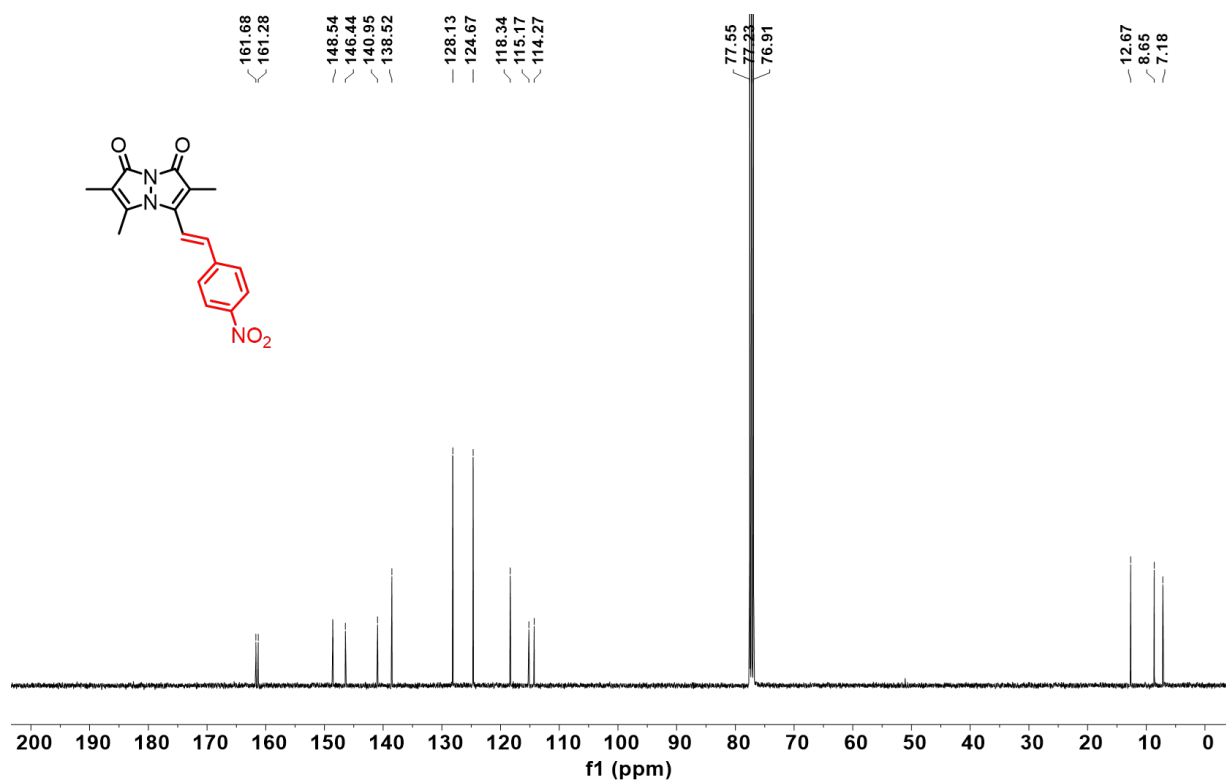
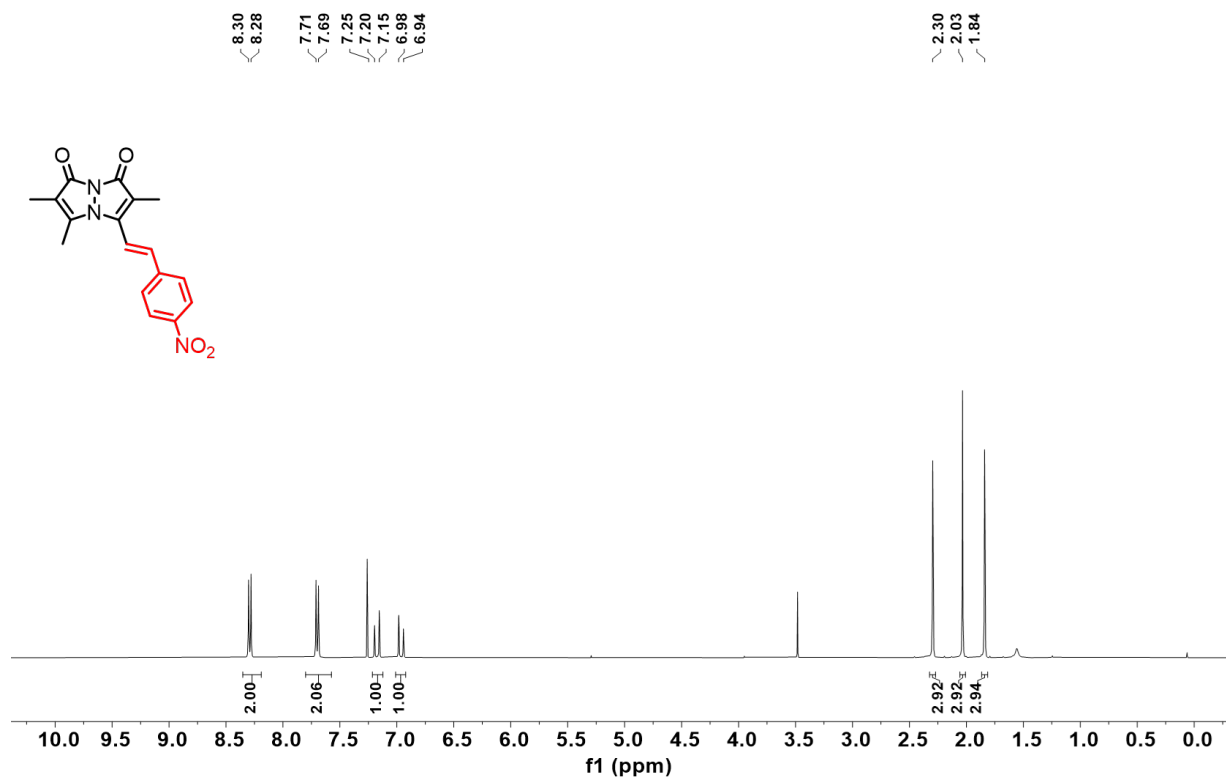


Fig. S30. ¹H NMR and ¹³C NMR spectrum of **5a** in CDCl₃.

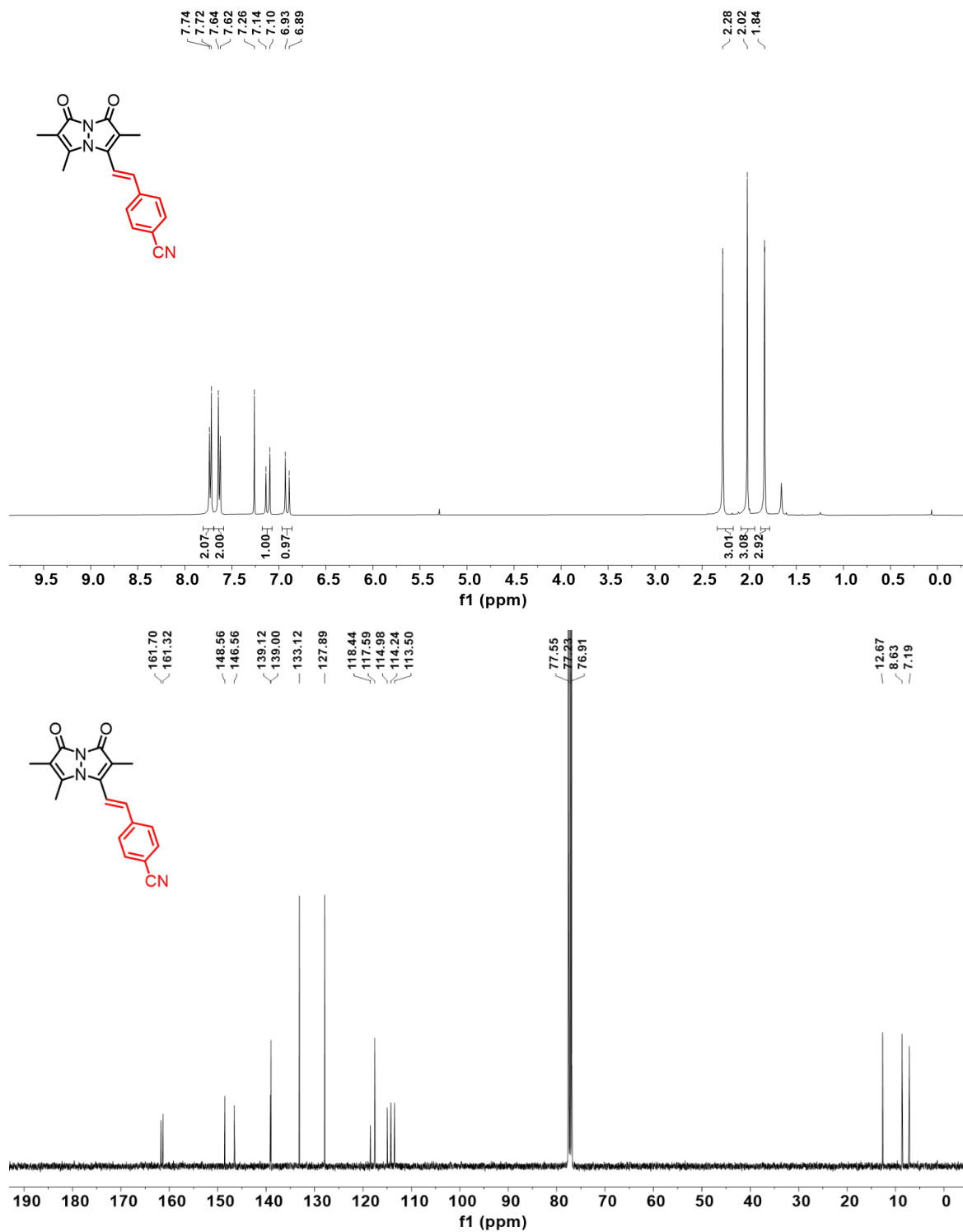


Fig. S31. ¹H NMR and ¹³C NMR spectrum of **5b** in CDCl₃.

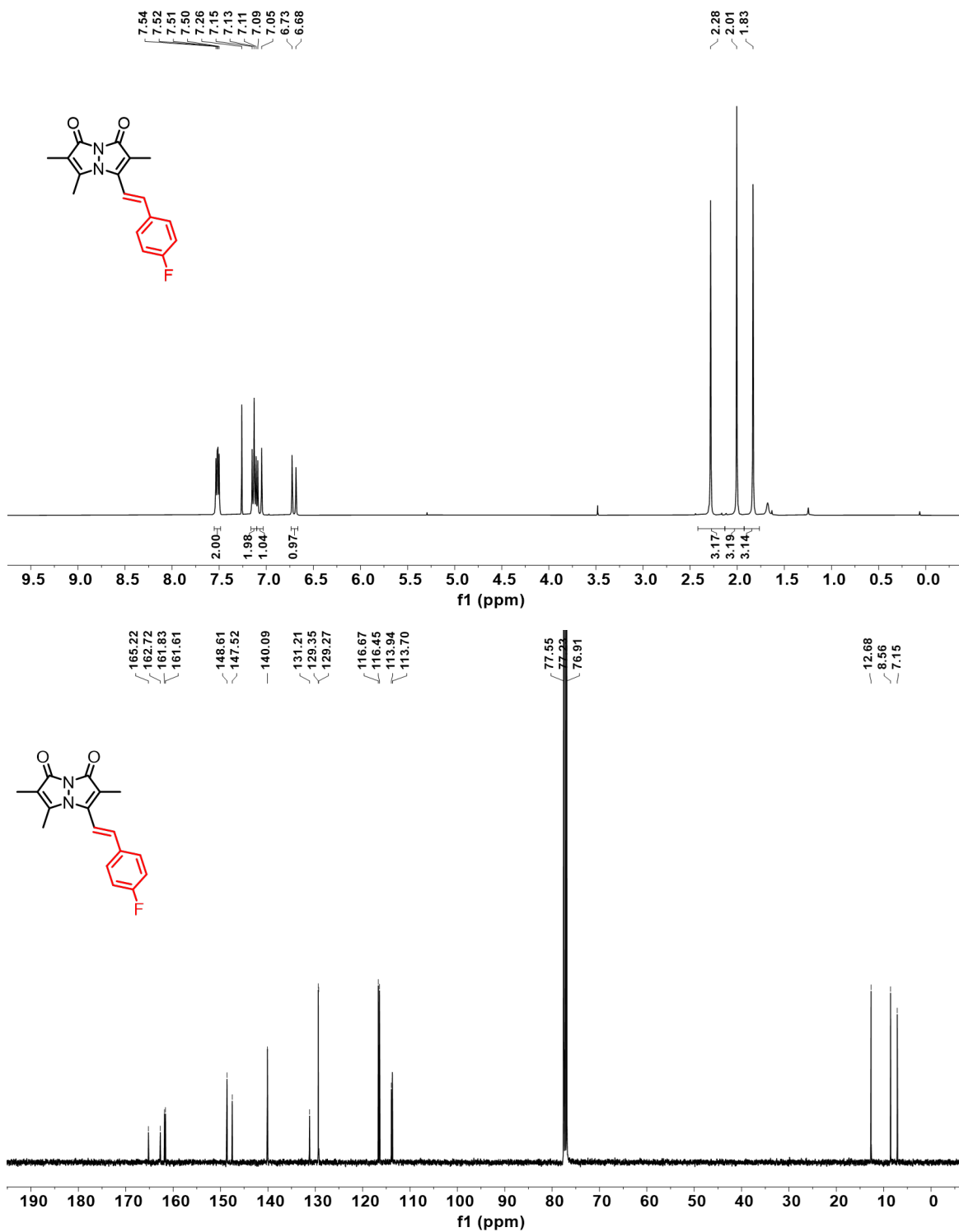


Fig. S32. ¹H NMR and ¹³C NMR spectrum of **5c** in CDCl₃.

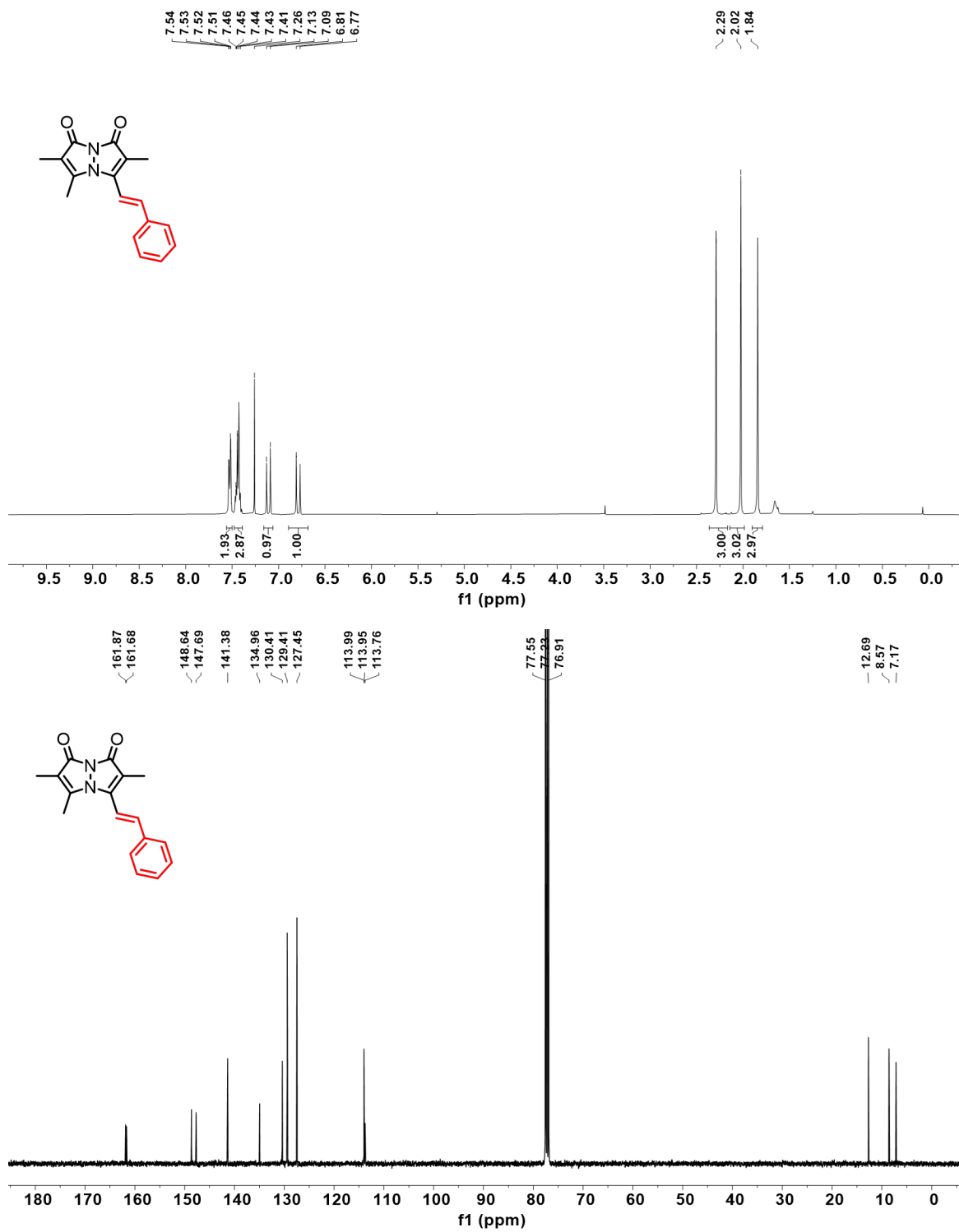


Fig. S33. ¹H NMR and ¹³C NMR spectrum of **5d** in CDCl₃.

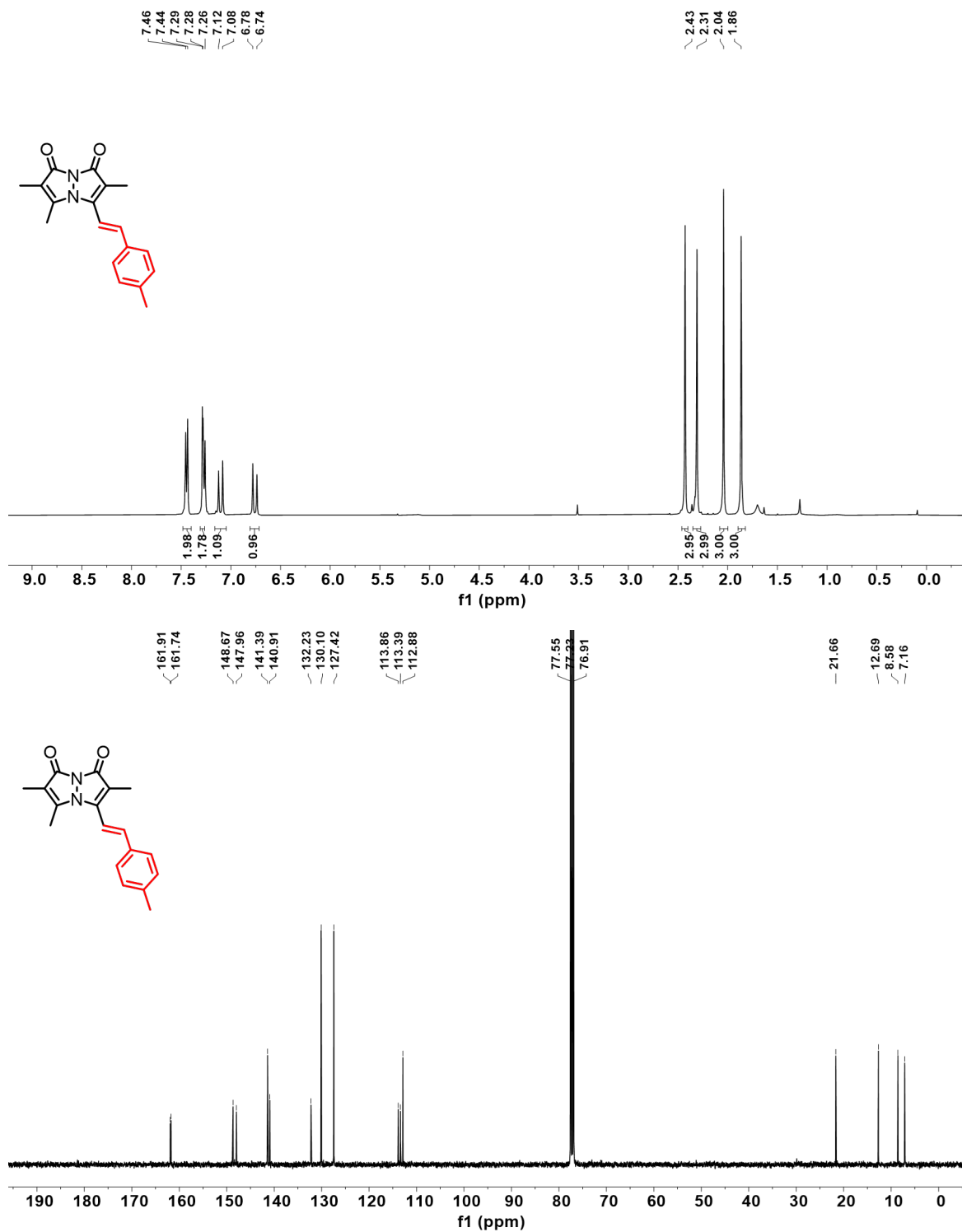


Fig. S34. ¹H NMR and ¹³C NMR spectrum of **5e** in CDCl₃.

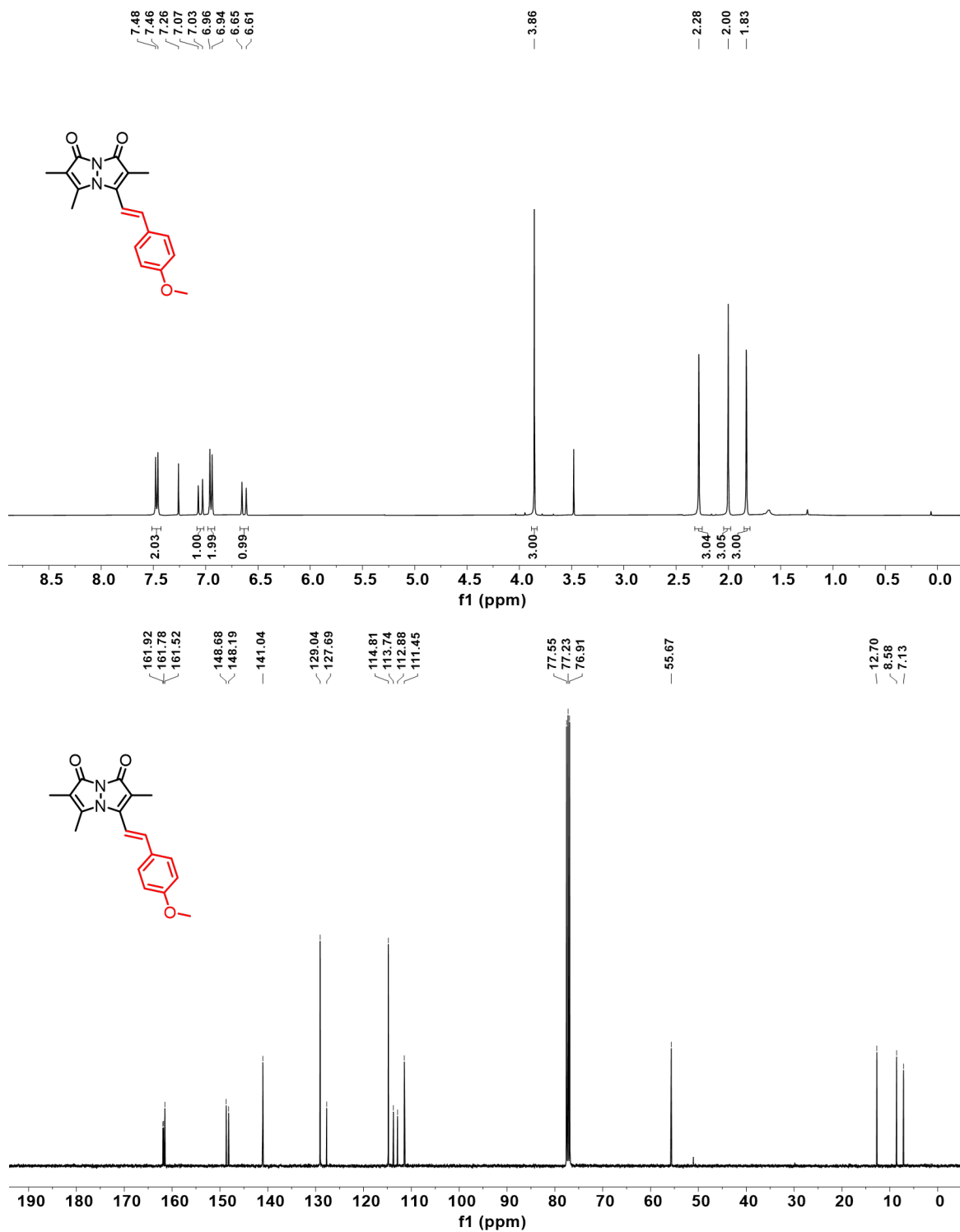


Fig. S35. ¹H NMR and ¹³C NMR spectrum of **5f** in CDCl₃.

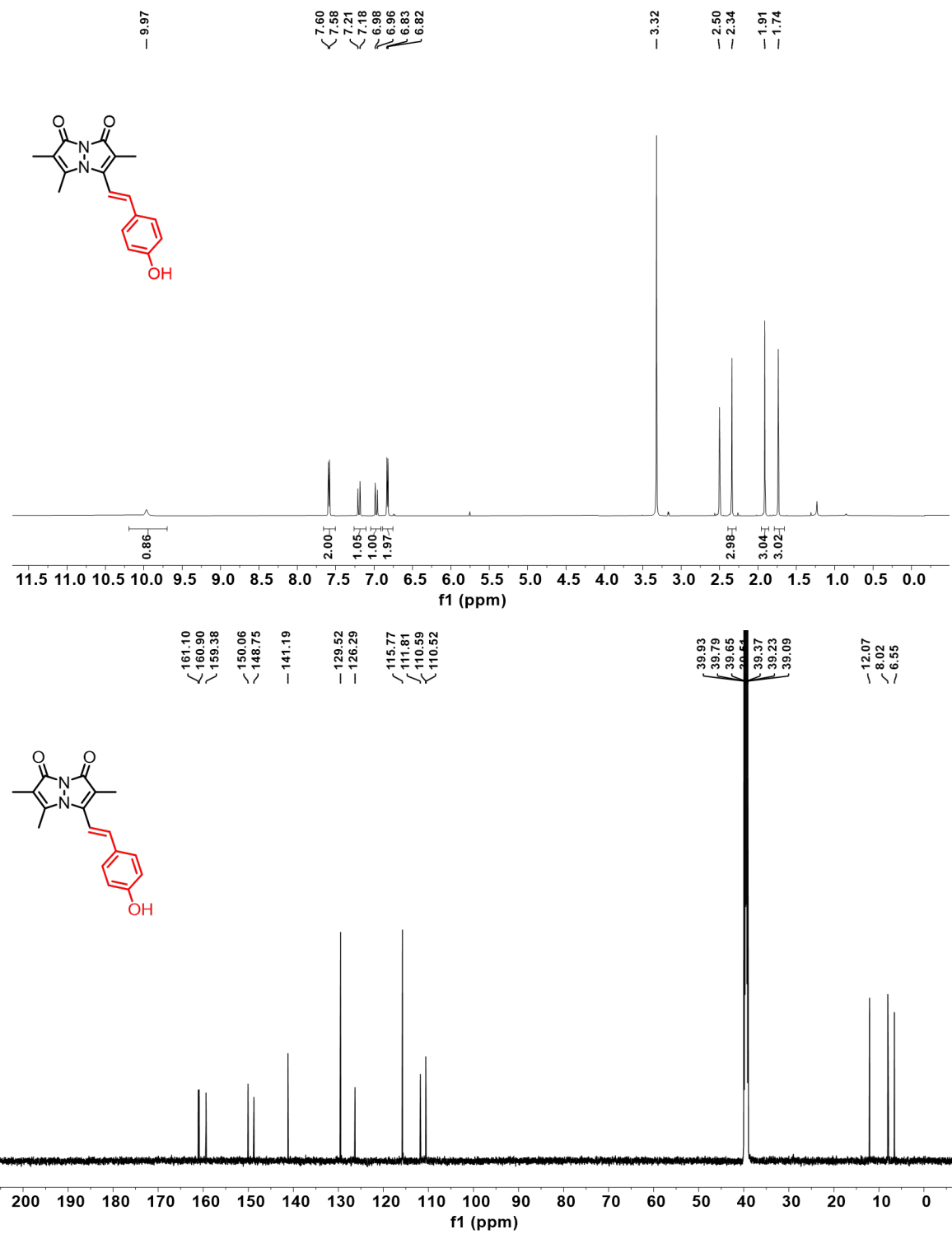


Fig. S36. ¹H NMR and ¹³C NMR spectrum of **5h** in CDCl₃.

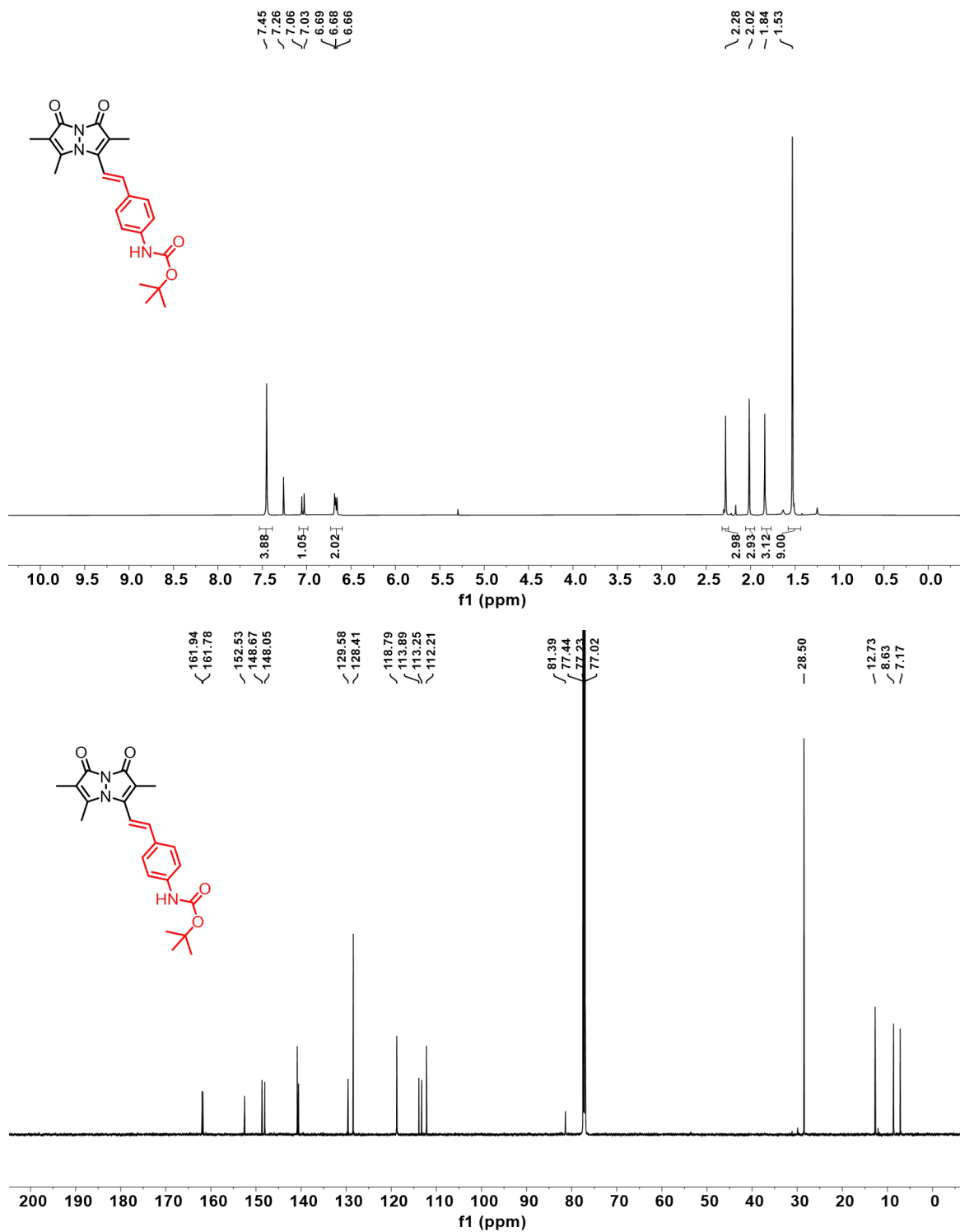


Fig. S37. ¹H NMR and ¹³C NMR spectrum of **5i** in CDCl₃.

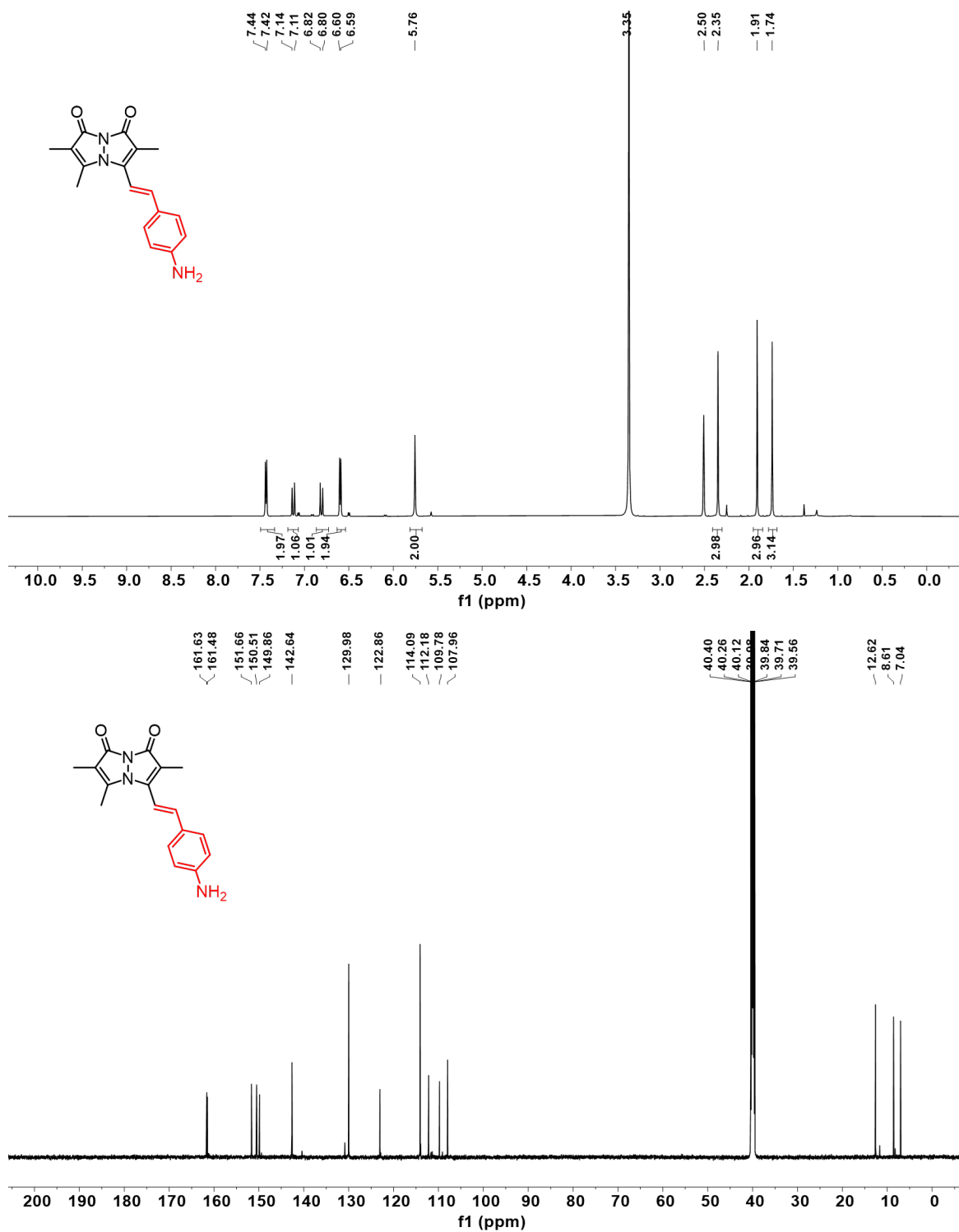


Fig. S38. ¹H NMR and ¹³C NMR spectrum of **5j** in CDCl₃.

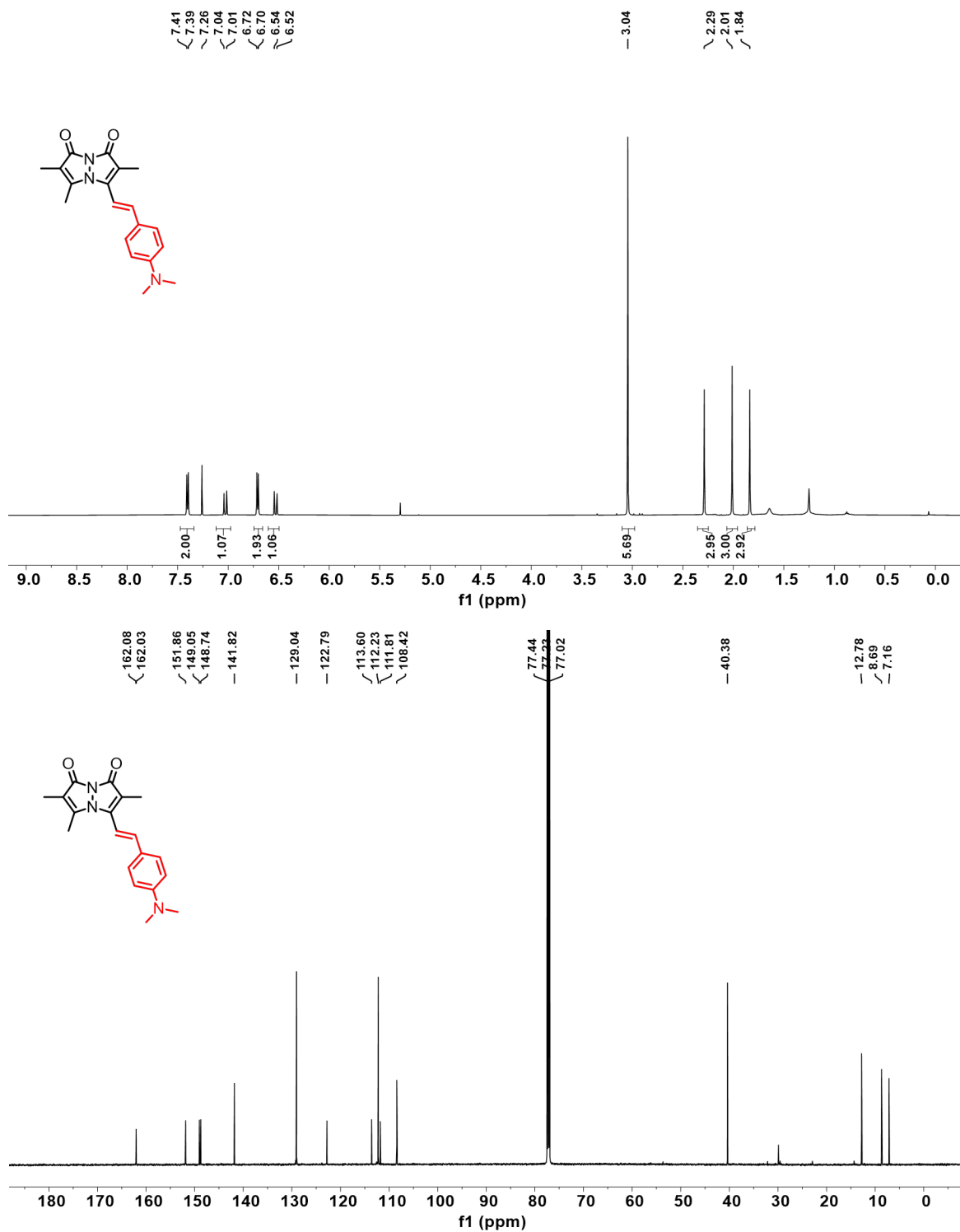
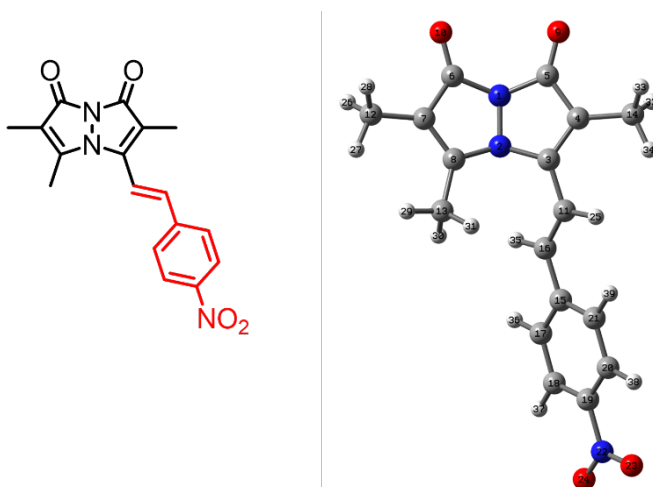


Fig. S39. ¹H NMR and ¹³C NMR spectrum of **5k** in CDCl₃.

Cartesian coordinates of the optimized geometries: 5a

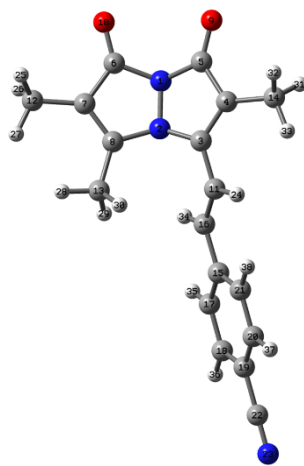
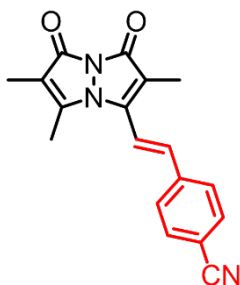
optimized at # APFD/6-311+G (2d, p) at ground state



N	-3.579474	0.239347	-0.572001	C	2.833122	0.762288	0.763210
N	-2.299302	-0.179095	-0.279420	N	6.346465	-0.179185	0.021334
C	-1.565537	0.948845	0.101344	O	6.904811	0.459678	0.899523
C	-2.370043	2.04777	0.092737	O	6.934219	-0.879406	-0.788087
C	-3.696554	1.628687	-0.316770	H	0.248439	1.664982	0.987488
C	-4.497548	-0.789201	-0.239320	H	-4.721945	-3.673432	-0.185264
C	-3.678545	-1.868992	0.272888	H	-3.502670	-3.848146	1.080706
C	-2.386686	-1.454747	0.287703	H	-5.037600	-3.03964	1.425392
O	-4.714624	2.276812	-0.463436	H	-1.511011	-3.083121	1.301642
O	-5.702171	-0.711177	-0.385578	H	-0.554378	-2.49759	-0.061723
C	-0.138163	0.916306	0.304655	H	-0.592096	-1.576429	1.441256
C	-4.257531	-3.17677	0.671821	H	-2.135087	4.051378	-0.599358
C	-1.194392	-2.188545	0.768133	H	-2.688372	3.912896	1.064510
C	-2.020095	3.470545	0.321110	H	-0.993617	3.588994	0.667770
C	2.137264	0.054229	-0.227891	H	0.267664	-0.57914	-1.098809
C	0.689924	0.099489	-0.362846	H	2.335367	-1.297757	-1.891595
C	2.863078	-0.739992	-1.125457	H	4.805826	-1.430819	-1.746577
C	4.241194	-0.821114	-1.053632	H	4.751503	1.232565	1.609710
C	4.895858	-0.100635	-0.066021	H	2.296741	1.368714	1.483134
C	4.207909	0.690472	0.847159				

Cartesian coordinates of the optimized geometries: 5b

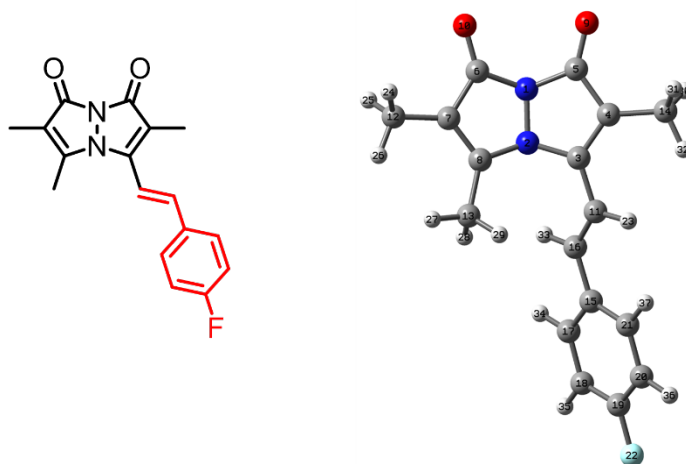
optimized at # APFD/6-311+G (2d, p) at ground state



<i>Atom</i>	<i>X</i>	<i>Y</i>	<i>Z</i>		<i>Atom</i>	<i>X</i>	<i>Y</i>	<i>Z</i>
N	-3.175423	0.260862	-0.566947		C	4.616648	0.629971	0.863327
N	-1.896895	-0.170511	-0.285469		C	3.242428	0.715587	0.779611
C	-1.157479	0.944302	0.122826		C	6.742536	-0.238066	0.024200
C	-1.957814	2.046319	0.143090		N	7.891747	-0.310201	0.095217
C	-3.285923	1.644018	-0.275238		H	0.659186	1.626515	1.030180
C	-4.097905	-0.770661	-0.258242		H	-4.646372	-3.057872	1.354389
C	-3.284010	-1.866479	0.227124		H	-4.338909	-3.653211	-0.272395
C	-1.990056	-1.458914	0.250790		H	-3.116984	-3.866005	0.985267
O	-4.301799	2.299709	-0.404539		H	-1.121964	-3.116456	1.223149
O	-5.302436	-0.683402	-0.401663		H	-0.162738	-2.501284	-0.125440
C	0.269405	0.898653	0.326914		H	-0.195702	-1.617838	1.399826
C	-3.869206	-3.180533	0.595312		H	-1.735349	4.070576	-0.490987
C	-0.801166	-2.210297	0.712134		H	-2.250466	3.881592	1.180182
C	-1.600701	3.461198	0.408041		H	-0.566325	3.567162	0.734720
C	2.541104	0.035246	-0.226156		H	0.667988	-0.561324	-1.114802
C	1.093903	0.095273	-0.360914		H	2.731421	-1.281349	-1.917760
C	3.262673	-0.744463	-1.138830		H	5.189959	-1.441945	-1.779180
C	4.640341	-0.838321	-1.066582		H	5.152796	1.156947	1.643875
C	5.322094	-0.147649	-0.062807		H	2.710114	1.311865	1.511384

Cartesian coordinates of the optimized geometries: 5c

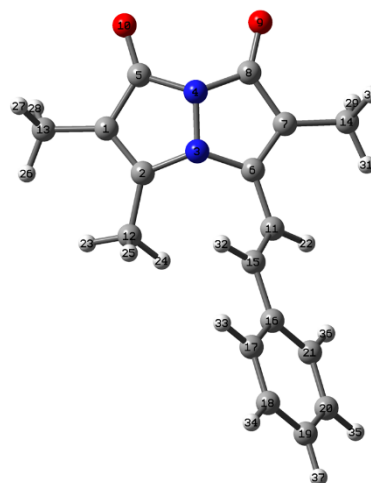
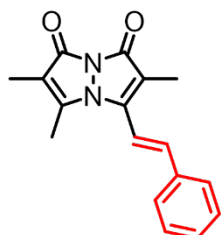
optimized at # APFD/6-311+G (2d, p) at ground state



N	-2.940634	0.265317	-0.574339	C	4.863449	0.615525	0.850855
N	-1.662558	-0.162997	-0.284168	C	3.487470	0.720354	0.765164
C	-0.924636	0.954461	0.122747	F	6.867657	-0.310086	0.032808
C	-1.730303	2.053997	0.139873	H	0.889452	1.639890	1.032950
C	-3.053538	1.649989	-0.283024	H	-4.419956	-3.047326	1.348618
C	-3.862576	-0.765402	-0.266313	H	-4.096245	-3.651200	-0.271777
C	-3.050403	-1.858413	0.226952	H	-2.885225	-3.853401	0.997900
C	-1.756784	-1.448802	0.256245	H	-0.895841	-3.097266	1.250120
O	-4.070855	2.303377	-0.420497	H	0.069405	-2.500109	-0.102334
O	-5.067378	-0.681000	-0.415796	H	0.034083	-1.598097	1.411261
C	0.499815	0.907164	0.334622	H	-1.549150	4.086614	-0.483067
C	-3.635595	-3.171995	0.597277	H	-1.996761	3.880263	1.205419
C	-0.571043	-2.197833	0.729708	H	-0.330078	3.580946	0.692055
C	-1.375553	3.470289	0.404394	H	0.892251	-0.565592	-1.092101
C	2.769777	0.016419	-0.211649	H	2.936086	-1.362491	-1.854576
C	1.324526	0.094452	-0.344175	H	5.409747	-1.557231	-1.709364
C	3.477427	-0.805984	-1.096075	H	5.427051	1.154112	1.603992
C	4.857002	-0.923153	-1.025983	H	2.968499	1.354440	1.475065
C	5.525296	-0.205740	-0.050540				

Cartesian coordinates of the optimized geometries: 5d

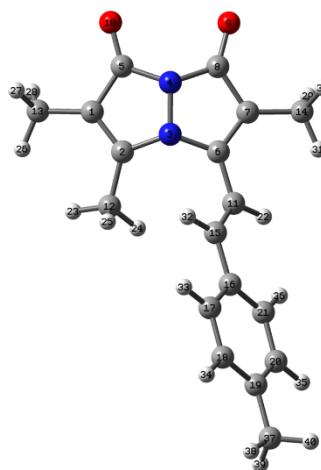
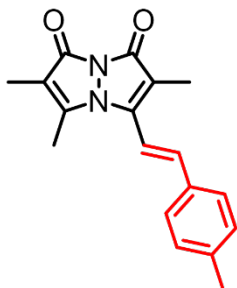
optimized at # APFD/6-311+G (2d, p) at ground state



<i>Atom</i>	<i>X</i>	<i>Y</i>	<i>Z</i>		<i>Atom</i>	<i>X</i>	<i>Y</i>	<i>Z</i>
C	2.709914	-1.832463	0.225581		C	-5.246127	0.515995	0.848202
C	1.409734	-1.444149	0.255490		C	-3.870391	0.649007	0.767610
N	1.294170	-0.159992	-0.284690		H	-1.286086	1.601905	1.033804
N	2.564860	0.289121	-0.575629		H	0.576230	-3.107511	1.247925
C	3.503719	-0.726227	-0.268001		H	-0.377549	-1.623640	1.411811
C	0.538398	0.945285	0.122637		H	-0.399628	-2.523895	-0.102915
C	1.326058	2.057825	0.139010		H	2.578508	-3.829978	0.996711
C	2.655571	1.675352	-0.284636		H	3.785097	-3.607579	-0.273874
O	3.662362	2.344850	-0.422207		H	4.099800	-2.998366	1.346279
O	4.706860	-0.621797	-0.418015		H	1.576046	3.892986	1.192083
C	-0.885040	0.875175	0.335675		H	1.093914	4.084192	-0.488728
C	0.236614	-2.212701	0.729022		H	-0.093610	3.559635	0.710065
C	3.317091	-3.136151	0.595505		H	-1.256938	-0.605626	-1.088710
C	0.948475	3.468072	0.403993		H	-3.285927	-1.439487	-1.839931
C	-1.698027	0.049185	-0.341131		H	-5.739037	-1.674864	-1.695042
C	-3.142746	-0.049529	-0.205861		H	-5.795144	1.062227	1.608254
C	-3.838510	-0.888292	-1.084753		H	-3.357878	1.295592	1.471769
C	-5.217823	-1.020856	-1.003798		H	-7.004924	-0.419607	0.031143
C	-5.926887	-0.317912	-0.037317					

Cartesian coordinates of the optimized geometries: 5e

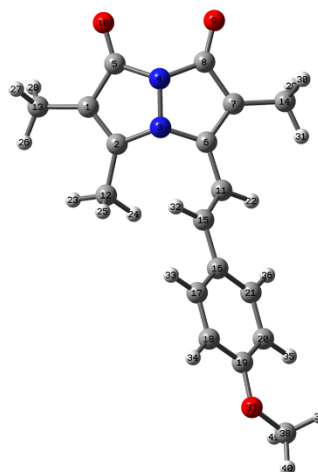
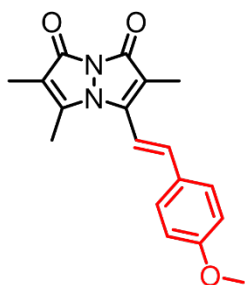
optimized at # APFD/6-311+G (2d, p) at ground state



C	3.070078	-1.860922	0.227749	C	-3.474271	0.744994	0.739199
C	1.776834	-1.449510	0.255399	H	-0.867442	1.645650	1.024305
N	1.684888	-0.163980	-0.285366	H	0.913646	-3.094354	1.253370
N	2.964107	0.262556	-0.573975	H	-0.017275	-1.594474	1.405569
C	3.884083	-0.769163	-0.264711	H	-0.048066	-2.502711	-0.104128
C	0.947375	0.954511	0.120914	H	2.900993	-3.855508	0.999014
C	1.756077	2.052445	0.140984	H	4.113621	-3.655628	-0.269416
C	3.078435	1.647113	-0.280523	H	4.436673	-3.051889	1.351139
O	4.097234	2.298981	-0.416762	H	2.013296	3.873482	1.219264
O	5.089457	-0.686652	-0.412848	H	1.592913	4.088829	-0.475053
C	-0.476641	0.909291	0.330510	H	0.353889	3.582613	0.678824
C	0.590023	-2.197064	0.728502	H	-0.869912	-0.570536	-1.089569
C	3.652858	-3.175361	0.599012	H	-2.915764	-1.393706	-1.826325
C	1.403244	3.469171	0.406758	H	-5.364556	-1.584920	-1.686467
C	-1.302868	0.094741	-0.346286	H	-5.391145	1.202459	1.563025
C	-2.747060	0.020586	-0.217093	H	-2.959312	1.397568	1.436356
C	-3.457394	-0.818583	-1.080832	C	-7.051771	-0.307866	0.042536
C	-4.838882	-0.926145	-1.001731	H	-7.454403	-1.004901	-0.693987
C	-5.560168	-0.202665	-0.055847	H	-7.355856	-0.649544	1.036384
C	-4.848901	0.633241	0.813359	H	-7.524107	0.666022	-0.117445

Cartesian coordinates of the optimized geometries: 5f

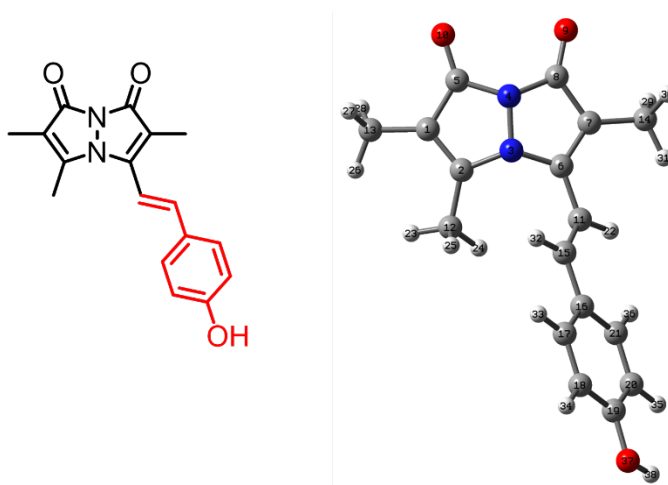
optimized at # APFD/6-311+G (2d, p) at ground state



<i>Atom</i>	<i>X</i>	<i>Y</i>	<i>Z</i>		<i>Atom</i>	<i>X</i>	<i>Y</i>	<i>Z</i>
C	-3.446200	-1.838591	-0.276992		H	0.541438	1.643281	-0.943973
C	-2.148797	-1.439083	-0.271126		H	-1.279797	-3.080489	-1.269761
N	-2.057387	-0.159619	0.283364		H	-0.327862	-1.589703	-1.377411
N	-3.339375	0.276313	0.546031		H	-0.345832	-2.519092	0.119449
C	-4.261005	-0.743455	0.205758		H	-3.276860	-3.830202	-1.056259
C	-1.299839	0.955620	-0.096592		H	-4.524183	-3.624279	0.176994
C	-2.100339	2.060372	-0.129338		H	-4.792317	-3.006970	-1.448364
C	-3.434223	1.664419	0.258733		H	-2.294779	3.883461	-1.219885
O	-4.450579	2.324258	0.377669		H	-1.961162	4.096311	0.493879
O	-5.469138	-0.651025	0.325817		H	-0.666868	3.585073	-0.595354
C	0.126682	0.899003	-0.272905		H	0.469095	-0.606180	1.133040
C	-0.959107	-2.194329	-0.724530		H	2.484080	-1.476213	1.909800
C	-4.032471	-3.143902	-0.674231		H	4.942752	-1.698278	1.823043
C	-1.729215	3.475933	-0.377183		H	5.067252	1.154188	-1.386023
C	0.929241	0.064057	0.410714		H	2.650168	1.368280	-1.302024
C	2.371776	-0.029707	0.318174		O	6.505065	-0.484961	0.258520
C	3.051664	-0.896525	1.187834		C	7.318075	0.235923	-0.655869
C	4.424268	-1.027010	1.147049		H	7.222238	1.314051	-0.501505
C	5.171042	-0.290131	0.223998		H	8.341103	-0.070618	-0.450012
C	4.513242	0.576235	-0.657142		H	7.063477	-0.013603	-1.689484
C	3.135643	0.695831	-0.602681					

Cartesian coordinates of the optimized geometries: 5h

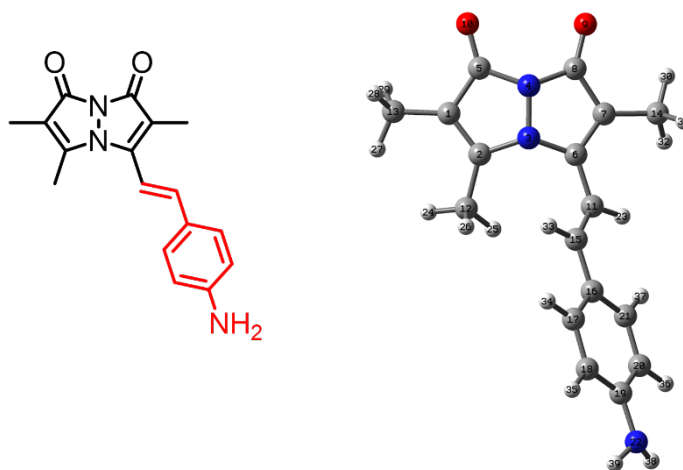
optimized at # APFD/6-311+G (2d, p) at ground state



<i>Atom</i>	<i>X</i>	<i>Y</i>	<i>Z</i>		<i>Atom</i>	<i>X</i>	<i>Y</i>	<i>Z</i>
C	3.048615	-1.860249	0.230659		C	-4.866416	0.632282	0.816450
C	1.756340	-1.445499	0.260393		C	-3.492027	0.741684	0.737568
N	1.666039	-0.161822	-0.284406		H	-0.881487	1.659965	1.019156
N	2.945935	0.260908	-0.576889		H	0.893664	-3.082103	1.272191
C	3.863825	-0.771868	-0.266685		H	-0.036507	-1.580389	1.413439
C	0.931322	0.959592	0.120865		H	-0.069643	-2.500998	-0.088599
C	1.744827	2.054909	0.139832		H	2.877025	-3.850748	1.012066
C	3.064113	1.645978	-0.283817		H	4.083837	-3.660884	-0.263310
O	4.084731	2.294844	-0.423949		H	4.417059	-3.050497	1.352661
O	5.069440	-0.692943	-0.417456		H	1.990355	3.870842	1.231852
C	-0.491263	0.917355	0.331736		H	1.608725	4.095021	-0.470446
C	0.569702	-2.188832	0.740665		H	0.341734	3.592151	0.654227
C	3.629032	-3.174874	0.605095		H	-0.882794	-0.570788	-1.079316
C	1.396030	3.473095	0.404436		H	-2.922723	-1.402804	-1.820871
C	-1.318480	0.097349	-0.340095		H	-5.383442	-1.602108	-1.684893
C	-2.759586	0.018258	-0.214127		H	-5.416661	1.198589	1.562396
C	-3.468018	-0.827572	-1.078533		H	-2.982510	1.398119	1.434721
C	-4.843948	-0.945864	-1.010871		O	-6.894922	-0.361001	-0.030536
C	-5.550898	-0.213064	-0.061028		H	-7.273460	0.189750	0.664064

Cartesian coordinates of the optimized geometries: 5j

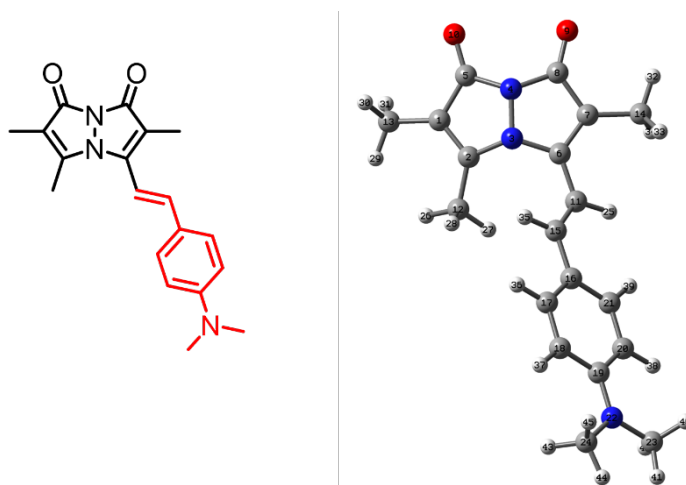
optimized at # APFD/6-311+G (2d, p) at ground state



<i>Atom</i>	<i>X</i>	<i>Y</i>	<i>Z</i>	<i>Atom</i>	<i>X</i>	<i>Y</i>	<i>Z</i>
C	3.081408	-1.848353	0.231110	C	-3.498769	0.795146	0.687872
C	1.784247	-1.448140	0.256855	N	-6.943441	-0.261643	-0.015747
N	1.680041	-0.168352	-0.292572	H	-0.872871	1.702911	0.948720
N	2.956703	0.268569	-0.583102	H	0.940397	-3.075330	1.299254
C	3.884567	-0.752193	-0.267633	H	-0.020578	-1.588775	1.389855
C	0.933274	0.946284	0.109520	H	-0.015614	-2.549407	-0.088058
C	1.739843	2.049399	0.136995	H	2.930978	-3.834954	1.026755
C	3.060724	1.656705	-0.286326	H	4.131361	-3.643278	-0.254207
O	4.079603	2.310756	-0.424387	H	4.465014	-3.018386	1.356060
O	5.090449	-0.661258	-0.415815	H	2.249754	4.068494	0.528531
C	-0.485109	0.914330	0.312086	H	0.768395	3.883066	-0.415454
C	0.606097	-2.202366	0.740911	H	0.754963	3.549048	1.316988
C	3.675339	-3.155020	0.612375	H	-0.884451	-0.641861	-1.023831
C	1.353124	3.458646	0.406931	H	-2.921592	-1.525693	-1.708771
C	-1.319903	0.065624	-0.321896	H	-5.364564	-1.708015	-1.587095
C	-2.756177	0.004219	-0.205322	H	-5.419347	1.319993	1.463080
C	-3.468304	-0.895092	-1.013267	H	-2.991488	1.495993	1.342797
C	-4.842865	-1.002185	-0.948064	H	-7.398099	0.100343	0.808224
C	-5.574563	-0.203894	-0.056422	H	-7.383503	-1.087220	-0.391848
C	-4.869983	0.698068	0.762702				

Cartesian coordinates of the optimized geometries: 5k

optimized at # APFD/6-311+G (2d, p) at ground state



<i>Atom</i>	<i>X</i>	<i>Y</i>	<i>Z</i>		<i>Atom</i>	<i>X</i>	<i>Y</i>	<i>Z</i>
C	3.780493	-1.863968	0.305634		C	-6.952480	-1.139366	-0.783171
C	2.489388	-1.443184	0.315750		H	-0.120728	1.777481	0.870805
N	2.404138	-0.185737	-0.284632		H	1.622994	-3.007947	1.432773
N	3.687405	0.220452	-0.591535		H	0.680517	-1.506725	1.448625
C	4.599659	-0.800361	-0.235149		H	0.676654	-2.537892	0.019039
C	1.672505	0.955329	0.071119		H	3.598134	-3.817637	1.173089
C	2.497476	2.046437	0.057217		H	4.808214	-3.689795	-0.106473
C	3.811082	1.618517	-0.347719		H	5.141618	-3.010819	1.481717
O	4.839328	2.251983	-0.514302		H	2.957887	4.113926	-0.025743
O	5.807409	-0.733942	-0.385595		H	1.247881	3.751657	-0.307958
C	0.255392	0.954131	0.272521		H	1.909836	3.678620	1.325986
C	1.300877	-2.158864	0.831999		H	-0.167138	-0.658967	-0.988639
C	4.354214	-3.163573	0.738709		H	-2.217200	-1.556730	-1.622431
C	2.129321	3.470092	0.274325		H	-4.632990	-1.700659	-1.515759
C	-0.593752	0.088194	-0.323164		H	-4.654645	1.522154	1.364421
C	-2.027348	0.054964	-0.210908		H	-2.254114	1.641707	1.240173
C	-2.754717	-0.877105	-0.966653		H	-6.793898	1.784463	0.585150
C	-4.129023	-0.960762	-0.907576		H	-8.027714	0.533370	0.755897
C	-4.871541	-0.097370	-0.069125		H	-6.694139	0.607543	1.911714
C	-4.137743	0.841757	0.699983		H	-6.653658	-2.161949	-0.529588
C	-2.766543	0.908092	0.626064		H	-8.015547	-1.038595	-0.579201
N	-6.226296	-0.163696	0.000723		H	-6.796379	-0.990993	-1.857035
C	-6.964960	0.738093	0.858599					

REFERENCES

1. Kosower, E. M.; Pazhenchevsky, B. Synthesis and Properties of syn- and anti- 1,5 Diazabicyclo[3.3.0]octadienediones (9, 10-Dioxabimanes). *J. Am. Chem. Soc.* **1980**, *102*, 15, 4983–4993.
2. Ishita Neogi, Partha J. Das, and Flavio Grynszpan. Dihalogen and Solvent-Free Preparation of syn-Bimane. *Synlett* **2018**, *29*, 1043–1046.
3. Gaussian 16, Revision C.01, Frisch, M. J.; Trucks, G. W.; Schlegel, H. B.; Scuseria, G. E.; Robb, M. A.; Cheeseman, J. R.; Scalmani, G.; Barone, V.; Petersson, G. A.; Nakatsuji, H.; Li, X.; Caricato, M.; Marenich, A. V.; Bloino, J.; Janesko, B. G.; Gomperts, R.; Mennucci, B.; Hratchian, H. P.; Ortiz, J. V.; Izmaylov, A. F.; Sonnenberg, J. L.; Williams-Young, D.; Ding, F.; Lipparini, F.; Egidi, F.; Goings, J.; Peng, B.; Petrone, A.; Henderson, T.; Ranasinghe, D.; Zakrzewski, V. G.; Gao, J.; Rega, N.; Zheng, G.; Liang, W.; Hada, M.; Ehara, M.; Toyota, K.; Fukuda, R.; Hasegawa, J.; Ishida, M.; Nakajima, T.; Honda, Y.; Kitao, O.; Nakai, H.; Vreven, T.; Throssell, K.; Montgomery, J. A., Jr.; Peralta, J. E.; Ogliaro, F.; Bearpark, M. J.; Heyd, J. J.; Brothers, E. N.; Kudin, K. N.; Staroverov, V. N.; Keith, T. A.; Kobayashi, R.; Normand, J.; Raghavachari, K.; Rendell, A. P.; Burant, J. C.; Iyengar, S. S.; Tomasi, J.; Cossi, M.; Millam, J. M.; Klene, M.; Adamo, C.; Cammi, R.; Ochterski, J. W.; Martin, R. L.; Morokuma, K.; Farkas, O.; Foresman, J. B.; Fox, D. J. Gaussian, Inc., Wallingford CT, 2016.
4. Lougee, M. G.; Pagar, V. V.; Kim, H. J.; Pancoe, S. X.; Chia, W. K.; Mach, R. H.; Garcia, B. A.; Petersson, E. J. Harnessing the Intrinsic Photochemistry of Isoxazoles for the Development of Chemoproteomic Crosslinking Methods. *Chem. Commun.*, **2022**, *58*, 9116–9119.
5. Fung, H. Y. J.; McKibben, K. M.; Ramirez, J.; Gupta, K.; Rhoades, E. Structural Characterization of Tau in Fuzzy Tau: Tubulin Complexes. *Structure* **2020**, *28* (3), 378–384.
6. Stine, W. B.; Jungbauer, L.; Yu, C.; Ladu, M. J. Preparing Synthetic A β in Different Aggregation States. *Methods Mol. Biol.* **2011**, *670*, 13–32.
7. Ferrie, J. J.; Lengyel-Zhand, Z.; Janssen, B.; Lougee, M. G.; Giannakoulis, S.; Hsieh, C. J.; Pagar, V. V.; Weng, C. C.; Xu, H.; Graham, T. J. A.; Lee, V. M. Y.; Mach, R. H.; Petersson, E. J. Identification of a Nanomolar Affinity A-Synuclein Fibril Imaging Probe by Ultra-High Throughput: In Silico Screening. *Chem. Sci.* **2020**, *11* (47), 12746–12754.
8. Haney, C. M.; Cleveland, C. L.; Wissner, R. F.; Owei, L.; Robustelli, J.; Daniels, M. J.; Canyurt, M.; Rodriguez, P.; Ischiropoulos, H.; Baumgart, T.; Petersson, E. J., Site-Specific Fluorescence Polarization for Studying the Disaggregation of α -Synuclein Fibrils by Small Molecules. *Biochemistry* **2017**, *56* (5), 683–691.
9. Marotta, N. P.; Ara, J.; Uemura, N.; Lougee, M. G.; Meymand, E. S.; Zhang, B.; Petersson, E. J.; Trojanowski, J. Q.; Lee, V. M. Y., Alpha-synuclein from patient Lewy bodies exhibits distinct pathological activity that can be propagated in vitro. *Acta Neuropathol. Commun.* **2021**, *9* (1), 188.
10. Volpicelli-Daley, L. A.; Luk, K. C.; Patel, T. P.; Tanik, S. A.; Riddle, D. M.; Stieber, A.; Meaney, D. F.; Trojanowski, J. Q.; Lee, V. M.-Y. Exogenous α -Synuclein Fibrils Induce Lewy Body Pathology Leading to Synaptic Dysfunction and Neuron Death. *Neuron* **2011**, *72* (1), 57–71.